CHAPTER 1

Long-Range DNA Charge Transport

Adapted from: Delaney, S., and Barton, J. K. (2003) *J. Org. Chem. 68*, 6475.

1.1 Deoxyribonucleic Acid as a Medium for Charge Transport Reactions.

The inner core of double helical DNA is composed of a stacked array of aromatic, heterocyclic base pairs (Figure 1.1). This array of π-orbitals resembles a one-dimensional aromatic crystal, and it was suggested shortly after elucidation of the double helical structure of DNA that the base stack might provide a pathway for charge transport (CT) reactions (*1*). Numerous solid-state π-stacked arrays have been identified and these materials tend to exhibit semiconductive or conductive behavior, especially in the presence of dopants (*2*). However, double helical DNA, as a molecular π-stack in solution, presents a unique, well-defined system in which to explore CT. Critical to the characterization of DNA CT was the ability to construct, through chemical synthesis, well-defined DNA assemblies with pendant probes of the CT process. Through a variety of spectroscopic, biochemical, and biophysical studies, it is now established that the DNA π-stack can, indeed, provide a medium for CT (*3*-*6*). Interestingly, the differences between DNA as a molecular π-stacked array and π-stacked solids may be as important as the chemical similarities in characterizing DNA CT chemistry.

Efficient CT chemistry is observed when both the charge donor and acceptor are electronically coupled into the base stack. To this end, we have exploited various intercalating donors and acceptors, covalently tethered to the ends of a double helix and we have monitored the reaction spectroscopically (*7*). We have also learned that DNA CT can yield chemistry at a distance (*8*). Thus, the DNA itself can directly participate in the redox chemistry, functioning as the electron donor. Of the nucleic acid bases free in solution, guanine (G) is the easiest to oxidize (E_0 = 1.3, 1.4, 1.6, and 1.7 V vs. NHE for G, A, C, and T, respectively) (*9*), and photooxidants bound to DNA can promote

oxidative damage at a remote guanine site through DNA CT. Using a variety of DNA-bound oxidants, many laboratories have now probed the factors affecting DNA CT and the yield of resultant oxidative damage. As a result, scientists are now asking not *if* DNA can mediate CT but rather *how* this process occurs.

Given that DNA CT can be efficient and lead to chemistry over long molecular distances, we can also begin to ask what are the biological consequences and opportunities for DNA CT. Does DNA CT play some role in the oxidative damage of the genome? Are there regions of the genome to which damage is funneled through CT? How is long-range oxidative damage affected by packaging of the DNA within chromatin? Additionally, does DNA CT offer a means of long-range signaling between proteins bound to DNA?

1.2 Oxidative DNA Damage via Charge Transport. Oxidative DNA damage at a distance was demonstrated first in an oligonucleotide assembly containing two 5'-GG-3' sites spatially separated from a tethered photooxidant, $[Rh(phi)_2bpy']^{3+}$ (phi = phenanthrenequinone diimine; bpy' = 4'-methylbipyridine-4-butyric acid) (*8*). High resolution NMR studies (*10*) and a recent 1.2 Å crystal structure (*11*) of a phi complex of rhodium bound to DNA reveal intercalative binding of the photooxidant from the major groove; importantly, these complexes bind with minimal perturbation of the surrounding bases. The phi ligand inserts deeply into the base stack and behaves essentially like an additional base pair. The rich photochemistry of phi complexes of rhodium allows not only for the initiation of long-range CT chemistry, but also identifies the exact binding site of the photooxidant (Figure 1.2) (*12*). When irradiated at high energy (λ = 313 nm) these complexes promote direct DNA strand cleavage by hydrogen atom abstraction from

the sugar ring near the photoexcited intercalated phi ligand, marking the site of intercalation. Irradiation at lower energy ($\lambda \geq 365$ nm) generates a potent photooxidant (E_0 ($Rh^{3+*/2+}$) ~ 2 V vs. NHE) that leads to damage of the guanine bases in DNA. Piperidine treatment results in strand breakage neighboring the damaged bases (*13*) and the yield of damage products can be analyzed by gel electrophoresis.

Remarkably, in the assemblies designed, oxidative DNA damage was observed at both 5'-GG-3' sites, located 17 and 34 Å from the site of rhodium binding (*8*). Specifically, damage was observed at the 5'-G of the 5'-GG-3' guanine doublets. *Ab initio* molecular orbital calculations have revealed the HOMO for stacked guanines is localized on the 5'-G of guanine doublets (*14*). This 5'-G reactivity is now considered the hallmark of long-range CT chemistry; non-specific reaction at guanine bases suggests instead an alternate chemistry, such as reaction with reactive oxygen species.

Since these first studies with the rhodium intercalator, organic intercalators such as naphthalene diimide (NDI) (*15*), ethidium (*16*) and modified anthraquinones (*17*) have been used to promote long-range oxidative DNA damage. Modified nucleotides such as 5-cyano-benzene deoxyuridine (*18*) and 4'-pivaloyl deoxythymine (*19*) have also been photolysed to generate hot base and sugar radicals, respectively, that lead to oxidative guanine damage from a remote site. The ability to affect long-range chemistry with a family of such varied oxidants indicates that the ability to mediate CT is a characteristic of the DNA duplex, not the oxidant utilized. Use of the full family of oxidants results in damage patterns consistent with CT, oxidation of the 5'-G of 5'-GG-3' sites.

1.3 Distance Dependence of DNA Charge Transport. To probe systematically the distance dependence of long-range oxidative damage, a series of 28 base pair

duplexes containing tethered $[Rh(phi)_2bpy']^{3+}$ and both proximal and distal 5'-GG-3' sites was constructed (*20*). The proximal guanine doublet was fixed with respect to the rhodium intercalator, while the distal guanine doublet was marched out in 2 base pair increments relative to the photooxidant binding site. The ratio in yield of damage at the distal versus proximal guanine doublets provides a measure of the relative efficiency of the CT reaction. Over distances of 75 Å, the yield of oxidative damage was not significantly diminished, suggesting a very shallow distance dependence. Further evidence for a shallow distance dependence in DNA CT was observed using a 63 base pair duplex containing either tethered $[Rh(phi)_2bpy']^{3+}$ or $[Ru(bpy')(dppz)(phen)]^{2+}$ (dppz = dipyridophenazine; phen = 1,10-phenanthroline); the assemblies also contained six 5'-GG-3' sites located 31 to 197 Å from the metallointercalator (Figure 1.3) (*20*). Extraordinarily, in both assemblies, oxidative damage was observed at all 5'-GG-3' sites including that almost 200 Å from the site of charge injection. Damage over this distance regime has been confirmed in analogous experiments using a tethered anthraquinone moiety as photooxidant (*21*). These experiments made clear that DNA CT can proceed over biologically significant distances.

While oxidative damage over long-range has been seen using a variety of oxidants, it has become increasingly clear that variations do occur in the efficiency of long-range reaction depending upon the oxidant employed. It had been proposed that differences seen with rhodium photooxidants versus anthraquinone photooxidants might reflect aggregation by the rhodium tethered species (*22*). The possible clustering of metallointercalators on DNA was probed earlier using NMR and no evidence for such clustering was seen (*23*). Moreover, in examinations of tethered duplex assemblies under

the conditions utilized for CT studies, no aggregation was observed. Nonetheless, recent work (*24*) in our laboratory to compare directly oxidative DNA damage by a phi complex of rhodium, a dipyridophenazine complex of ruthenium, and modified anthraquinones under identical conditions and using identical sequences has shown that the amount of damage seen at a 5'-GG-3' site proximal versus distal to the tethered oxidant varies significantly with the photooxidant. The differences we observe likely arise from several factors that depend upon the oxidant employed including the efficiency of back electron transfer, extent of coupling with the base pair stack (*25*) and energetics of the oxidant. Understanding mechanistically the basis for these differences is something we need still to achieve.

1.4 Sensitivity of DNA Charge Transport to Base Stacking. While charge migration through DNA is possible over long molecular distances, it is nonetheless modulated by intervening DNA structure and stacking. DNA CT is exquisitely sensitive to static and dynamic perturbations in base stacking. An effectively coupled aromatic π-array is requisite for long-range CT and variations in stacking can lead to substantial changes in efficiency and yield (Figure 1.4). As an example, we found that the introduction of base bulges between 5'-GG-3' sites located distal and proximal to a tethered rhodium intercalator resulted in significant diminutions in the distal/proximal ratios of oxidative damage (*26*). Upon the insertion of a 5'-ATA-3' bulge the amount of charge reaching the distal site was attenuated by 75%, clearly reflecting the importance of an intact base stack.

Introducing a series of base-pair mismatches between 5'-GG-3' sites located distal and proximal to a tethered, intercalated ruthenium(III) oxidant also produced

decreased distal/proximal ratios of oxidative damage, in fact to extents similar to those seen with base bulges (*27*). A systematic examination of base mismatches revealed that some mismatches severely destabilize the helix, while others yield more subtle variations. The ratio of distal/proximal oxidative damage varies in the order GC ~ GG ~ GT ~ GA > AA > CC ~ TT ~ CA ~ CT. The purine-purine mismatches do not greatly diminish CT to the distal guanine doublet, while introduction of a pyrimidine-pyrimidine mismatch results in significantly attenuated yields of oxidative damage. The extent of long-range guanine oxidation was compared with the thermodynamic stability of the mismatch-containing duplexes and although a correlation exists, the trend most closely correlates with base-pair opening lifetimes derived from ^{1}H-NMR measurements of imino proton exchange rates; this parameter reflects the dynamical motion of the mismatch and extent of stacking with the adjacent base pairs. In general, purine-purine mismatches do not greatly perturb the base stack; these mispairs are able to hydrogen bond and the larger aromatic surface area of the purines allows for significant coupling with the bases above and below the mismatch. However, in a pyrimidine-pyrimidine mismatch, lack of proper hydrogen bonding and small stacking surface area make these mismatches particularly destabilizing to the helix. These results further implicate base stacking and dynamics in modulating long-range oxidative damage in DNA.

In addition to base bulges and mismatches, some DNA-binding proteins that perturb the DNA structure also can modulate long-range oxidative DNA damage (Figure 1.5) (*28*). Methyltransferase *Hha*I (M.*Hha*I) methylates a cytosine in 5'-G*CGC-3' sequences by flipping out the cytosine into its active site and inserting a glutamine side chain in its place (*29*). This glutamine side chain creates a non-aromatic plug within the

base stack and, as a result, when M.*Hha*I is bound between two 5'-GG-3' sites on a rhodium tethered assembly, oxidative damage to the distal site is greatly diminished. Interestingly, when a mutant enzyme, that inserts a heterocyclic, aromatic tryptophan into the base stack was tested, charge transport to the distal guanine site was restored (*28*). This result is consistent with the idea that tryptophan, resembling a DNA base when inserted in the π-stack, completes the π-stack and thus does not disrupt long-range CT. Hence, depending on the specific nature of the interaction, DNA-binding proteins can regulate long-range CT both positively and negatively.

It is important to emphasize that the sensitivity of DNA CT in metal-tethered duplexes to these perturbations in intervening base pair structure underscores that the path for charge transport is necessarily through the base pair stack. Oxidative damage cannot, for example, arise in these systems from aggregration or intermolecular reaction. Indeed a photophysical study of photoinduced electron transfer between two tethered intercalators provided the first indication of the sensitivity of CT to intervening mismatches and early compelling evidence that long-range CT through the DNA π-stack could occur (*30*).

1.5 Charge Transport through Different DNA Structures. DNA duplexes modified to contain tethered photooxidants provide well-defined systems in which to explore long-range CT chemistry. However, other π-stacked arrays have demonstrated efficiency in mediating oxidative DNA damage (Figure 1.6). In DNA/RNA hybrids, containing both ribo- and deoxyribonucleotide strands, a pendant ethidium photooxidant can promote oxidative damage from a distance of 35 Å (*31*). These hybrids adopt an A-like structure and possess a narrower major groove than B-DNA. For this reason, use of

metallointercalators does not result in efficient CT; the oxidant cannot intercalate within the narrow groove and is therefore not well coupled to the π-stack. Ethidium, however, does intercalate in A-form helices and can promote efficient CT. These results underscore the importance of efficient coupling of the charge donor and acceptor with the base stack.

Another base-stacked array in which CT was explored is the triple helix. Triplex structures furthermore provide a means to introduce a photooxidant site-specifically to a long DNA fragment. An NDI intercalator attached to the center of a 16 base pair triplex-forming oligonucleotide (TFO) was selectively targeted to a single site on a ~ 250 base pair restriction fragment (*32*). Oxidative DNA damage was observed over at least 85-130 Å in each direction from the site of binding. Notably, however, the CT reaction was significantly more efficient to the 3' side of the triplex. Interestingly, when NDI or $[Rh(phi)_2bpy']^{3+}$ are covalently tethered to the 5'-end of the TFO, significant amounts of damage were observed only in the immediate vicinity of oxidant binding, suggesting the base stacking is distorted at the 5'-end of the triplex-duplex junction so as to interrupt CT. Triplex targeting to a restriction fragment to yield oxidative damage provided us with an estimate of the distance distribution of genomic charge transport of ~ 200 Å around the site of radical injection.

Multiple-stranded DNA assemblies, in addition to double and triple-stranded arrays, provide unique base stacks in which to explore CT. Four-way DNA junctions (also called Holliday junctions) are composed of four partially complementary DNA strands that form parallel base stacks which rapidly exchange between different stacking isomers. Photoactivation of a tethered rhodium complex, displaying photocleavage and

therefore intercalation in only one arm of the assembly, results in oxidative damage in all arms of the four-way junction (*33*). These assemblies are relatively mobile and interchange between different stacking isomers provides multiple π-stacked pathways and, hence oxidative damage is possible in all arms of the four-way junction. In contrast, similar experiments utilizing a tethered anthraquinone moiety revealed CT in only two of the four arms of the four-way junction. While it was proposed (*22*) that the differences seen reflected aggregation by the rhodium tethered species, instead we consider that the variations among oxidants seen reflect variations in the time scale for CT, which may vary with the oxidant employed.

To restrain the flexibility of the four-way junction, DNA double-crossover (DX) assemblies were also constructed (*34*). DX assemblies are composed of a collection of partially complementary strands annealed into one supermolecule which has two connected, but spatially separated, π-stacks. Unlike a four-way junction, DX assemblies are relatively rigid and when $[Rh(phi)_2bpy']^{3+}$ is tethered to one end of the DX, yet constrained so as to only allow intercalation into one base stack, oxidative G damage is observed selectively down the base stack bearing the metallointercalator. Remarkably, despite tight packing, no CT crossover to the adjacent base stack was observed; the two base stacks are effectively insulated from one another. These data underscore also the importance of the π-stacked array as the critical path for CT.

To explore CT in a secondary DNA structure which may be biologically relevant, duplex/quadruplex conjugates were constructed (*35*). In these assemblies composed of adjacent duplex and guanine quadruplex regions, the guanines in the stracked quadruplex were found to be more efficient traps of oxidative damage damage than a 5'-GG-3'

guanine doublet in the duplex region. Furthermore, the pattern of oxidative damage in the quadruplex region is distinct from that observed in duplex DNA. These differences may be useful for identifying DNA sequences *in vivo* which may be forming quadruplexes. This will be discussed further in Chapter 6.

1.6 Gating of CT by Dynamical Motions. Biochemical experiments probing the distance dependence or effect of helix-destabilizing mismatches, bulges, or non-aromatic side chains measure only a change in *yield* of CT products; might there also be a change in CT *rate*? To address this question, assemblies containing a tethered ethidium photooxidant and 7-deazaguanine as the electron donor, with donor-acceptor distances 6-24 Å, were constructed and their ability to support long-range CT examined spectroscopically (*36*). Ultrafast transient absorption spectroscopy revealed biphasic kinetics for the CT with populations having two time constants, 5 and 75 picoseconds. The 5 ps component was assigned to direct CT from 7-deazaguanine, while the 75 ps component corresponded to the orientation time of ethidium within its binding site to align in a conformation allowing CT. Interestingly, with increasing donor/acceptor separation, the two components decreased in yield but not significantly in their decay times. The *rate* of CT was independent of donor/acceptor separation while the *yield* decreased significantly. These data suggested to us first that dynamical motions within the π-stack gate long-range CT. Recent studies of base-base CT as a function of temperature, both time resolved and steady state, highlight the role of base dynamics in modulating CT and provide additional support for the idea that intervening base motions serve to gate the CT process.

1.7 Towards a Mechanistic Understanding of Long-Range Charge Transport.

Based upon many experiments that established long-range oxidative damage to DNA, the focus of research has shifted from questions of *whether* long-range CT occurred to *how* charge propagates through the base stack. Our first interest was in determining experimentally the scope and parameters governing DNA CT. As we do so, now we and others can begin to address mechanistically how DNA CT proceeds. There are two general mechanistic possibilities: tunneling through the DNA, forming a 'virtual' bridge between the donor and acceptor, and charge hopping between discrete base orbitals (Figure 1.7) (*37*). In a tunneling mechanism, the DNA orbitals are energetically higher than the donor and acceptor and the charge tunnels through the bridge without formally occupying it. With only virtual occupation of the DNA bridge, the rate of CT would show exponential dependence on donor/acceptor separation. In contrast to tunneling, in a hopping mechanism, the donor and acceptor orbitals are close in energy to the bridge. Thus in thermally induced hopping, charge transiently occupies the bridge orbitals, hopping from one low energy site to the next. So long as hopping to the next 'stepping stone' is faster than radical trapping, charge would be able to propagate through the base stack with a very shallow distance dependence.

Bixon and Jortner proposed a theoretical model to explain the sequence-dependence associated with long-range oxidative damage and the shallow distance dependence. They first proposed sequential hopping between guanine bases with tunneling through A-T base pairs (*38*). Utilizing yield measurements of oxidative DNA damage as a function of intervening sequence, Giese, Jortner, and coworkers offered experimental support for this guanine hopping model of CT through DNA (*39*). They

observed decreased yields of guanine oxidation with increasing separation of guanine ‘stepping stones’ by TA steps.

We considered whether base dynamics might also explain the sequence-dependence in efficiency of DNA CT observed. By inserting 5’-TA-3’ steps, which are known to be quite flexible, into the bridge, the base-base coupling is significantly altered; this could also explain the diminished yields of oxidative damage. To probe more directly the notion that charges tunnel through TA steps, we therefore varied the length of AA, TT, and AT tracts intervening two 5’-GG-3’ sites and monitored the yield of oxidative damage using a tethered rhodium intercalator (*40*). Significant damage at the distal guanine doublet site was observed in all cases with up to 10 A’s, T’s or alternating AT sequence intervening. The distal/proximal ratio of oxidative damage was consistently higher for assemblies containing all A’s intervening; this we attributed to significant stacking overlap of the purine tract. Moreover, increasing the number of A’s between the guanine doublets only slightly decreased the guanine oxidation ratio and, remarkably, an increase in oxidation ratios was observed increasing from four to eight intervening T’s or AT sequence. In fact, guanine oxidation was observed through up to five TA steps with no significant loss of yield over that distance. Furthermore, insertion of a GC pair in this TA tract actually decreased the oxidative damage yield, inconsistent with a guanine hopping model.

Based upon our results and those of Schuster, the model of Giese and Jortner for sequence-dependent CT was recently revised to distinguish unistep superexchange tunneling over ‘short’ $(A\text{-}T)_n$ bridges ($n < 3\text{-}4$), and thermally induced hopping over ‘long’ $(A\text{-}T)_n$ bridges ($n > 3\text{-}4$) (*38*). We consider, however, that sequence-dependent

DNA dynamics and flexibilities can gate CT. Rather than hopping from guanine to guanine, we have proposed that CT over long molecular distances might be best considered as *domain hopping* (*20, 40*), where charge is transiently delocalized over sequence-dependent domains defined by local structure. Variations in length and sequence contribute to the conformational dynamics of the helix, and these may define a delocalized domain. Accordingly, inserting a GC pair into the TA tract may have disrupted a local domain and the resultant yield of CT. Recent experiments using photoexcited 2-aminopurine (*Ap), a fluorescent nucleobase analog, in combination with time-resolved (*41*) and steady-state fluorescence quenching (*42*), have shown that base dynamics play a significant role in modulating propagation of charge through DNA. Domains over which charge may be delocalized are defined by sequence and dynamics; a domain size of ~ 4 base pairs has been characterized. CT between these domains is gated by DNA conformations; higher temperatures provide increased base fluctuations which in turn allow access to more CT active conformations and facilitate CT.

Schuster and coworkers have proposed phonon-assisted polaron hopping between guanine bases (*43*). In this model, based on yield measurements of oxidative damage, transient formation of polarons in DNA allows for charge delocalization over regions of sequence; propagation of these polarons throughout the helix is aided by phonons. Counterion distribution may be a critical factor in considering phonon-assisted polaron hopping (*44*). By simply varying the position of phosphate termini with respect to a tethered rhodium intercalator, we were able to modulate the amount of long-range guanine oxidation (*45*). In one case, sequences containing two spatially separated 5'-GG-3' sites, six intervening A's, and a tethered rhodium intercalator were examined for their

ability to mediate long-range CT. With a 5'-^{32}P-end label (5'-OPO_3^{2-}, 3'-OH) a distal/proximal ratio of 5.2 was obtained. By simply 3'-end labeling the duplex (5-OH, 3'-PO_2^--OR) instead, the ratio dropped to 0.4. Thus moving the negative charge to the end proximal to the rhodium intercalator dramatically decreased oxidative damage at the distal guanine doublet. Analogous fluorescence measurements of electron transfer between photoexcited 2-aminopurine and G did not show significant modulations in fluorescence as a function of charge distribution at the duplex termini. This led to a proposal of altered oxidation potentials at the distal relative to proximal guanine doublet sites as a function of charge at the termini. Assuming the results reflect a change in the thermodynamic potential at the 5'-GG-3' sites, then one can roughly calculate the internal longitudinal dielectric constant of DNA based on the these data. High values ranging from 30-300, depending on extent of screening of the pendant charges by counterions, are obtained; thus these results pointed to the possibility that a high longitudinal polarizability of DNA may play a part in the mechanism for DNA CT (*46*).

There is, however, much we still do not understand mechanistically. We cannot yet account for many variations seen with different oxidants; in some cases CT appears to be rate limiting, but in other cases, not. Clearly a critical feature we have learned, irrespective of the methodology employed, is the sensitivity of DNA CT to nucleic acid structure, both statically and dynamically. To delineate further these differences depending upon oxidant and nucleic acid structure, we need to look not just at the irreversible oxidative damage found at long distance but also more directly to monitor the radicals formed and their rates of formation.

1.8 Spectroscopic Identification of Radical Intermediates in Long-Range CT.

Following our biochemical experiments designed to establish oxidative chemistry from a distance, using the rhodium intercalator primarily, we therefore became interested in characterizing the timescales and radical intermediates in the long-range CT process. Dipyridophenazine complexes of ruthenium(II) possess remarkable photophysical properties and, given their avid intercalative binding to DNA, thus provide a unique spectroscopic handle. Luminescence of these dppz complexes is evident in organic solvents; however, in aqueous solution the luminescence is quenched by proton transfer to the phenazine nitrogens (*47*). Upon intercalative binding to DNA, these phenazine nitrogens are protected from solvent and luminescence is restored; binding to DNA thus sensitively modulates the luminescent properties, and hence these complexes have been dubbed 'molecular light switches.' These complexes furthermore provide a valuable spectroscopic handle for DNA CT. Photoexcitation of dppz complexes of Ru(II) yields a metal-to-ligand charge transfer excited state which is localized on the dppz ligand. Quenching of this excited state by a non-intercalating, diffusible species (e.g., $[Ru(NH_3)_6]^{3+}$ or $[Co(NH_3)_5Cl]^{2+}$) generates *in situ* a powerful Ru(III) oxidant (E_0 ($Ru^{3+/2+}$) ~ 1.5 V vs. NHE) that is capable of oxidizing guanines from a distance (*48*).

The flash/quench technique, coupled with transient absorption spectroscopy, has been applied effectively in characterizing the resultant neutral guanine radical in duplex DNA; deprotonation of the cation radical must occur faster than the 10^{-7} s time scale of the experiment (*48*). We have also utilized flash/quench experiments in characterizing radical products in peptide/DNA assemblies (*49*) and a protein/DNA complex (*50*). In particular, CT and radical trapping were examined in DNA assemblies in the presence of

a site-specifically bound methyltransferase *Hha*I mutant. The methyltransferase mutant, which can flip out a base and insert a tryptophan side chain within the DNA cavity, was found to activate long-range hole transfer through the base pair stack. Protein-dependent DNA charge transport was observed over 50 Å with guanine radicals formed > 10^6 s^{-1}; hole transport through DNA over this distance was found not to be rate-limiting. Thus, the flash/quench technique, originally designed to study CT in proteins (*51*), provides a method to generate powerful ground state oxidants and to follow the formation of radical intermediates associated with long-range DNA CT chemistry.

Assemblies containing 4-methylindole (M) as the electron donor embedded between two G bases, for greater stability, as well as a tethered ruthenium intercalator were also constructed to explore long-range DNA CT spectroscopically (*52*). The methylindole radical cation is particularly amenable as an artificial base in these studies because of its strong absorptivity at 600 nm and its relatively low oxidation potential (1 V vs. NHE). To explore the distance dependence of radical formation, the separation between the ruthenium oxidant and M was varied over 17-37 Å with only intervening A-T base pairs composing the DNA bridge. Formation of the M radical at all distances was found to be coincident with quenching of the ruthenium excited state to form the Ru(III) oxidant. Thus the rate of formation of the radical at long-range across a path of AT bases is $\geq 10^7$ s^{-1} and over this distance regime CT is not rate limiting.

Additional assemblies containing a pendant ruthenium oxidant and M as the charge donor were constructed to examine spectroscopically the effects of intervening sequence on long-range CT (*53*). Sequences contained either a G or inosine (I) at the hole injection site with the intervening sequence to the GMG oxidation site varied as all

A's, all T's, or containing an intervening AA mismatch. In the presence of the intervening mismatch, consistent with measurements of long-range oxidative damage, no indole cation radical was formed. In comparing assemblies containing inosine and guanine, inosine is harder to oxidize than G by ~ 200 mV, and the initial expectation might have been that hole injection into the bridge would be less efficient for sequences containing I at the injection site. In fact, rapid radical formation was observed with either G or I at the injection site, except for the mismatch-containing assembly. Remarkably, in sequences containing I at the injection site and no intervening guanines, formation of radical product was also observed at rates $\geq 10^7\ s^{-1}$. Even more intriguing, the 600 nm signal is significantly larger for sequences containing I at the injection site, indicative of a higher yield of radical formation. Biochemical analysis of analogous assemblies where GGG was substituted for GMG suggests these differences can be accounted for based upon the extent of radical localization at the injection site and subsequent reaction with Q^{red}. Thus the yield of oxidative damage at a site spatially separated from the oxidant can be modulated sensitively by reactivity at the injection site; the sequence determines the extent of hole localization and hence the probability of hole propagation. This sensitivity in long-range oxidative damage to the DNA sequence surrounding hole injection was seen also with capped anthraquinone moieties (*54*) and will be discussed in Chapter 4.

Assemblies containing a pendant ruthenium oxidant have also been used recently to examine competition between two distinct trapping sites in DNA (*55*). These assemblies contain both 5'-GMG-3' and 5'-GGG-3' triple guanine sites. Using transient absorption spectroscopy to monitor DNA radical intermediates on a short time scale and biochemical experiments to examine oxidative damage products which form on a longer

time scale, charge equilibration between the two distinct sites is observed. These experiments demonstrate that charge equilibrates over the entire duplex before being trapped at a particular site(s). This chemistry will be discussed further in Chapter 5.

1.9 Electrochemical Detection of Base Stacking Perturbations and Applications for DNA Sensing. A variety of experimental techniques have been shown to be useful in probing DNA mediated CT. Analysis of oxidative damage yields by biochemical means has provided invaluable insight into the effects of DNA sequence conformations and base stacking perturbations. Spectroscopy has allowed us to explore more vigorously rates of CT reactions and has revealed an exquisite sensitivity to dynamical base motions. Additionally, we have developed an electrochemical probe of DNA mediated CT, and this electrochemistry may lead to powerful diagnostic applications of DNA CT.

Exploiting molecular self-assembly of thiol-modified DNA duplexes on gold electrodes, we are able to monitor electrochemically the reduction of a redox active intercalator bound to the DNA at a site remote from the gold surface (Figure 1.8) (*56*). Reduction of the distantly bound intercalator is monitored by cyclic voltammetry or chronocoulometry and is a direct probe of the efficiency of CT through the intervening DNA bridge. It is notable that applying a negative potential to the DNA film and monitoring the reduction of a redox active intercalator exploits *electron* transport through the base stack; this is in contrast to biochemical and spectroscopic assays which rely on *electron hole* transport. Mechanistically, this process is not well understood, as the DNA bridge orbitals are thought to be significantly higher in energy than the applied potentials, although the energies may be altered in stacked DNA or the films described here. If not

perturbed significantly in energy, thermally induced hopping would be hard to reconcile. Nonetheless, these electrochemical experiments have served to support results of the biochemical and spectroscopic studies and confirm the superb sensitivity of CT reactions to base stacking.

In fully hybridized DNA duplexes containing a single base mismatch, the electrocatalytic signal of methylene blue, a redox active intercalator, coupled to $[Fe(CN_6)]^{3-}$ distinguished all single base mismatch-containing DNA from perfectly matched duplexes (*57*). Remarkably, even thermodynamically stable GT and GA mismatches, notoriously difficult to identify by means of differential hybridization, are detected and distinguished from well-matched sequences. Furthermore, physiologically relevant base lesions and 'hot spot' mutations can be readily discerned.

In studies analogous to biochemical assays utilizing M.*Hha*I, the effect on CT of DNA-binding proteins has also been explored electrochemically (*58*). In general, it is observed that CT yields correlate with protein-dependant alterations in DNA base stacking. Base-flipping enzymes such as uracil DNA glycosylase, TATA-binding protein which crystallography reveals kinks DNA 90° upon binding (*59*), and M.*Hha*I drastically diminish CT out to the distant redox probe. In agreement with biochemical assays (*28*), binding of a mutant M.*Hha*I, which inserts an aromatic, heterocyclic amino acid into the π-stack, does not disrupt CT out to the redox probe (*58*). Similarly, proteins that bind DNA without perturbing the base stack, such as restriction endonuclease R.*Pvu*II and the transcription factor Antennapedia homeodomain, do not significantly lessen the yield of CT. Hence, protein binding is able to modulate DNA CT both negatively and positively,

depending on the specific nature of the DNA-protein interactions and the extent of helix perturbation.

1.10 Biological Consequences. Our observations concerning the sensitivity of DNA CT to structure, mismatches, lesions, and binding by proteins, as well as the fact that DNA CT can proceed over long molecular distances all beg the question of whether DNA CT is physiologically relevant and indeed important. Might some DNA-binding proteins utilize DNA mediated CT for long-range signaling or activation? Perhaps DNA-binding proteins containing redox active cofactors or structural elements such as flavins or Fe-S clusters take advantage of DNA CT for communication *in vivo*. Additionally, CT chemistry provides an approach to sensing base stacking perturbations and lesions; might Nature take advantage of this chemistry?

Before considering these possibilities, it is first necessary to demonstrate that long-range oxidative damage can occur in DNA as packaged within the cell. *In vivo*, DNA is not floating free in solution, but rather packaged and protected in nucleosome core particles (NCP). In eukaryotes double helical DNA is wrapped around a core of positively charged histone proteins. A crystal structure of a NCP has been determined for a histone octamer and a 146 base pair palindromic DNA sequence (*60*). The DNA is highly bent as it wraps ~ 1.5 times around the outside of the histone octamer. Remarkably, using a rhodium intercalator tethered to the 5'-end of the DNA, guanine bases within the NCP were oxidized from a distance of over 80 Å (Figure 1.9) (*61*). Perhaps binding to the histone core stabilizes a base stacking conformation particularly suited to long-range oxidative damage. More importantly, these results concerning long-range damage have to be considered in the context of our thinking about DNA packaging

within chromatin. Our intuition suggests that packaging DNA in NCP protects it from damage; in fact DNA within chromatin is well protected from solution-borne oxidants. Despite this protection from solution-borne radicals, however, this packaged DNA is quite susceptible to oxidative damage through long-range CT mediated by the base stack.

Further evidence suggesting the possibility of CT damage *in vivo* comes from long-range oxidative damage demonstrated in whole nuclei (*62*). Treatment of *HeLa* nuclei with a rhodium intercalator, followed by photoactivation, results in oxidative DNA damage. This damage is revealed by treatment with base excision repair enzymes and amplification of the genomic DNA by ligation-mediated PCR. Oxidative damage has been probed in exon 5 of the p53 gene and in the transcriptionally active PGK1 promotor; damage at the 5'-G of guanine doublets and triplets was observed, the hallmark of DNA mediated CT. Moreover, in the PGK1 promotor, oxidative damage occurs at protein-bound sites that are inaccessible to rhodium. Protein footprinting analyses allowed us to conclude CT damage occurs over distances of at least 34 Å, and potentially further. Thus, on transcriptionally active DNA within the nucleus, long-range CT can result in oxidative base lesions.

The demonstration of long-range oxidative damage in NCP and nuclei extends DNA CT as a feasible mechanism for the generation of cellular base lesions. Perhaps organisms have evolved to protect the genetic code from CT damage. Certain regions of the genome may have evolved to be more or less susceptible to long-range oxidative DNA damage. After statistical analysis of the human genome, Heller has proposed a means of cathodic DNA protection, similar to the way in which Zn^{2+} protects steel (*63*). The number of 5'-GGG-3' triple guanine sites is elevated in the regions flanking protein-

coding exons and it is suggested that charges injected into DNA might be funneled to these sacrificial G-rich introns. Telomeric DNA, located at the ends of all linear chromosomes, is also G-rich and charges may be funneled to these non-coding regions. Damage is trapped preferentially in a guanine quadruplex rather than duplex DNA (*35*), and guanine quadruplexes have been proposed to form at telomeres. Understanding how damage may be funneled to certain sites and insulated at other sites could be an important element in biochemical mechanisms for DNA damage and its repair (*64*).

As described in this thesis, we have continued to explore both the fundamental mechanistic questions and possible biological consequences of DNA CT. As detailed in Chapter 2, we examined the importance of electronic communication with the π-stack as provided by intercalation. We have also begun to consider the possibility of electron versus electron hole transport through the double helix, as described in Chapter 3. We further probed the sequence dependence of DNA CT using a combination of spectroscopic and biochemical analyses, as shown in Chapter 4. Charge equilibration between two distinct sites in DNA is illustrated in Chapter 5. Finally, Chapter 6 describes experiments to further explore the biological possibilities of DNA CT; oxidative damage in guanine quadruplexes is probed.

1.11 RERFERENCES

(1) Györgi, A. S. (1960) *Proc. Natl. Acad. Sci. U. S. A. 46*, 1444. (b) Eley, D. D., and Spivey, D. I. (1962) *Trans. Faraday Soc*. *58*, 411.

(2) Miller, J. S., and Epstein, A. J. (1994) *Angew. Chem. Int. Ed*. *33*, 385. (b) Fox, M. A. (1992) *Acc. Chem. Res*. *25*, 569. (c) Marks, T. J. (1985) *Science 227*, 881.

(3) Núñez, M. E., and Barton, J. K. (2000) *Curr. Opin. Chem. Biol*. *4*, 199.

(4) Schuster, G. B. (2000) *Acc. Chem. Res. 33*, 253.

(5) Giese, B. (2002) *Ann. Rev. Biochem. 71*, 51.

(6) Lewis, F. D., Letsinger, R. L., and Wasielewski, M. R. (2001) *Acc. Chem. Res. 34*, 159.

(7) Murphy, C. J., Arkin, M. A., Jenkins, Y., Ghatlia, N. D., Bossmann, S. H., Turro, N. J., and Barton, J. K. (1993) *Science 262*, 1025.

(8) Hall, D. B., Holmlin, R. E., and Barton, J. K. (1996) *Nature 382*, 731.

(9) Steenken, S., and Jovanovic, S. V. (1997) *J. Am. Chem. Soc*. *119*, 617.

(10) Hudson, B. P., and Barton, J. K. (1998) *J. Am. Chem. Soc*. *120*, 6877.

(11) Kielkopf, C. L., Erkkila, K. E., Hudson, B. P., Barton, J. K., and Rees, D. C. (2000) *Nat. Struc. Biol*. *7*, 117.

(12) Sitlani, A., Long, E. C., Pyle, A. M., and Barton, J. K. (1992) *J. Am. Chem. Soc*. *114*, 2303.

(13) Burrows, C. J., and Muller, J. G. (1998) *Chem. Rev*. *98*, 1109.

(14) Prat, F., Houk, K. N., and Foote, C. S. (1998) *J. Am. Chem. Soc*. *120*, 845.

(15) Saito, I., Takayama, M., Sugiyama, H., Nakatani, K., Tsuchida, A., and Yamamoto, M. (1995) *J. Am. Chem. Soc*. *117*, 6406.

(16) Hall, D. B., Kelley, S. O., and Barton, J. K. (1998) *Biochemistry 37*, 15933.

(17) Gasper, S. M., and Schuster, G. B. (1997) *J. Am. Chem. Soc*. *119*, 12762.

(18) Nakatani, K., Dohno, C., and Saito, I. (1999) *J. Am. Chem. Soc*. *121*, 10854.

(19) Meggers, E., Kusch, D., Spichty, M., Wille, U., and Giese, B. (1998) *Angew. Chem. Int. Ed*. *37*, 460.

(20) Núñez, M. E., Hall, D. B., and Barton, J. K. (1999) *Chem. Biol*. *6*, 85.

(21) Ly, D., Sanii, L., and Schuster, G. B. (1999) *J. Am. Chem. Soc*. *121*, 9400.

(22) Fahlman, R. P., Sharma, R. D., and Sen, D. (2002) *J. Am. Chem. Soc*. *124*, 12477.

(23) Franklin, S. J., Treadway, C. R., and Barton, J. K. (1998) *Inorg. Chem. 37*, 5198.

(24) Williams, T. T., Dohno, C., Stemp, E. D. A., and Barton, J. K. (2004) Manuscript submitted.

(25) Delaney, S., Pascaly, M., Bhattacharya, P. K., Han, K., and Barton, J. K. (2002) *Inorg. Chem. 41*, 1966.

(26) Hall, D. B., and Barton, J. K. (1997) *J. Am. Chem. Soc. 119*, 5045.

(27) Bhattacharya, P. K., and Barton, J. K. (2001) *J. Am. Chem. Soc. 123*, 8649. (b) Bhattacharya, P. K., Cha, J., and Barton, J. K. (2002) *Nuc. Acids Res. 30*, 4740.

(28) Rajski, S. R., and Barton, J. K. (2001) *Biochemistry 40*, 5556. (b) Rajski, S. R., Kumar, S., Roberts, R. J., and Barton, J. K. (1999) *J. Am. Chem. Soc. 121*, 5615.

(29) Cheng, X. D., Kumar, S., Posfai, J., Pflugrath, J. W., and Roberts, R. J. (1993) *Cell 74*, 299.

(30) Kelley, S. O., Holmlin, R. E., Stemp, E. D. A., and Barton, J. K. (1997) *J. Am. Chem. Soc. 119*, 9861.

(31) Odom, D. T., and Barton, J. K. (2001) *Biochemistry 40*, 8727.

(32) Núñez, M. E., Noyes, K. T., Gianolio, D., McLaughlin, L. W., and Barton, J. K. (2000) *Biochemistry 39*, 6190.

(33) Odom, D. T., Dill, E. A., and Barton, J. K. (2000) *Chem. Biol. 7*, 475.

(34) Odom, D. T., Dill, E. A., and Barton, J. K. (2001) *Nuc. Acids Res. 29*, 2026.

(35) Delaney, S., and Barton, J. K. (2003) *Biochemistry 42*, 14159.

(36) Wan, C., Fiebig, T., Kelley, S. O., Treadway, C. R., Barton, J. K., and Zewail, A. H.(1999) *Proc. Nat. Acad. Sci. U. S. A. 96*, 6014.

(37) Marcus, R. A., and Sutin, N. (1985) *Biochim. Biophys. Acta*. *811*, 265.

(38) Bixon, M., and Jortner, J. (2002) *Chem. Phys*. *281*, 393. (b) Jortner, J., Bixon, M., Voityuk, A. A., and Rösch, N. (2002) *J. Phys. Chem*. *A 106*, 7599.

(39) Bixon, M., Giese, B., Wessely, S., Langenbacher, T., Michel-Beyerle, M. E., and Jortner, J. (1999) *Proc. Nat. Acad. Sci. U. S. A. 96*, 11713. (b) Giese, B., Wessely, S., Spormann, M., Lindemann, U., Meggers, E., and Michel-Beyerle, M. E. (1999) *Angew. Chem. Int. Ed*. *38*, 996.

(40) Williams, T. T., Odom, D. T., and Barton, J. K. (2000) *J. Am. Chem. Soc*. *122*, 9048.

(41) O'Neill, M. A., Becker, H.-C., Wan, C., Barton, J. K., and Zewail, A. H. (2003) *Angew. Chem. Int. Ed*. *42*, 5896.

(42) O'Neill, M. A., and Barton, J. K. (2004) Manuscript submitted.

(43) Henderson, P. T., Jones, D., Hampikian, G., Kan, Y., and Schuster, G. B. (1999) *Proc. Nat. Acad. Sci. U. S. A. 96*, 8353.

(44) Barnett, R. N., Cleveland, C. L., Joy, A., Landman, U., and Schuster, G.B. (2001) *Science 294*, 567.

(45) Williams, T. T., and Barton, J. K. (2001) *J. Am. Chem. Soc*. *124*, 1840.

(46) Hartwich, G., Caruana, D. J., de Lumley-Woodyear, T., Wu, Y. B., Campbell, C. N., and Heller, A. (1999) *J. Am. Chem. Soc*. *121*, 10803.

(47) Friedman, A. E., Chambron, J.-C., Sauvage, J.-P., Turro, N. J., and Barton, J. K. (1990) *J. Am. Chem. Soc*. *112*, 4960. (b) Jenkins, Y., Friedman, A. E., Turro, N. J., and Barton, J. K. (1992) *Biochemistry 31*, 10809. (c) Olson, E. J. C., Hu, D., Hormann, A., Jonkman, A. M., Arkin, M. R., Stemp, E. D. A., Barton, J. K., Barbara, P. F. (1997) *J. Am. Chem. Soc*. *119*, 11458.

(48) Stemp, E. D. A., Arkin, M. R., and Barton, J. K. (1997) *J. Am. Chem. Soc*. *119*, 2921.

(49) Wagenknecht, H. A., Stemp, E. D. A., and Barton, J. K. (2000) *Biochemistry 39*, 5483.

(50) Wagenknecht, H. A., Rajski, S. R., Pascaly, M., Stemp, E. D. A., and Barton, J. K. (2001) *J. Am. Chem. Soc*. *123*, 4400.

(51) Chang, I.-J., Gray, H. B., and Winkler, J. R. (1991) *J. Am. Chem. Soc*. *113*, 7056.

(52) Pascaly, M., Yoo, J., and Barton, J. K. (2002) *J. Am. Chem. Soc*. *124*, 9083.

(53) Yoo, J., Delaney, S., Stemp, E. D. A., and Barton, J. K. (2003) *J. Am. Chem. Soc*. *125*, 6640.

(54) Sanii, L., and Schuster, G. B. (2000) *J. Am. Chem. Soc*. *122*, 11545.

(55) Delaney, S., Yoo, J., Stemp, E. D. A., and Barton, J. K. (2004) Submitted.

(56) Kelley, S. O., Jackson, N. M., Hill, M. G., and Barton, J. K. (1999) *Angew. Chem. Int. Ed*. *38*, 941.

(57) Boon, E. M., Ceres, D. M., Drummond, T. G., Hill, M.G., and Barton, J. K. (2000) *Nat. Biotech. 18*, 1096. (b) Kelley, S. O., Boon, E. M., Barton, J. K., Jackson, N. M., and Hill, M. G. (1999) *Nuc. Acids Res. 27*, 4830.

(58) Boon, E. M., Salas, J. E., and Barton, J. K. (2002) *Nat. Biotech*. *20*, 282.

(59) Kim, Y. C., Geiger, J. H., Hahn, S., and Sigler, P. B. (1993) *Nature 365*, 512. (b) Kim, J. L., Nikolov, D. B., and Burley, S. K. (1993) *Nature 365*, 520.

(60) Luger, K., Mäder, A., Richmond, R., Sargent, D., and Richmond, T. J. (1997) *Nature 389*, 251.

(61) Núñez, M. E., Noyes, K. T., and Barton, J. K. (2002) *Chem. Biol*. *9*, 403.

(62) Núñez, M. E, Holmquist, G. P., and Barton, J. K. (2001) *Biochemistry 40*, 12465.

(63) Friedman, K. A., and Heller, A. (2001) *J. Phys. Chem. B 105*, 11859.

(64) Rajski, S. R., Jackson, B. A., and Barton, J. K. (2000) *Mut. Res*. *447*, 49.

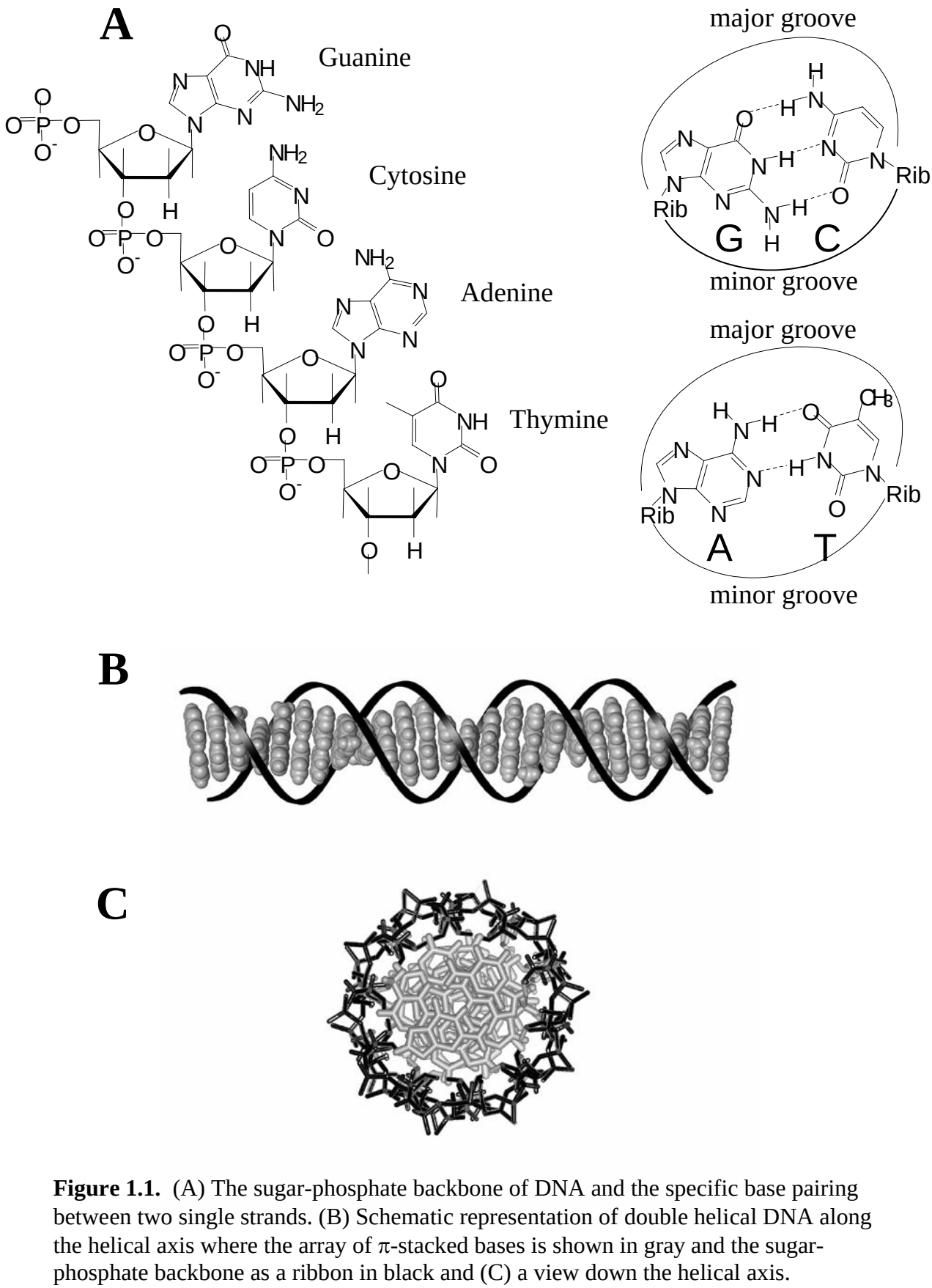

Figure 1.1. (A) The sugar-phosphate backbone of DNA and the specific base pairing between two single strands. (B) Schematic representation of double helical DNA along the helical axis where the array of π-stacked bases is shown in gray and the sugar-phosphate backbone as a ribbon in black and (C) a view down the helical axis.

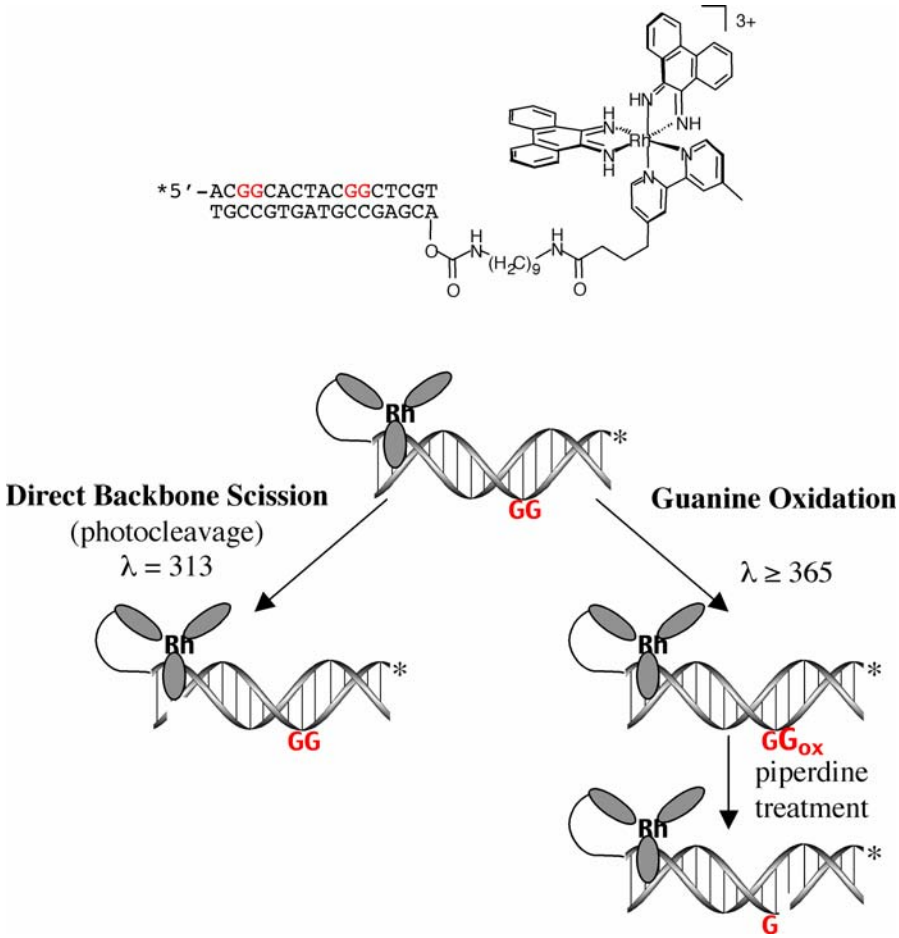

Figure 1.2. Shown above is the first DNA assembly in which long-range oxidative damage to guanine bases was observed using a tethered photooxidant. Damage to DNA by the photooxidant $[Rh(phi)_2(bpy')]^{3+}$ can occur by two distinct paths. After irradiation at high energy, a short range reaction, which identifies the site of intercalation occurs (left side). Long-range CT, which promotes oxidative damage (G_{ox}) at a distance occurs after low energy excitation (right side). These two mechanisms allow for clear delineation of site of radical generation and site of CT damage enabling long-range chemistry to be identified.

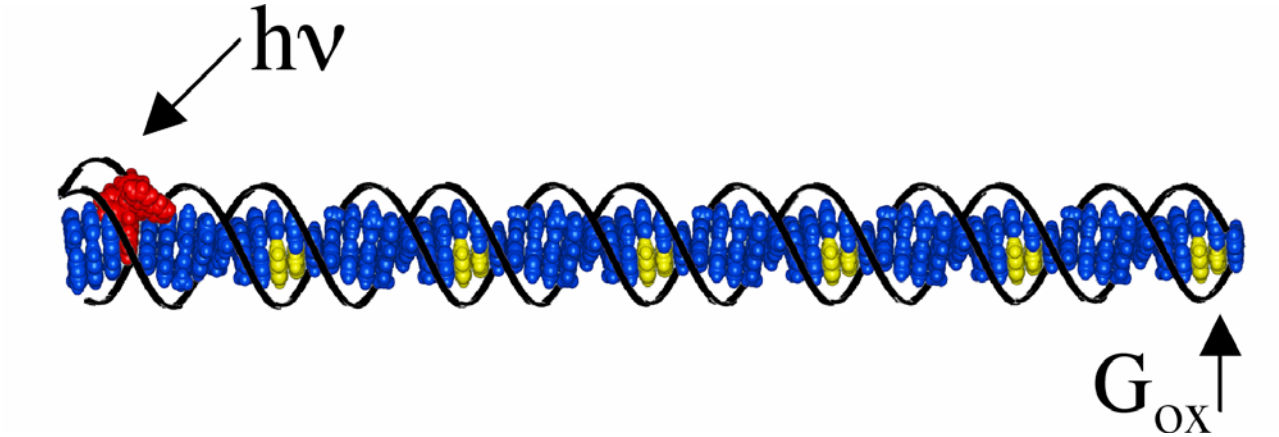

Figure 1.3. Schematic representation of a DNA duplex with a tethered rhodium photooxidant containing six 5'-GG-3' guanine doublets up to 200 Å from the metallointercalator binding site. Oxidative damage at each of the guanine doublet sites, as a result of photoexcitation of the rhodium intercalator, has been demonstrated.

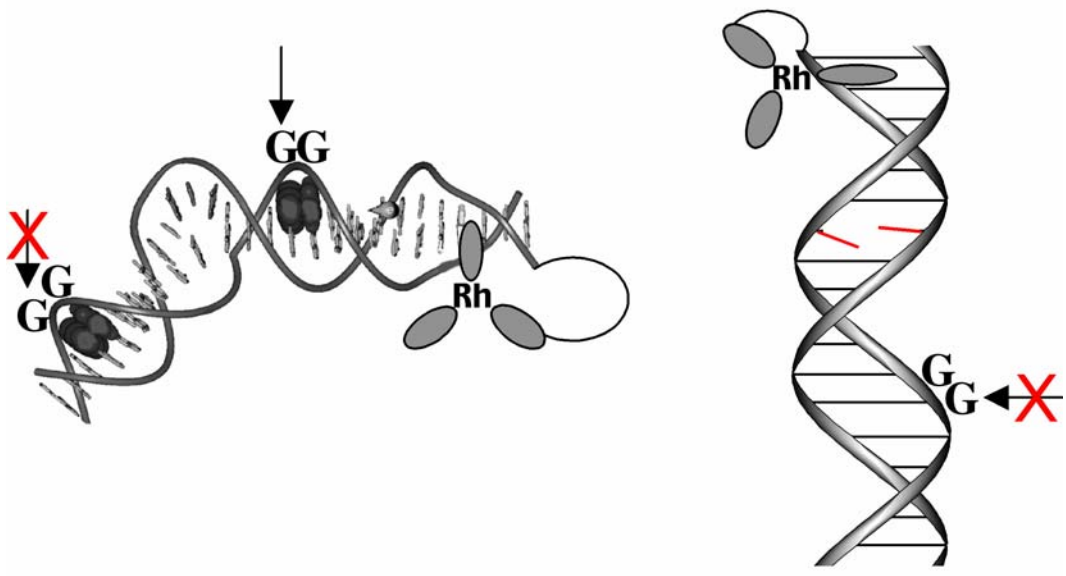

Figure 1.4. Schematic representations of some of the base stacking perturbations that have been examined using guanine oxidation ratios. A duplex with a 5'-ATA-3' base bulge (left) and a mismatch containing DNA duplex (right). Both mismatches and base bulges attenuate the amount of CT through the duplex by disrupting the π-stacking array. After photo-excitation of the oxidant no long-range guanine oxidation is observed in assemblies containing a perturbation in the π-stack.

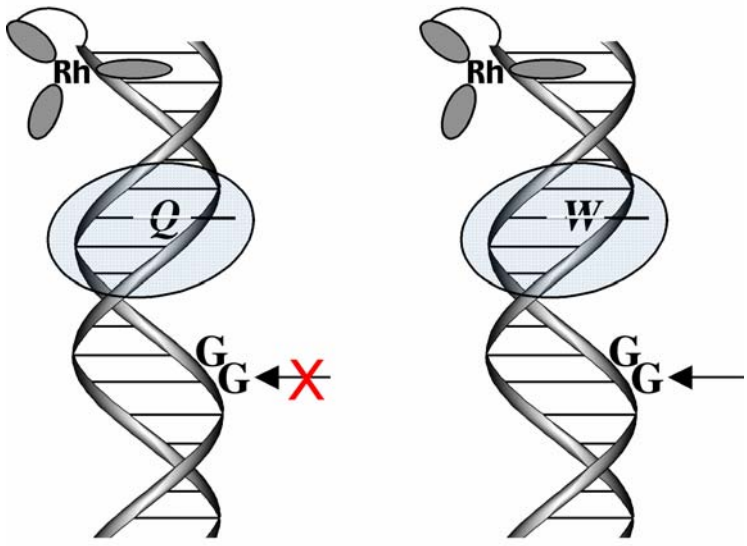

Figure 1.5. Schematic illustrations of a DNA-binding protein modulating CT, both positively and negatively. M.*Hha*I binds to DNA and inserts a hydrophobic glutamine residue into the base stack (left) which does not allow for efficient CT. The amino acid side chain acts as a hydrophobic 'plug' in the aromatic base-stacking array which disrupts CT. On the other hand, a mutant M.*Hha*I which inserts instead an aromatic tryptophan residue (right) does not disrupt the π-array and allows for CT. Depending on the nature of the DNA/protein interaction, DNA-binding proteins can regulate CT both positively and negatively.

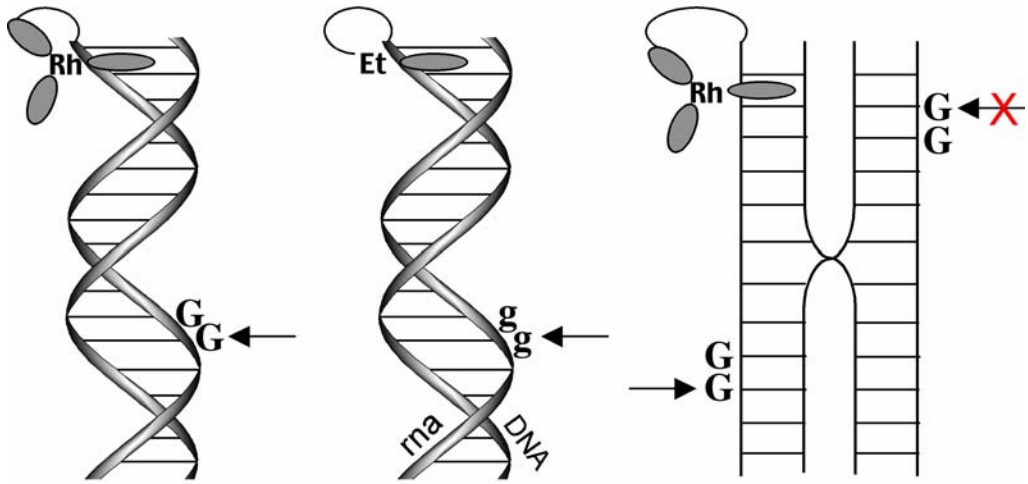

Figure 1.6. Schematic illustrations of some of the DNA structures studied for their ability to mediate CT. A DNA duplex (left), a DNA/RNA hybrid containing a tethered ethidium photooxidant (center), and a DNA four-way junction (right). All three DNA structures provide an intact base-stacking array, as is requisite for CT chemistry. Following excitation of the photooxidant, these DNA structures all efficiently mediate long-range oxidative damage.

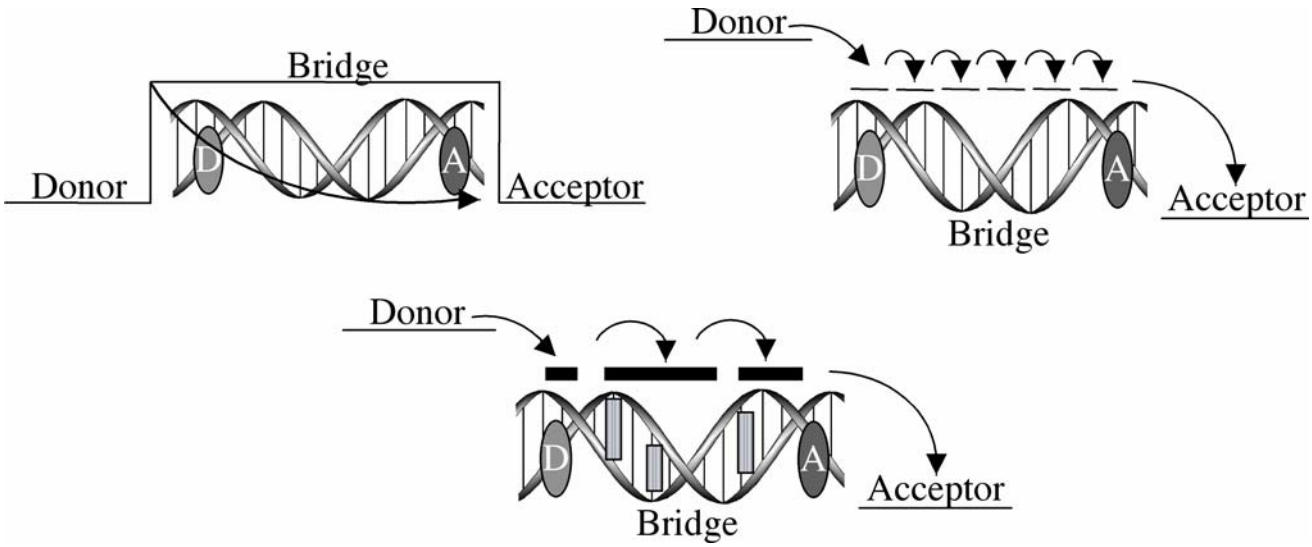

Figure 1.7. Schematic representations of three possible mechanisms for DNA CT. In superexchange (top left), the charge tunnels from the donor (D) to the acceptor (A) through the bridge. An exponential decrease in the rate of CT with increasing bridge length is expected. In a hopping mechanism (top right), charge occupies the bridge hopping between discrete molecular orbitals. If hopping is faster than radical trapping, the charge should be able to migrate over long molecular distances. In a domain hopping mechanism (bottom), charge occupies the bridge by delocalizing over several bases. This domain hops along the bridge to travel from donor to acceptor. As in a pure hopping mechanism, the charge should be able to travel long distances.

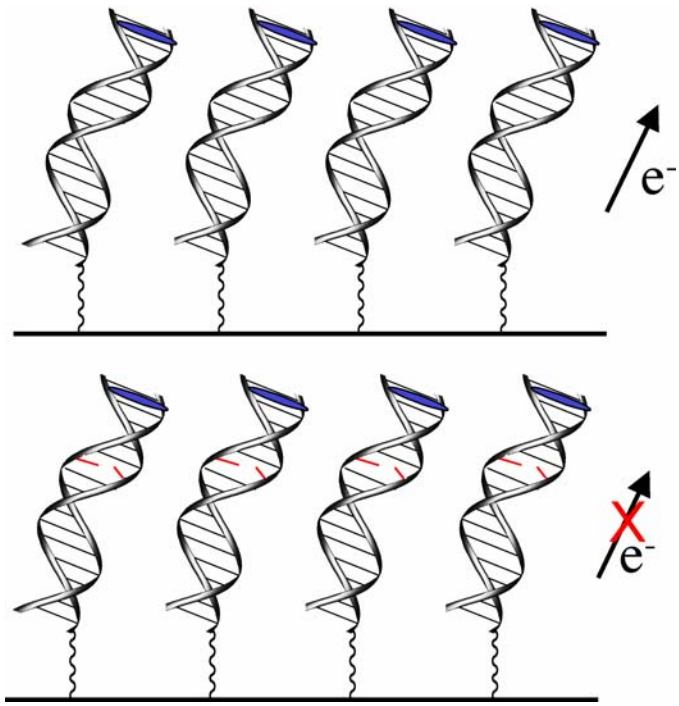

Figure 1.8. Schematic illustrations of electrochemistry experiments utilizing DNA films self-assembled on a gold surface. The reduction of a redox active intercalator is monitored after electron transport through the DNA (top). The efficiency of reduction of the intercalator is a measure of the ability of the intervening π-stack to support CT and can be used to monitor for stacking perturbations. In the presence of a mismatch (bottom) the base stack is perturbed and electron transport to the redox probe is diminished.

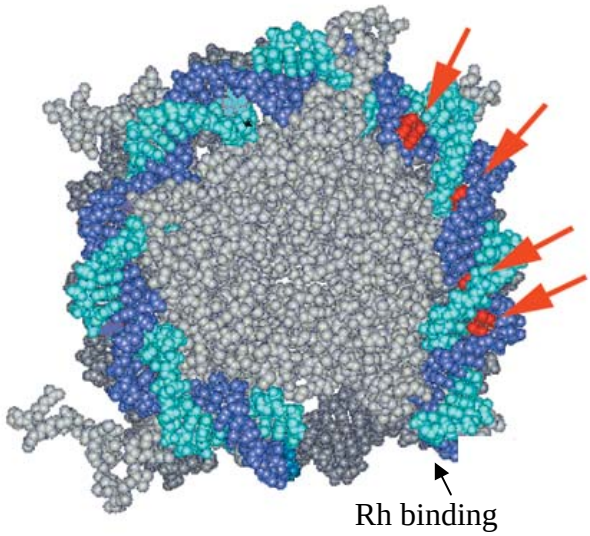

Figure 1.9. In a nucleosome core particle the DNA is wrapped ~ 1.5 times around an octamer of histone proteins. The site of rhodium attachment and binding is indicated. Oxidative damage is observed at guanine doublets (arrows) located over 80 Å from the site of rhodium intercalation after photoactivation. (The picture was adapted from PDB coordinates 1aoi, reference 60).

CHAPTER 2

Oxidative DNA Damage by Ruthenium Complexes Containing the Dipyridophenazine Ligand or Its Derivatives: A Focus on Intercalation

Adapted from: Delaney, S., Pascaly, M., Bhattacharya, P., Han, K., and Barton, J. K. (2002) *Inorg. Chem. 41*, 1966.

** Experiments comparing DNA charge transport using noncovalently bound and covalently tethered ruthenium complexes were performed by Dr. Pratip Bhattacharya.

2.1 INTRODUCTION

Charge transport (CT) through DNA has been shown to require proper stacking of the π-orbitals of the heterocyclic nucleobases (*1*). When base bulges (*2*), mismatches (*3, 4*) or non-aromatic residues (*5, 6*) are inserted into the π-stack, charge transport is efficiently shut off. When properly stacked, the DNA π-array has been shown to mediate guanine oxidation at sites 200 Å from a remotely bound oxidant (*7, 8*). Oxidative damage to DNA from a distance is therefore necessarily sensitive to the intervening DNA sequence and structure (*9-12*).

Besides proper π-stacking, energetic driving force is a requirement for charge transfer reactions. Guanine is the easiest nucleobase to oxidize with a potential of 1.29 V vs. NHE (*13*). *Ab initio* molecular orbital calculations predict that in a 5'-GG-3' guanine doublet, the bulk of the HOMO lies on the 5'-G, which has a lower oxidation potential than a single guanine (*14, 15*).

The work presented here was designed to address a third aspect considered to affect the oxidation of guanine sites in DNA: the ability of the oxidant to intercalate into the π-stack. This intercalation is proposed to result in more effective coupling to the DNA π-array and more efficient hole injection, facilitating long-range charge migration through the π-stack. To explore this hypothesis, octahedral ruthenium(II) complexes (Figure 2.1) bearing the intercalating dppz ligand or derivatives thereof, $[Ru(bpy)_2(dppz)]^{2+}$ (dppz = dipyridophenazine), $[Ru(bpy)_2(dppx)]^{2+}$ (dppx = 7,8-dimethyldipyridophenazine), $[Ru(bpy)_2(dpq)]^{2+}$ (dpq = dipyridoquinoxaline) and $[Ru(bpy)_2(dpqC)]^{2+}$ (dpqC = dipyrido-6,7,8,9-tetrahydrophenazine), have been prepared, and both their binding interactions and oxidative reactions with DNA have been

characterized. Dppz complexes of ruthenium have been extensively studied owing to their unique luminescence properties when bound to DNA (*16, 17*). The binding of dpq and dpqC complexes of ruthenium to DNA has been explored structurally using NMR methods (*18, 19*). These complexes vary both in their ability to stack intercalatively within the DNA helix and in their efficiency in promoting oxidative DNA damage.

Oxidative damage to DNA is generated with these ruthenium complexes through a flash/quench experiment (*20*). The flash/quench methodology, originally developed to explore charge transport reactions in proteins (*21*), has been effectively applied in characterizing transient radical intermediates in the DNA CT process (*6*) and in generating protein/DNA crosslinks (*22, 23*). Scheme 2.1 illustrates the series of reactions associated with the flash/quench experiment. The cycle is initiated by visible light, which excites the intercalated ruthenium(II) complex. The excited ruthenium(II) complex, *Ru(II), is then quenched by a nonintercalating electron acceptor, Q, such as $[Ru(NH_3)_6]^{3+}$, methyl viologen (MV^{2+}) or $[Co(NH_3)_5Cl]^{2+}$, so as to form Ru(III) *in situ*. This species can be reduced back to Ru(II) either through recombination with reduced quencher (Q^-) or by CT with guanine (G). The oxidized guanine radical can then return to its resting state by reaction with reduced quencher or undergo further reaction to form a family of oxidative products, G_{ox} (*24*).

In addition to Ru(II) complexes that contain derivatives of the dppz ligand, $[Ru(phen)_3]^{2+}$ and $[Ru(bpy)_3]^{2+}$, which possess the necessary driving force to oxidize DNA but do not intercalate as well as complexes containing the dppz ligand, have been examined. The importance of intercalation into the π-stack is also explored by

comparing oxidative DNA damage resulting from covalently bound derivatives of ruthenium complexes containing bpy versus dppz ligands.

2.2 METHODS

2.2.1 Materials. $[Ru(bpy)_3]Cl_2$ and $[Ru(phen)_3]Cl_2$ were purchased from Aldrich and recrystallized from water prior to use. $[Ru(NH_3)_6]Cl_3$ was purchased from Aldrich and was used as received. Calf thymus DNA (ct-DNA) was purchased from Amersham and was dialysed against a buffer of 10 mM NaCl, 20 mM sodium phosphate, pH 7.85 prior to use. Phosphoramidites were from Glen Research and were used as received.

2.2.2 Metal Complex Synthesis. The ligands dipyrido[3,2-a:2',3'-c]phenazine (dppz), 7,8-dimethyldipyrido[3,2-a:2',3'-c]phenazine (dppx), dipyrido[3,2-*d*:2',3'-*f*]quinoxaline (dpq) and dipyrido[3,2-*a*:2',3'-*c*]-(6,7,8,9-tetrahydro)phenazine (dpqC) were prepared according to literature protocols (*18, 19*) as was $Ru(bpy)_2Cl_2{\cdot}2H_2O$ (*25*). The bis(bpy) ruthenium complexes containing the third ligand L = dppz, dppx, dpq, or dpqC, $[Ru(bpy)_2(L)]Cl_2$, were synthesized by heating 1.2 equiv. L with $Ru(bpy)_2Cl_2{\cdot}2H_2O$ at 150 ºC in ethylene glycol for 1 hour. Solid NH_4PF_6 was used to precipitate the orange-red solid which was then washed with H_2O and diethyl ether. Complexes were purified on alumina columns equilibrated with dichloromethane and eluted with acetonitrile. Water soluble chloride salts were then obtained using a Sephadex QAE-25 ion-exchange resin equilibrated with 0.2 M KCl and eluted with acetonitrile. The three-ligand complex $[Ru(bpy')(dppz)(phen)]Cl_2$ (bpy' = 4-butyric acid-4'-methyl-2,2'-bipyridine) was prepared according to literature procedures (*25, 26*), and

$[Ru(bpy)_2(bpy')]Cl_2$ was prepared from $Ru(bpy)_2Cl_2 \cdot 2H_2O$ (*25*). For all complexes prepared, ^{1}H-NMR and FAB-MS analyses agreed with values expected.

Extinction coefficients for complexes were obtained as follows: accurate measurements of ruthenium concentrations were made using a Perkin-Elmer/Sciex Elan 5000A ICP-MS and $[Ru(bpy)_3]Cl_2$ as calibrant, and absorbance measurements were collected using a Varian 300 Bio Spectrophotometer. Ten replicates of concentration and absorbance for each sample were used to calculate extinction coefficients at 450 nm as follows: $[Ru(bpy)_2(dppx)]^{2+}$, $\varepsilon = 21{,}000 \pm 600\ M^{-1}$; $[Ru(bpy)_2(dpq)]^{2+}$, $\varepsilon = 14{,}200 \pm 400\ M^{-1}$; $[Ru(bpy)_2(dpqC)]^{2+}$, $\varepsilon = 14{,}300 \pm 500\ M^{-1}$; $[Ru(bpy)_2(dppz)]^{2+}$, $\varepsilon = 21{,}400 \pm 600\ M^{-1}$.

2.2.3 Electrochemistry. Ground state oxidation and reduction potentials for the ruthenium complexes were obtained on a Bioanalytical Systems (BAS) Model CV-50W electrochemical analyzer. A glassy carbon working electrode, Ag/AgCl reference electrode and Pt auxillary electrode were used in a single cell sample apparatus. Solutions of racemic metal complex (1mM) in dry acetonitrile (Fluka; stored over molecular sieves) containing 100 mM tetrabutylammonium hexaflourophosphate were degassed with argon prior to use and voltammagrams were collected using a 100 mV/s scan rate. $E_{1/2}$ values were taken as the average of the voltage of maximum current for the forward and reverse electrochemical processes. Potentials are reported in volts versus NHE.

2.2.4 Luminescence. Emission and excitation spectra were obtained on an ISS-K2 spectroflourometer. Emission intensities were determined by integration of the luminescence spectrum and standardized against $[Ru(bpy)_3]^{2+}$ as a calibration for the

instrument. Solutions containing 10 μM racemic metal complex and 1 mM nucleotides ct-DNA in 10 mM NaCl, 20 mM sodium phosphate, pH 7.85 were excited at 450 nm and emission was monitored from 500-800 nm. Excitation spectra were obtained by monitoring at the emission maximum while varying excitation wavelength from 250-600 nm. Luminescence polarization data were obtained using an ISS-K2 spectrofluorometer in an L-configuration. Samples consisted of 10 μM racemic metal complex in 10 mM NaCl, 20 mM sodium phosphate, pH 7.85. When present, ct-DNA concentration was 1 mM nucleotides and glycerol samples contained 60% glycerol by volume. Samples were irradiated at 450 nm and emission was monitored at 610 nm using a 495 nm cut-off filter.

To determine excited state lifetimes, time-resolved emission measurements were conducted using a pulsed YAG-OPO laser (λ_{ex} = 470 nm). Laser powers ranged from 3-4 mJ/pulse. To obtain luminescence lifetimes, τ, time-resolved emission data were fit to $y(t) = 100[C_1\exp(-t/\tau_1) + (1-C_1)\exp(-t/\tau_2)]$ by a nonlinear least-squares method with convolution of the instrument response function using in-house software as described previously (*27*). Errors in lifetimes and percent contributions are estimated to be ± 10%. All complexes were purified by HPLC prior to luminescence measurement using a Dynamax 300 Å C18 reverse-phase column (Rainin) on a Hewlett-Packard 1100 HPLC (95% 30 mM NH_4OAc/5% acetonitrile to 100% acetonitrile over 60 min). Samples consisted of 10 μM racemic metal complex, 10 mM NaCl, 20 mM sodium phosphate, pH 7.85. For determining excited state lifetimes of metal complexes bound to DNA, 1 mM nucleotides ct-DNA was present. In luminescence quenching studies, samples contained, in addition, 80 μM $[Ru(NH_3)_6]^{3+}$ or 100 μM $[Rh(phi)_2(dmb)]^{3+}$ (phi = 9,10-

phenanthrenequinone diimine; dmb = 4,4'-dimethyl-2,2'-bipyridine). The luminescence traces of the complexes in water were fit to a monoexponential function ($C_1 = 1$).

2.2.5 Determination of Binding Constants to DNA. Luminescence titrations on an ISS-K2 fluorometer were performed to determine affinity constants for the ruthenium complexes with ct-DNA. Ct-DNA, ranging from 10^{-7} M to 10^{-3} M, was titrated into solutions containing racemic metal complex, 10 mM NaCl, 20 mM sodium phosphate, pH 7.85. For each metal complex, multiple experiments were conducted at a constant metal concentration ranging from 0.25-10 μM. An excitation wavelength of 450 nm was used and total luminescence intensity was recorded from 500-800 nm and corrected for dilution. The fraction of complex bound to ct-DNA was calculated from the equation $C_B = C_T[(F-F_F)/(F_B - F_F)]$, where C_T is the total concentration of metal complex, F the observed luminescence intensity, at a given ct-DNA concentration, F_F the intensity of unbound complex and F_B the intensity of fully bound complex. Binding data was analyzed in the form of Scatchard plots (*28*).

2.2.6 Determination of Enantioselectivity. A double stranded DNA cellulose (Sigma) column was rinsed with 10 mM NaCl, 20 mM sodium phosphate, pH 7.85 buffer to remove unbound DNA. Then 100 μL of 100 μM *rac*-$[Ru(bpy)_2(dpq)]^{2+}$ or *rac*-$[Ru(bpy)_2(dpqC)]^{2+}$ was loaded onto the column and eluted with 1 mL of buffer. Following this elution, 1 mL 5 M NaCl was loaded onto the column and the eluant collected. Circular dichroism measurements were performed on both fractions using a AVIV Circular Dichroism Spectrometer 62A DS.

2.2.7 Oligonucleotide Synthesis. Oligonucleotides were synthesized on an ABI 392 DNA/RNA synthesizer, using standard phosphoramidite chemistry (*29*). DNA was

synthesized with a 5'-dimethoxy trityl (DMT) protecting group and was purified by HPLC using a Dynamax 300 Å C18 reverse-phase column (Rainin) on a Hewlett-Packard 1100 HPLC (95% 30 mM NH_4OAc/5% acetonitrile to 84% 30 mM NH_4OAc/16% acetonitrile over 25 min). The DMT group was removed by incubation with 80% glacial acetic acid for 12 min at ambient temperature, and then re-purified by HPLC (100% 30 mM NH_4OAc to 75% 30 mM NH_4OAc/25% acetonitrile over 40 min). Quantification was done on a Beckman DU 7400 Spectrophotometer using the ε_{260} values estimated for single stranded DNA (*30*).

Ruthenium-tethered 17-mer oligonucleotides were prepared as described previously (*31*) and were purified on a Dynamax 300 Å C18 reverse-phase column (Rainin) on a Hewlett-Packard 1050 HPLC (85% 30 mM NH_4OAc/15% acetonitrile to 75% 30 mM NH_4OAc/25% acetonitrile over 40 min.). The ruthenium-conjugated oligonucleotides were characterized by mass spectrometry and quantitated using the following extinction coefficients: $[Ru(bpy')(dppz)(phen)]^{2+}$ modified oligonucleotides ε_{432} = 19,000 $M^{-1}cm^{-1}$; $[Ru(bpy)_2(bpy')]^{2+}$ modified oligonucleotides ε_{453} = 21,000 $M^{-1}cm^{-1}$.

2.2.8 Assay of Oxidative DNA Damage. For experiments conducted using noncovalently bound ruthenium, single strands containing the guanine doublet site were 5'-^{32}P end-labeled using standard protocols (*32*) and annealed to the complementary strand in an aerated buffer of 10 mM NaCl, 20 mM sodium phosphate, pH 7.85. Oligonucleotide duplexes (8 μM) containing 16 μM racemic metal complex and 160 μM $[Ru(NH_3)_6]^{3+}$ as an electron accepting quencher were irradiated at 450 nm with a 1000 W Hg/Xe lamp equipped with a monochromator. Irradiation times varied from 0-30 min.

After irradiation, samples were treated with 10% piperidine at 90 °C for 30 min., dried, and electrophoresed through a 20% denaturing polyacrylamide gel. The extent of damage was quantitated by phosphorimagery (ImageQuant).

For experiments conducted using ruthenium-tethered oligonucleotides, single strand complements to the ruthenium-modified oligonucleotides were 5'-^{32}P end-labeled as described (*32*) and annealed in an aerated buffer of 5 mM NaCl, 35 mM Tris-HCl, pH 8.0. Oligonucleotide duplexes (2.5 μM) with 25 μM $[MV]^{2+}$ as an electron accepting quencher were irradiated for 5 min. at 432 nm using a 1000 W Hg/Xe lamp equipped with a monochromator. After irradiation, samples were treated with 10% piperidine at 90 °C for 30 min, dried, and electrophoresed through a 20% denaturing polyacrylamide gel. The extent of damage was quantitated by phosphorimagery (ImageQuant).

2.3 RESULTS

2.3.1 Redox Characteristics of Metal Complexes. The reversible oxidation waves corresponding to the Ru(III)/Ru(II) couples are observed between 1.45 and 1.57 V (Table 2.1). According to these values, all of the Ru(III) complexes, once generated *in situ* by flash/quench are capable of oxidizing guanines in the DNA duplex. The electrochemical reduction of these complexes is ligand-based, where the first reduction is centered on the dppz (or dppz derivative) and the subsequent reductions involve the ancillary ligands (*35*). As can be seen in Table 2.1, the first reduction wave can be tuned by derivatizing the dppz ligand, which is inherently easy to reduce due to its aromatic size, providing a large area for charge delocalization. Adding methyl groups at the 7 and 8 positions of dppz, yielding dppx, donates electron density toward the ring system,

resulting in a ligand that is ~ 80 mV harder to reduce. Removing the terminal ring of dppz, yielding dpq, produces a ligand which is less aromatic and ~ 310 mV more difficult to reduce. Along a similar line, removing the aromaticity of the terminal ring from dppz, yielding dpqC, again results in loss of aromaticity and a ligand which is ~ 340 mV harder to reduce.

Values for $E_{0/0}$ are also presented in Table 2.1. The values presented allow the calculation of excited state reduction potentials of the complexes (*2+/+), which is a critical parameter when considering guanine oxidation directly from the excited state. Based upon the excited state redox potentials of these complexes, the ruthenium complexes with dppz and dppx ligands possess excited state potentials that should be capable of guanine oxidation.

2.3.2 Luminescence Characteristics in the Absence and Presence of DNA. Table 2.2 shows the excited state lifetimes along with their emission maxima obtained in water, ct-DNA and in the presence of oxidative quenchers. As described earlier, $[Ru(bpy)_2(dppz)]^{2+}$ and $[Ru(bpy)_2(dppx)]^{2+}$ behave as luminescent 'light switches'; no detectable luminescence is apparent in aqueous solution, but upon intercalation, the phenazine nitrogens are protected from aqueous quenching and the complexes emit (*37*). Luminescence decay traces for the dppz and dppx complexes bound to DNA show biexponential decays in emission, which we have assigned to two general orientations (side-on and head-on) for intercalation of the complexes into the duplex (*38*); these orientations are supported also by NMR results (*39*).

In contrast to $[Ru(bpy)_2(dppz)]^{2+}$ and $[Ru(bpy)_2(dppx)]^{2+}$, the complexes $[Ru(bpy)_2(dpq)]^{2+}$ and $[Ru(bpy)_2(dpqC)]^{2+}$ do not show 'light switch' behavior. Altering

the electronic structure of the dppz ligand to yield dpq and dpqC results in complexes that emit in aqueous solvents in the absence of DNA. However, both $[Ru(bpy)_2(dpq)]^{2+}$ and $[Ru(bpy)_2(dpqC)]^{2+}$ display 2-5 fold luminescence enhancements upon the addition of DNA. These complexes also display biexponential decays in emission when bound to DNA. These luminescence characteristics in the presence of DNA are reminiscent of those seen earlier with $[Ru(phen)_3]^{2+}$ and derivatives (*40, 41*).

In the presence of the oxidative quencher $[Ru(NH_3)_6]^{3+}$, all the DNA-bound ruthenium complexes examined display shorter excited state lifetimes indicative of dynamic quenching by the groove-bound ruthenium hexammine. The longer lived component is assigned as the DNA-bound species; in the presence of quencher, this excited state lifetime is shortened, resulting in two shorter lived components. $[Rh(phi)_2(dmb)]^{3+}$ has been shown to intercalate into DNA via the phi ligand and quench the emission of intercalating ruthenium complexes effectively via DNA mediated CT (*36*). Quenching by $[Rh(phi)_2(dmb)]^{3+}$ was observed with all the ruthenium complexes examined, suggesting the intimate association of all of the ruthenium complexes with DNA.

2.3.3 Binding Affinities Determined through Luminescence Titration and Support for an Intercalative Binding Mode. Spectroscopic titrations of the ruthenium complexes with ct-DNA were carried out over a range of metal concentrations. Table 2.3 shows the results obtained through Scatchard analyses of the data. As expected, the dppz and dppx complexes possess intercalative binding affinities for DNA that are significantly higher than for the dpq and dpqC complexes.

Because of the low binding affinities found for the dpq and dpqC complexes, additional experiments were carried out to probe whether binding to DNA by these complexes was primarily through an intercalative binding mode. Earlier studies with $[Ru(phen)_3]^{2+}$ indicated a mixture of binding modes (*40, 42, 43*). Values for luminescence polarization are shown in Table 2.4. In buffer and 60% glycerol there is no significant polarization observed for the complexes. In the presence of ct-DNA, there is an increase in polarization observed for all of the complexes, while the highest values of polarization are obtained in the presence of both ct-DNA and 60% glycerol. For these samples containing both ct-DNA and glycerol, the luminescence polarization values for $[Ru(bpy)_3]^{2+}$ and $[Ru(phen)_3]^{2+}$ are smallest, while $[Ru(bpy)_2(dppz)]^{2+}$ and $[Ru(bpy)_2(dppx)]^{2+}$ display the largest degree of luminescence polarization. Certainly the values for the luminescence polarization depend in part on the luminescent lifetimes of the complexes; hence all values are expected to be significantly lower than for fluorescent intercalators such as ethidium (20 ns excited state lifetime) (*44*). Given that the bound excited state lifetimes for the dpq and dpqC complexes are in the microsecond range, the values obtained indicate that, despite the low polarization values, these complexes are held in a relatively rigid environment bound to DNA. The values obtained therefore are consistent with intercalative binding.

The intercalative binding mode was also probed through measurements of enantioselectivity associated with binding to DNA. Right-handed metal complexes bound through intercalation are favored in binding to the right-handed helix whereas the left handed isomer is generally favored for a groove-bound mode with B-form DNA (*45*). Enantioselectivity in DNA binding was probed by examining fractions eluted from a

DNA cellulose column (*46*). The circular dichroism spectra obtained for the fractions collected from the DNA cellulose column for $[Ru(bpy)_2(dpq)]^{2+}$ are shown in Figure 2.2. Spectra for $[Ru(bpy)_2(dpqC)]^{2+}$ showed identical patterns. Comparison with literature spectra (*39*) indicates that the less favored isomer, eluting with lower salt concentrations, corresponds to the Λ-enantiomer while the Δ-enantiomer, eluting with 5 M NaCl, binds preferentially to DNA. These data are therefore also consistent with intercalative binding.

2.3.4 Oxidative Damage by Noncovalently Bound Ruthenium Complexes. Ruthenium(III) complexes, generated *in situ* using the flash/quench technique, effectively damage DNA via hole transport chemistry followed by irreversible reaction of the guanine radical produced. Figure 2.3 shows the oligonucleotide sequence employed for these experiments as well as the results for the family of ruthenium complexes tested. It is evident that the damage obtained for all complexes resides solely on the 5'-G of the 5'-GG-3' guanine doublet. This site is considered to be that of lowest oxidation potential within the oligonucleotide based upon empirical and theoretical studies (*14, 15*), and damage at the 5'-G of 5'-GG-3' sites is generally taken as a hallmark of CT damage (*9*). All of the ruthenium complexes examined produce this characteristic damage pattern, and increasing irradiation time leads to increased amounts of damage. Figure 2.4 shows the comparison of efficiencies for the different complexes.

Figure 2.5 shows the oxidative damage obtained after piperidine treatment of the oligonucleotides irradiated with the ruthenium complexes but in the absence of quencher. This damage is strikingly different from that in Figure 2.3, in that here damage is observed at all guanines with little sequence preference. This damage is not consistent

with a CT reaction but is instead consistent with damage owing to reaction with singlet oxygen, formed by sensitization of the excited ruthenium complexes (*47*, *48*). Singlet oxygen reacts preferentially with guanines (*49*), and the slight variations in base damage along the oligomer observed probably reflect preferences in the sites of Ru(II) binding and/or differences in the accessibility of guanine to diffusion of molecular oxygen.

2.3.5 Oxidative Damage by Covalently Bound Ruthenium Complexes. To probe the importance of intercalation to oxidative damage by long-range CT most directly, we compared oxidative damage patterns for $[Ru(bpy)_2(bpy')]^{2+}$ and $[Ru(bpy')(dppz)(phen)]^{2+}$ covalently bound to DNA. The bpy complex shows no intercalative interaction with the duplex while the dppz complex binds avidly by intercalation. By tethering the two complexes to the DNA duplex, one can therefore distinguish the effects of intercalation from simply a low association with the helix.

Figure 2.6 shows the results. As is evident, there is no guanine damage on the duplex containing the covalently bound $[Ru(bpy)_2(bpy')]^{2+}$ (Lane 14) just as there is no guanine damage in the case of noncovalently bound $[Ru(bpy)_2(bpy')]^{2+}$ when the ratio of oligonucleotide to metal is 1:1 (Lane 10). It is noteworthy that significant damage at all guanines is evident at a higher concentration of noncovalent $[Ru(bpy)_2(bpy')]^{2+}$ (Lane 8). We attribute this oxidation to direct association of the ruthenium complex with the guanine site. Also, for comparison, the expected long-range guanine oxidation is observed with both the covalently (Lane 12) and noncovalently bound (Lanes 4, 6) dppz derivatives of ruthenium. Interestingly, in the case of noncovalently bound $[Ru(bpy)_2(dppz)]^{2+}$, damage is also observed at the adenine 5' to the proximal double guanine site. This adenine, as part of a purine tract, may be particularly susceptible to

oxidative damage. Control experiments confirm that the long-range guanine damage occurs intraduplex and is not a result of metal intercalation into DNA other than that to which it is covalently tethered (*7*).

2.4 DISCUSSION

2.4.1 Intercalative Binding by the Family of Ruthenium Complexes. The data shown here provide support for intercalative binding by the full family of ruthenium complexes. The binding affinity and extent of intercalation appears to correlate with the expanse of the ligand available for stacking between the DNA base pairs (*50*).

A series of luminescence measurements were useful in characterizing the intercalative interaction. Comparable studies were carried out more than a decade ago to characterize the interaction of $[Ru(phen)_3]^{2+}$ and derivatives with DNA (*40*), and analogous studies have been carried out more recently in characterizing various phenazine derivatives (*51*). As seen earlier, the dppz and dppx complexes display no detectable luminescence in aqueous solution yet exhibit intense luminescence in the presence of DNA (*37, 38*). This effect has been attributed to the deep intercalation of the phenazine moeity within the base stack, so as to protect the phenazine nitrogen atoms from water. In the case of dpq and dpqC complexes, extensive NMR studies have been used to characterize interactions with DNA (*18, 19*), but luminescence properties have not been previously explored. Lacking the phenazine moiety, luminescence for $[Ru(bpy)_2(dpq)]^{2+}$ and $[Ru(bpy)_2(dpqC)]^{2+}$ is observed in water even in the absence of DNA. Nonetheless the complexes do show 2-5 fold luminescence enhancements in the presence of DNA, consistent with partial intercalation. In the case of $[Ru(phen)_3]^{2+}$, we

had attributed comparable levels of luminescence enhancement to partial intercalation, rigidifying the complex within the helix, decreasing vibrational modes of relaxation (*40*). We also observe that, similarly to $[Ru(bpy)_2(dppz)]^{2+}$ and $[Ru(bpy)_2(dppx)]^{2+}$, the excited states of $[Ru(bpy)_2(dpq)]^{2+}$ and $[Ru(bpy)_2(dpqC)]^{2+}$ are quenched by groove-bound quenchers such as $[Ru(NH_3)_6]^{3+}$ and more efficiently by intercalating $[Rh(phi)_2(dmb)]^{3+}$, pointing to an intimate association with the DNA helix. The polarization of luminescence of $[Ru(bpy)_2(dpq)]^{2+}$ and $[Ru(bpy)_2(dpqC)]^{2+}$ are comparable to that of $[Ru(bpy)_2(dppz)]^{2+}$, despite their relatively long excited state lifetimes, and not to those of groove-bound $[Ru(bpy)_3]^{2+}$. Again, the polarization results support a rigid association of the complexes on the helix.

We also utilized measurements of enantioselectivity to distinguish the association with the right-handed helix by intercalation versus groove-binding. We had earlier seen that owing to symmetry and steric constraints, for an intercalative interaction, where the complex resembles a base pair in stacking within the helix, a right-handed Δ-configuration is favored for binding to right-handed duplex DNA; in contrast, for groove-binding against the right-handed helix, a complementary Λ-configuration is favored (*45*). Enantioselectivity experiments clearly show for $[Ru(bpy)_2(dpq)]^{2+}$ and $[Ru(bpy)_2(dpqC)]^{2+}$ that it is the Δ-enantiomer that is preferred in binding to the right-handed duplex, consistent with intercalation.

Based on binding affinity data, luminescence measurements, and the aromatic expanse of the intercalating ligand, there are three distinct classes within this family of ruthenium complexes. The first is composed of the dppz and dppx complexes; these display the highest binding affinities, reflecting deep intercalation within the helix. The

second group contains complexes that bind less avidly to DNA, presumably due to decreased aromatic size of the intercalating ligand, $[Ru(bpy)_2(dpq)]^{2+}$, $[Ru(bpy)_2(dpqC)]^{2+}$, and $[Ru(phen)_3]^{2+}$. $[Ru(phen)_3]^{2+}$ had been shown to bind to DNA through a mixture of binding modes (*40*). Because of the hydrophobicity associated with dpq and dpqC, a groove-binding association seemed reasonable to consider as a predominant mode of association. While a mixture of binding modes may result for these more weakly bound complexes, just as was seen earlier for $[Ru(phen)_3]^{2+}$, certainly the results described here are consistent with the presence of an intercalative interaction. The third class contains $[Ru(bpy)_3]^{2+}$; earlier studies had shown only the electrostatic association of this complex with DNA (*40*).

2.4.2 Different Modes of Reactivity. Photoactivation of the ruthenium complexes bound to DNA leads to two distinct routes for oxidative damage, and these routes may be distinguished by the pattern of reactivity along the duplex. When this family of ruthenium complexes is irradiated in the presence of DNA, but absence of quencher, damage is observed at all guanines. This damage is consistent with singlet oxygen-mediated chemistry and is dependent on the excited state lifetime as well as binding affinity of the ruthenium complex. Singlet oxygen has been shown to react preferentially with guanines along the helix (*49*). Since the reaction depends upon the diffusion of $^1O_2$ from the site of sensitization to guanine, if the binding of the ruthenium sensitizer is non-specific, then reaction at all guanines on the helix is expected. This reaction at all guanines is essentially what we observe for all of the complexes, and thus the pattern reflects also the non-specific association of the family of complexes with DNA.

When these ruthenium complexes are utilized in a flash/quench scheme, damage at the 5'-G of a 5'-GG-3' guanine doublet is observed, the hallmark of DNA mediated CT damage. This damage also depends upon the excited state lifetime of the metal complex. With this chemistry, however, a diffusible intermediate is not involved in generating the guanine radical. Instead the reactivity depends upon redox potentials, that of the ruthenium(III/II) couple, and that of the guanine. It is the oxidation potential of the 5'-G of 5'-GG-3' sites that appears to be lowest (*14, 15*), and hence the signature damage at 5'-G's. It is noteworthy that the guanine oxidation products are expected to be similar for singlet oxygen and CT damage (*24*), although the products have not been characterized here. Also important to note is that since CT damage can arise from a distance, the site of reactivity need not reflect the site of ruthenium binding.

Interestingly, a third mode of reactivity would be direct DNA oxidation from the Ru(II) excited state. From the excited state reduction potentials, both the dppz and dppx complexes appear to have the proper driving force to oxidize guanines from the excited state. However, this damage is not observed. A possible explanation comes from an examination of the Ru(II) excited state. The excited state results from a metal-to-ligand charge transfer, which is directed to the dppz or dppx ligand. When these complexes intercalate into DNA, the ligand which is in intimate contact with the π-stack and would ultimately accept an electron from guanine, therefore possesses additional electron density in the excited state. Most likely, then, because of the direction of the charge transfer, the driving force for this reaction is significantly less than expected.

2.4.3 Direct Correlation Between Intercalation and DNA Charge Transport. For the family of ruthenium complexes examined here, it is evident that there is a direct

correlation between binding affinity and efficiency of damage as a result of DNA mediated CT. Tighter intercalative binding results in greater amounts of oxidative DNA damage. Complexes that possess large aromatic ligands intercalate more avidly than those with less aromatic surface area, and also display greater amounts of oxidative damage. Thus $[Ru(bpy)_2(dppz)]^{2+}$ and $[Ru(bpy)_2(dppx)]^{2+}$ show the highest extent of CT damage, despite not having particularly long excited state lifetimes bound to DNA. $[Ru(bpy)_3]^{2+}$, although possessing a long excited state lifetime (*40*), shows no evidence for an intercalative association with DNA and shows little reactivity through CT chemistry. $[Ru(bpy)_2(dpq)]^{2+}$ and $[Ru(bpy)_2(dpqC)]^{2+}$ have intermediate levels of intercalative binding and show intermediate levels of oxidative damage through DNA charge transport.

The importance of intercalation is perhaps most directly illustrated in experiments comparing reactions of covalently bound ruthenium complexes. By tethering the complexes to the DNA duplex, one can distinguish the effects of intercalation from simply a low association with the helix. When the bpy complex is tethered to DNA, and thus linked to the helix, no DNA CT damage from a distance results; damage is evident only at the site of ruthenium association. We attribute this lack of reactivity at distal positions to the lack of coupling of the ruthenium oxidant into the base pair stack. However, in the case of a tethered dppz complex, extensive damage is observed across the helix and at a site distant from ruthenium intercalation. It is noteworthy that at high enough metal concentrations, guanine damage can be observed with noncovalent $[Ru(bpy)_3]^{2+}$; we attribute this damage to direct contact between guanine and $[Ru(bpy)_3]^{3+}$ generated in solution. Such reactivity by $[Ru(bpy)_3]^{3+}$ is precedented (*52*),

although no oxidative damage to DNA *from a distance* has been observed with $[Ru(bpy)_3]^{3+}$.

More subtle variations in efficiency with degree of intercalative binding have also been seen. Differences in efficiency of guanine oxidation via DNA CT are observed for Δ and Λ-enantiomers of Ru(II) and Rh(III) octahedral complexes (*36*). The Δ-enantiomer can intercalate deeply into the base pair stack, avoiding steric interactions with the sugar-phosphate backbone of the right-handed helix, and provide efficient coupling between the oxidant and the π-stack. Decreased amounts of CT damage are observed with the Λ-enantiomers.

Intercalation therefore serves sensitively to modulate long-range oxidative DNA damage. By studying a family of ruthenium complexes containing the dppz ligand or derivatives, the ability of the complex to intercalate into the DNA π-array has been found to affect directly the extent of DNA CT and resultant damage. Intercalation can lead to more effective coupling into the π-stack, resulting in more efficient hole injection and CT. These results require consideration in comparing reactions on DNA with different photooxidants. The source of charge injection into DNA is therefore a critical parameter in determining the extent of oxidative DNA damage from a distance.

2.5 REFERENCES

(1) Kelley, S. O., and Barton, J. K. (1999) *Met. Ions Biol. Syst*. *36*, 211. (b) Núñez, M. E., and Barton, J. K. (2000) *Curr. Opin. Chem. Biol*. *4*, 199.

(2) Hall, D. B., and Barton, J. K. (1997) *J. Am. Chem. Soc*. *119*, 5045.

(3) Bhattacharya, P. K., and Barton, J. K. (2001) *J. Am. Chem. Soc*. *123*, 8649.

(4) Boon, E. M., Ceres, D. M., Drummond, T. G., Hill, M. G., and Barton, J. K. (2000) *Nat. Biotech*. *18*, 1096.

(5) Rajski, S. R., and Barton, J. K. (2001) *Biochemistry 40*, 5556. (b) Rajski, S. R., Kumar, S., Roberts, R. J., and Barton, J. K. (1999) *J. Am. Chem. Soc*. *121*, 5615.

(6) Wagenknecht, H. A., Rajski, S. R., Pascaly, M., Stemp, E. D. A., and Barton, J. K. (2001) *J. Am. Chem. Soc*. *123*, 4400.

(7) Núñez, M. E., Hall, D. B., and Barton, J. K. (1999) *Chem. Biol*. *6*, 85.

(8) Ly, D., Sanii, L., and Schuster, G. B. (1999) *J. Am. Chem. Soc*. *121*, 9400.

(9) Hall, D. B., Holmlin, R. E., and Barton, J. K. (1996) *Nature 382*, 731.

(10) Schuster, G. B. (2000) *Acc. Chem. Res. 33*, 253.

(11) Giese, B. (2000) *Acc. Chem. Res*. *33*, 631.

(12) Williams, T. T., Odom, D. T., and Barton, J. K. (2000) *J. Am. Chem. Soc*. *122*, 9048.

(13) Steenken, S., and Jovanovic, S. V. (1997) *J. Am. Chem. Soc*. *119*, 617.

(14) Saito, I., Takayama, M., Sugiyama, H., Nakatani, K., Tsuchida, A., and Yamamoto, M. (1995) *J. Am. Chem. Soc*. *117*, 6406.

(15) Prat, F., Houk, K. N., Foote, C. S. (1998) *J. Am. Chem. Soc*. *120*, 845.

(16) Friedman, A. E., Chambron, J.-C., Sauvage, J.-P., Turro, N. J., and Barton, J. K. (1990) *J. Am. Chem. Soc*. *112*, 4960.

(17) Haq, I., Lincoln, P., Suh, D., Nordén, B., Chowdry, B. Z., and Chaires, J. B. (1995) *J. Am. Chem. Soc. 117*, 4788. (b) Lincoln, P., Broo, A., Nordén, B. (1996) *J. Am. Chem. Soc*. *118*, 2644.

(18) Collins, J. G., Sleeman, A. D., Aldrich-Wright, J. R., Greguric, I., and Hambley, T. W. (1998) *Inorg. Chem. 37*, 3133. (b) Collins, J. G., Aldrich-Wright, J. R., Greguric, I. D., and Pellegrini, P. A. (1999) *Inorg. Chem. 38*, 5502.

(19) Greguric, I., Aldrich-Wright, J. R., and Collins, J. G. (1997) *J. Am. Chem. Soc*. *119*, 3621.

(20) Stemp, E. D. A., Arkin, M. R., and Barton, J. K. (1997) *J. Am. Chem. Soc*. *119*, 2921.

(21) Chang, I.-J., Gray, H. B., and Winkler, J. R. (1991) *J. Am. Chem. Soc*. *113*, 7056.

(22) Stemp, E. D. A., and Barton, J. K. (2000) *Inorg. Chem*. *39*, 3868.

(23) Nguyen, K. L., Steryo, M., Kurbanyan, K., Nowitzki, K. M., Butterfield, S. M., Ward, S. R., and Stemp, E. D. A. (2000) *J. Am. Chem. Soc*. *122*, 3585.

(24) Burrows, C. J., and Muller, J. G. (1998) *Chem. Rev*. *98*, 1109. (b) Angelov, D., Spassky, A., Berger, M., and Cadet, J. (1997) *J. Am. Chem. Soc*. *119*, 11373.

(25) Amouyal, E., Homsi, A., Chambron, J.-C., and Sauvage, J.-P. (1990) *J. Chem. Soc., Dalton Trans. 6*, 1841.

(26) Strouse, G. F., Anderson, A. P., Schoonover, J. R., Meyer, T. J., and Keene, F. R. (1992) *Inorg. Chem*. *31*, 3004. (b) Anderson, P. A., Deacon, G. B., Haarmenn, K. H., Keene, F. R., Meyer, T. J., Reitsma, D. A., Skelton, B.W., Strouse, G. F., Thomas, N. C., Treadway, J. A., and Whit, A. H. (1995) *Inorg. Chem*. *34*, 6145.

(27) Holmlin, R. E., and Barton, J. K. (1995) *Inorg. Chem*. *34*, 7. (b) Holmlin, R. E., Stemp, E. D. A., and Barton, J. K. (1996) *J. Am. Chem. Soc*. *118*, 5236.

(28) Scatchard, G. (1949) *Ann. N.Y. Acad. Sci*. *51*, 660.

(29) Beaucage, S. L., and Caruthers, M. H. (1981) *Tet. Lett*. *23*, 1859. (b) Goodchild, J. (1990) *J. Bioconj. Chem*. *1*, 165.

(30) Warshaw, M. M., and Tinoco, I. Jr. (1966) *J. Mol. Biol*. *20*, 29.

(31) Holmlin, R. E., Dandliker, P. J., and Barton, J. K. (1999) *Bioconj. Chem*. *10*, 1122.

(32) Sambrook, J., Fritsch, E. F., and Maniatis, T. (1989) *Molecular Cloning: A Laboratory Manual*, 2nd ed., Cold Spring Harbor Laboratory, New York.

(33) Moucheron, C., Mesmaeker, A. K., and Choua, S. (1997) *Inorg. Chem. 36*, 584. (b) Chambron, J.-C., and Sauvage, J.-P. (1985) *Nouv. J. De. Chim. 9*, 527.

(34) Scott, S. M., Gordon, K. C., and Burrell, A. K. (1999) *J. Chem. Soc., Dalton Trans*. *16*, 2669.

(35) Fees, J., Ketterle, M., Klein, A., Fiedler, J., and Kaim, W. (1999) *J. Chem. Soc., Dalton Trans*. *15*, 2595.

(36) Arkin, M. R., Stemp, E. D. A., Holmlin, R. E., Barton, J. K., Hörmann, A., Olson, E. J. C., and Barbara, P. F. (1996) *Science 273*, 475.

(37) Turro, C., Bossmann, S. H., Jenkins, Y., Barton, J. K., and Turro, N. J. (1995) *J. Am. Chem. Soc. 117*, 9026. (b) Olson, E. J. C., Hu, D., Hormann, A., Jonkman, A.

M., Arkin, M. R., Stemp, E. D. A., Barton, J. K., and Barbara, P. F. (1997) *J. Am. Chem. Soc*. *119*, 11458.

(38) Hartshorn, R. M., and Barton, J. K. (1992) *J. Am. Chem. Soc*. *114*, 5919-5925. (b) Jenkins, Y., Friedman, A. E., Turro, N. J., and Barton, J.K. (1992) *Biochemistry 31*, 10809.

(39) Dupureur, C. M., and Barton, J .K. (1997) *Inorg. Chem*. *36*, 33. (b) Dupureur, C. M., and Barton, J. K. (1994) *J. Am. Chem. Soc*. *116*, 10286.

(40) Kumar, C. V., Barton, J. K., and Turro, N. J. (1985) *J. Am. Chem. Soc*. *107*, 5518.

(41) Barton, J. K., Goldberg, J. M., Kumar, C. V., and Turro, N. J. (1986) *J. Am. Chem. Soc*. *108*, 2081.

(42) Rehmann, J. P., and Barton, J. K. (1990) *Biochemistry 29*, 1701.

(43) Eriksson, M., Leijon, M., Hiort, C., Nordén, B., and Gräslund, A. (1994) *Biochemistry 33*, 5031-5040. (b) Marincola, F. C., Casu, M., Saba, G., Lai, A., Lincoln, P., and Nordén, B. (1998) *Chem. Phys*. *236*, 301.

(44) Le Pecq, J. B., and Paoletti, C. (1967) *J. Mol. Biol*. *27*, 87.

(45) Barton, J. K. (1986) *Science 233*, 727.

(46) Baker, D. A., Morgan, R. J., and Strekas, T. C. (1991) *J. Am. Chem. Soc*. *113*, 1411.

(47) Mei, H.-Y., and Barton, J. K. (1986) *J. Am. Chem. Soc*. *108*, 7414-7416. (b) Mei, H.-Y., and Barton, J. K. (1988) *Proc. Natl. Acad. Sci. U. S. A. 85*, 1339.

(48) Kelly, J. M., Tossi, A. B., McConnell, D. J., and Ohvign, C. (1985) *Nuc. Acid. Res*. *13*, 6017.

(49) Rougee, M., and Bensasson, R. V. (1986) *C.R. Acad. Sci. Ser. 2*. *302*, 1223.

(50) Pyle, A. M., Rehmann, J. P., Meshoyer, R., Kumar, C. V., Turro, N. J., and Barton, J. K. (1989) *J. Am. Chem. Soc*. *111*, 3051.

(51) Van Gijte, O., and Kirsch-De Mesmaeker, A. (1999) *J. Chem. Soc., Dalton Trans*. *6*, 951. (b) Lecomte, J. P., Kirsch-De Mesmaeker, A., Feeny, M. M., and Kelly, J. M. (1995) *Inorg. Chem*. *34*, 6481.

(52) Ropp, P. A., and Thorp, H. H. (1999) *Chem. Biol*. *6*, 599. (b) Yang, I. V., and Thorp, H. H. (2000) *Inorg. Chem*. *39*, 4969.

Table 2.1. Electrochemical Data[a] and $E_{0/0}$[b] for Ruthenium Complexes.

Complex	Metal Centered (*2+/+)	(3+/2+)	$E_{0/0}$	Ligand Centered L/L·⁻	bpy_1·⁻	bpy_2·⁻
$[Ru(bpy)_2(dppz)]^{2+}$ [c]	1.51	1.57	2.24	-0.73	-1.15	-1.39
$[Ru(bpy)_2(dppx)]^{2+}$	1.44	1.55	2.25	-0.81	-1.17	-1.39
$[Ru(bpy)_2(dpq)]^{2+}$ [c]	1.17	1.47	2.21	-1.04	-1.33	-1.48
$[Ru(bpy)_2(dpqC)]^{2+}$	1.21	1.45	2.28	-1.07	-1.27	-1.47
$[Ru(bpy)_3]^{2+}$ [c]	0.98	1.49	2.10	-1.12	-1.28	-1.51
$[Ru(phen)_3]^{2+}$ [c]	1.08	1.54	2.18	-1.10	-1.25	-1.42

[a] In dry CH_3CN with 100 mM tetrabutylammonium hexafluorophosphate; scan rate 100 mV/s. For all complexes examined, oxidation waves are reversible and reduction waves are irreversible. Potentials are reported in volts vs. NHE and uncertainty is estimated to be ± 50 mV. [b] Excitation and emission spectra were obtained in CH_3CN and the point of intersection, after normalization, was taken as $E_{0/0}$. $E_{0/0}$ values were obtained from the luminescent triplet excited state and are therefore underestimates of the actual values. [c] In agreement with literature values (*33*, *34*).

Table 2.2. Excited State Lifetimes for *rac*-Ruthenium Complexes (in nanoseconds).[a]

Complex	H_2O	ct-DNA	ct-DNA 80 μM $Ru(NH_3)_6^{3+}$[c]	ct-DNA 100 μM $Rh(phi)_2(dmb)^{3+}$[c]	Emission Max (nm)
$Ru(bpy)_2(dpq)^{2+}$	195 ± 11	1094 ± 39 (93%) 47 ± 4 (7%)	549 (93%) 217 (7%)	862 (47%) 167 (53%)	636
$Ru(bpy)_2(dpqC)^{2+}$	415 ± 26	965 ± 84 (90%) 68 ± 5 (10%)	532 (15%) 205 (85%)	672 (47%) 121 (53%)	609
$Ru(bpy)_2(dppz)^{2+}$[d]	b	450 ± 32 (35%) 50 ± 5 (65%)	207 (20%) 42 (80%)	115 (21%) 14 (79%)	627
$Ru(bpy)_2(dppx)^{2+}$	b	475 ± 44 (39%) 137 ± 9 (61%)	187 (48%) 53 (52%)	274 (52%) 30 (48%)	619
$Ru(bpy)_3^{2+}$[e]	406	420	-	-	-

[a] Samples consisted of 10 μM racemic metal complex, 10 mM NaCl, 20 mM sodium phosphate, pH 7.85. Lifetimes in water alone and ct-DNA are given as averages of three replicates. When present, ct-DNA concentration was 1 mM nucleotides. In fluorescence quenching studies, samples contained, in addition, 80 μM $Ru(NH_3)_6^{3+}$ or 100 μM $Rh(phi)_2(dmb)^{3+}$ (phi = 9,10-phenanthrenequinone diimine; dmb = 4,4'-dimethyl-2,2'-bipyridine). The luminescence traces of the complexes in water alone were fit to a monoexponential function ($C_1 = 1$). [b] Faster than instrument response. [c] Uncertainties estimated to be ± 10%. [d] Corresponds to literature value (*36, 40*). [e] Literature value (*40*).

Table 2.3. DNA Binding Properties for Ruthenium Complexes.[a]

Complex	K_b, M^{-1}	Metal/Nucleotides
$Ru(bpy)_2(dppz)^{2+}$[b,c]	$>10^6$	-
$Ru(bpy)_2(dppx)^{2+}$	$8.8\ (0.3) \times 10^6$	1/3
$Ru(bpy)_2(dpq)^{2+}$	$5.9\ (0.2) \times 10^4$	1/8
$Ru(bpy)_2(dpqC)^{2+}$	$8.5\ (0.2) \times 10^4$	1/4

[a] Ct-DNA, ranging from 10^{-7} M to 10^{-3} M, was titrated into solutions containing 0.25-10 μM racemic metal complex, 10 mM NaCl, 20 mM sodium phosphate, pH 7.85. An excitation wavelength of 450 nm was used and total luminescence intensity was recorded from 500-800 nm and corrected for dilution. [b] Literature value (*16*). [c] Values for $Ru(phen)_2(dppz)^{2+}$ are reported to be ~10^7 in 50 mM NaCl, 1 mM sodium cacodylate, pH 7 and ~10^6 in 50 mM NaCl, 5 mM Tris-HCl, pH 7.1 (*17*).

Table 2.4. Luminescence Polarization Data for Ruthenium Complexes.[a]

Complex	Medium			
	buffer	ct-DNA	60% glycerol	ct-DNA/ 60% glycerol
$[Ru(bpy)_3]^{2+}$	-0.0004	0.005	0.001	0.006
$[Ru(phen)_3]^{2+}$,[b]	-0.001	0.006	0.002	0.027
$[Ru(bpy)_2(dpq)]^{2+}$	-0.003	0.012	0.003	0.045
$[Ru(bpy)_2(dpqC)]^{2+}$	-0.003	0.017	0.003	0.060
$[Ru(bpy)_2(dppx)]^{2+}$	-	0.025	-	0.061
$[Ru(bpy)_2(dppz)]^{2+}$	-	0.029	-	0.070

[a] Samples consisted of 10 μM racemic metal complex in 10 mM NaCl, 20 mM sodium phosphate, pH 7.85. When present, ct-DNA concentration was 1 mM nucleotides and glycerol samples contained 60% glycerol by volume. Samples were irradiated at 450 nm and emission was monitored at 610 nm using a 495 nm cut-off filter. Uncertainties are estimated to be ±5%. [b] Comparable to literature values (*40*).

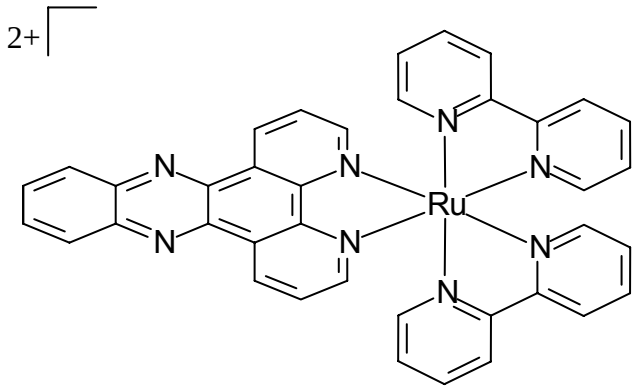

$Ru(bpy)_2(dppz)^{2+}$

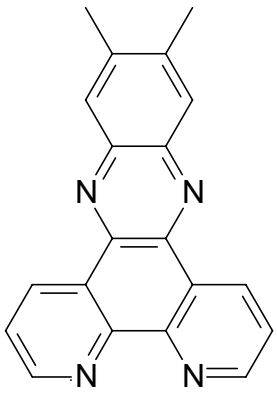

dppx

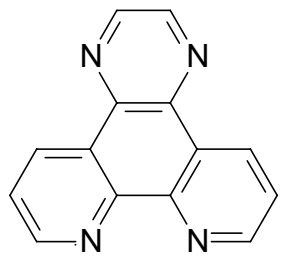

dpq

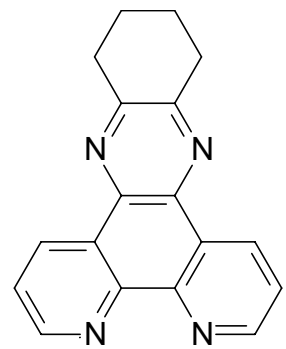

dpqC

Figure 2.1. Schematic illustrations of metal complexes used in this study.

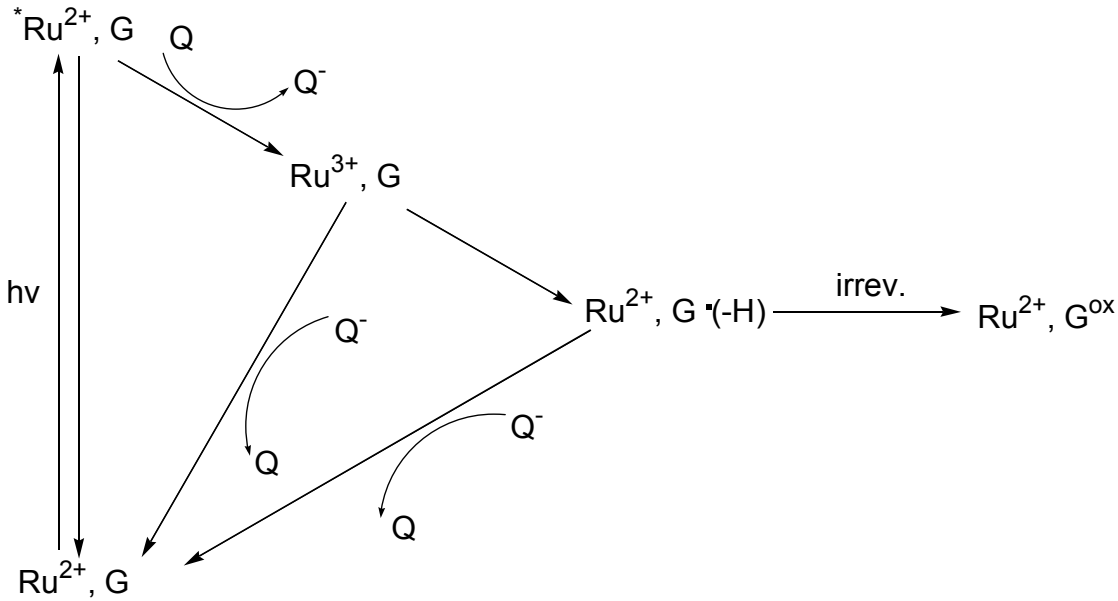

Scheme 2.1. Schematic illustration of the flash/quench methodology.

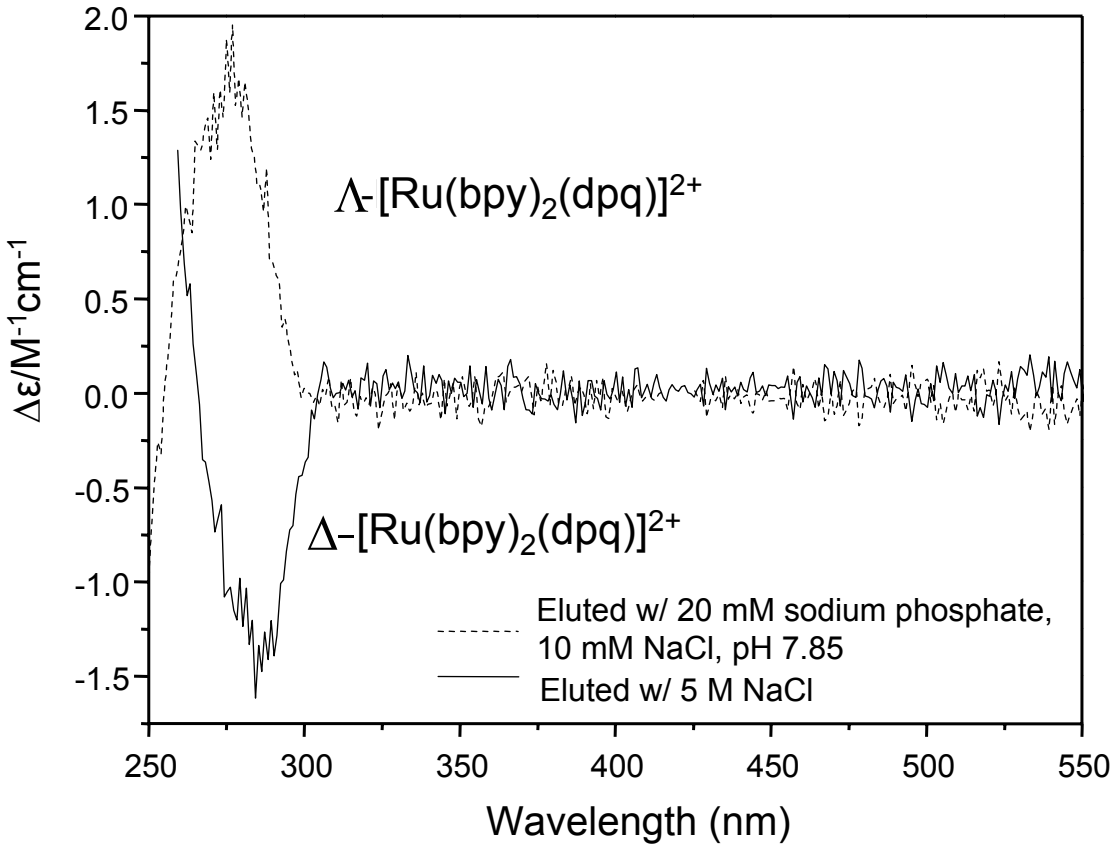

Figure 2.2. Circular dichroism for $[Ru(bpy)_2(dpq)]^{2+}$ eluted from DNA cellulose column with 10 mM NaCl, 20 mM sodium phosphate, pH 7.85 (dashed) and that eluted later with 5M NaCl (solid). Configurations were assigned based on literature spectra (*39*).

*5′-TGATCGGTGCGTCTGAGACT-3′
3′-ACTAGCCACGCAGACTCTGA-5′

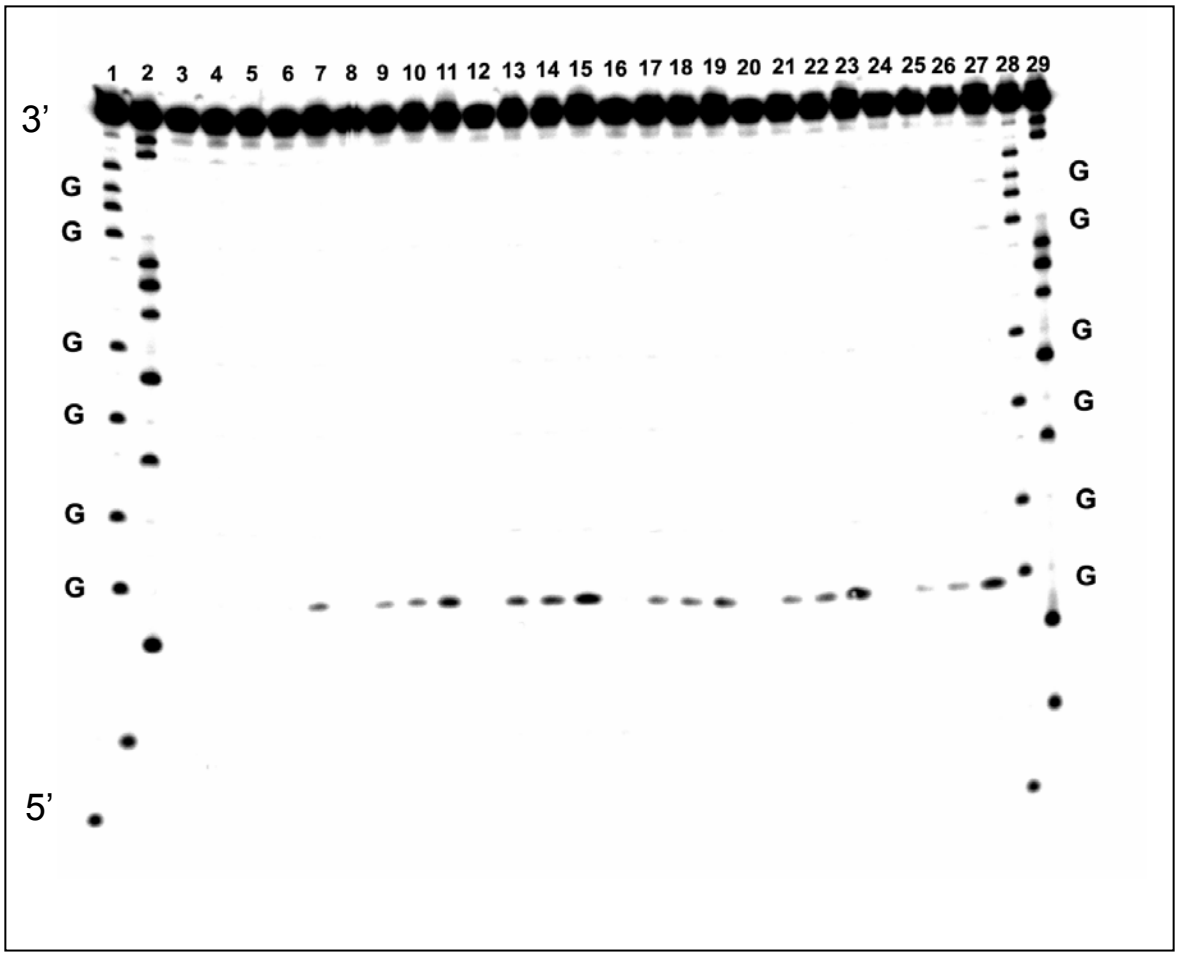

Figure 2.3. Oxidative Damage to DNA via Flash/Quench Method. Shown above is sequence of oligonucleotides used for electrophoresis experiments. The double guanine site has been underlined indicating site with the lowest oxidation potential; single guanines have also been underlined as these sites are susceptible to $^1O_2$ damage. Site of ^{32}P labeling is indicated by *. Shown below is the autoradiogram after oxidation of the oligonucleotide by $[Ru(bpy)_3]^{2+}$ in lanes 4,5,6, and 7; oxidation by $[Ru(phen)_3]^{2+}$ in lanes 8, 9, 10 and 11; and oxidation by $[Ru(bpy)_2(L)]^{2+}$ (L = dppz, dppx, dpq, dpqC) in lanes 12 through 27, respectively, using the flash/quench technique for increasing periods of time of irradiation: 0, 5, 10, 30 min within each series. Samples contain 8 μM oligonucleotide, 16 μM metal, and 160 μM $[Ru(NH_3)_6]^{3+}$. Lanes 1, 28 and 2, 29 show the damage patterns after Maxam-Gilbert sequencing reactions A+G and C+T, respectively. Lane 3 shows the damage pattern after irradiation for 30 min of the oligonucleotide in the presence of quencher but absence of metal.

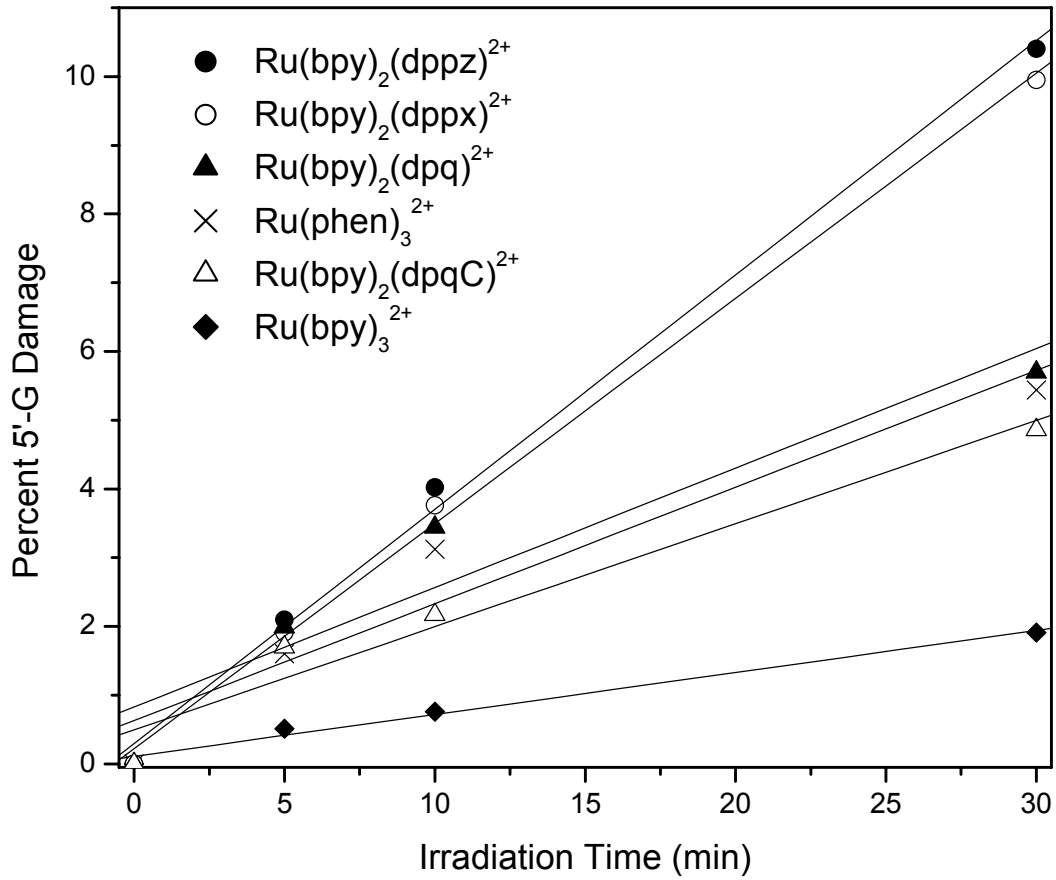

Figure 2.4. Plot of 5'-G damage versus irradiation time for family of ruthenium complexes showing relative efficiencies of oxidative damage.

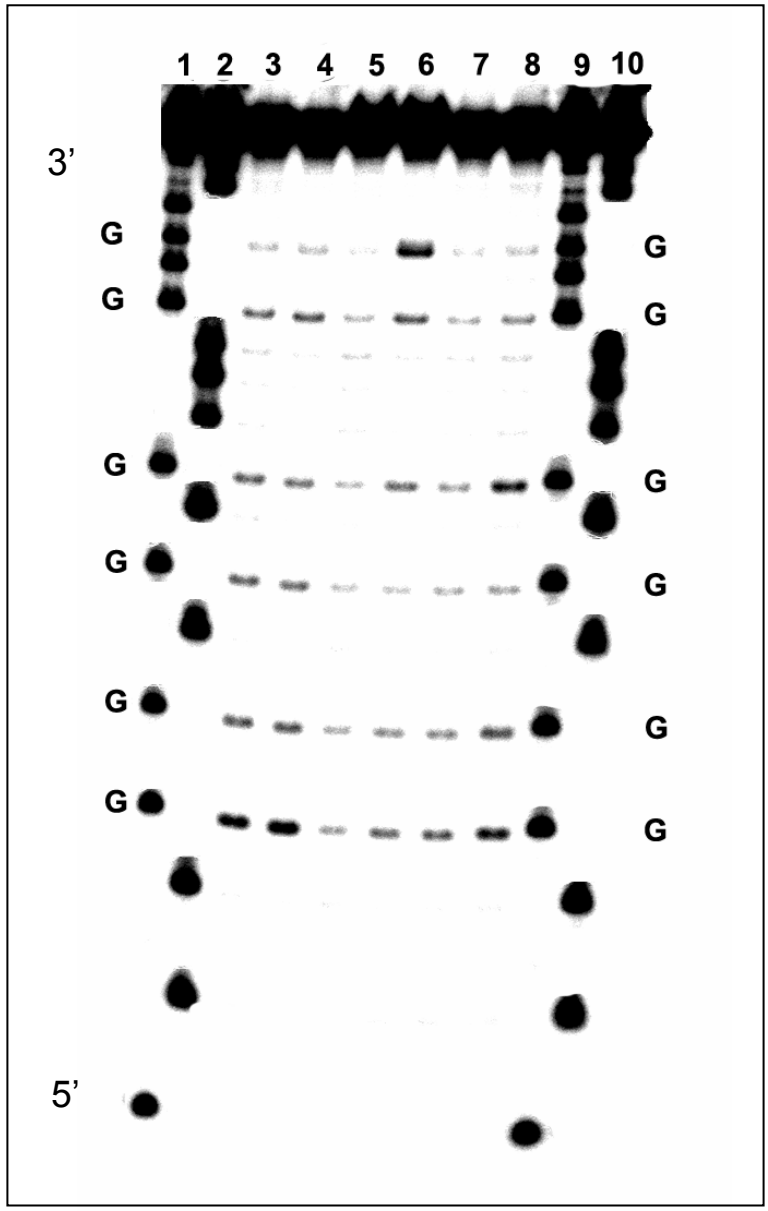

Figure 2.5. Oxidative DNA Damage via Singlet Oxygen Sensitization. Autoradiogram after denaturing polyacrylamide gel electrophoresis of ^{32}P-5'-TGATCGGTGCGTCTGAGACT-3' after oxidation of the oligonucleotide by the family of ruthenium complexes, in the absence of quencher. Samples contain 8 μM oligonucleotide and 16 μM metal, after 30 min of irradiation at 450 nm. Lanes 1, 9 and 2, 10 show damage patterns after Maxam-Gilbert sequencing reactions A+G and C+T, respectively. Lanes 3 through 8 show damage pattern after oxidation of the oligonucleotide by $[Ru(bpy)_3]^{2+}$, $[Ru(phen)_3]^{2+}$, and $[Ru(bpy)_2(L)]^{2+}$ (L = dppz, dppx, dpq, dpqC), respectively.

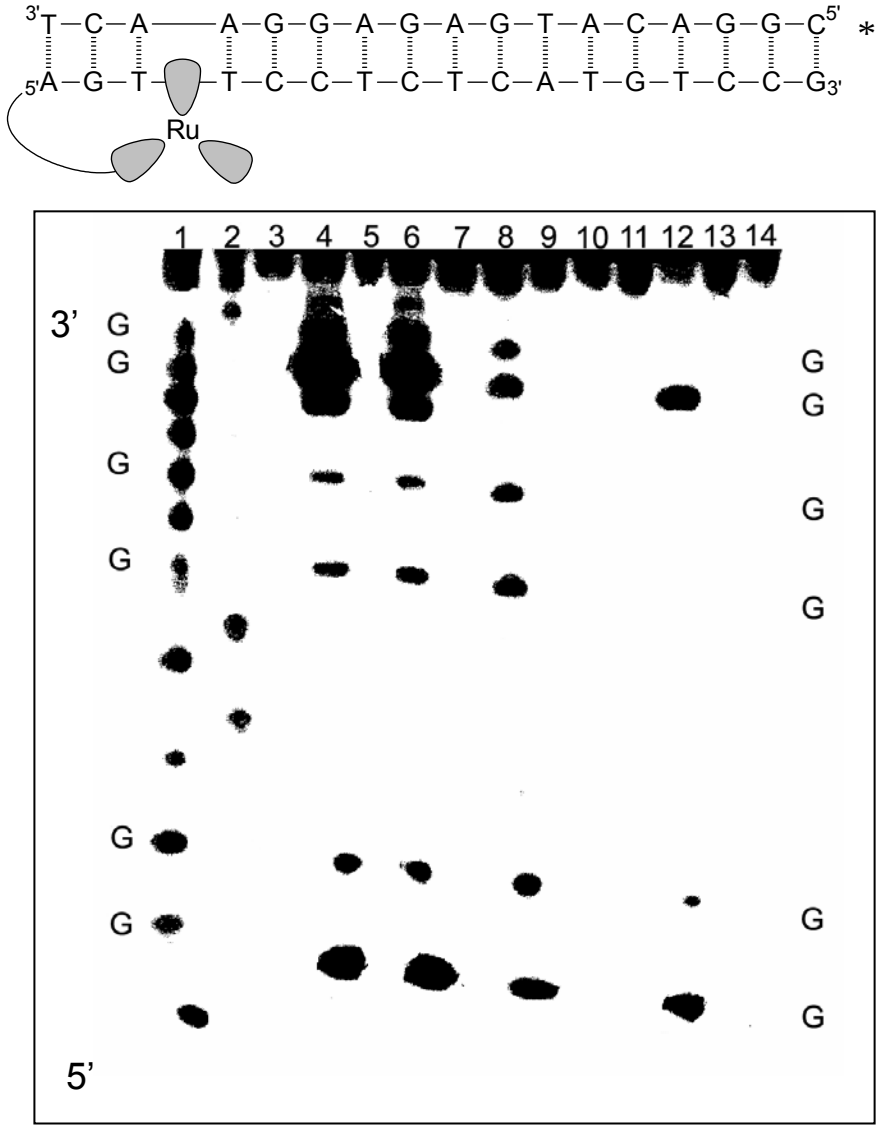

Figure 2.6. DNA Damage by Covalent Versus Noncovalent Ruthenium Complexes. Shown above is the ruthenium-oligonucleotide conjugate used in covalently tethered experiments. Site of ^{32}P labeling is indicated by *. Shown below is the autoradiogram of the ruthenium-oligonucleotide conjugate after oxidation by noncovalent and covalent bpy and dppz complexes. Samples contain 2.5 μM ruthenium-oligonucleotide and 25 μM MV^{2+} for covalently bound experiments. Noncovalently bound experiments utilized 2.5 μM oligonucleotides, 25 μM MV^{2+}, and indicated metal to DNA ratio. All irradiations were at 432 nm for 5 min. Lanes 1 and 2 show damage pattern after Maxam-Gilbert sequencing reactions A+G and C+T, respectively. Lanes 3, 4 and 5,6 show damage pattern for oxidation of the oligonucleotide by $[Ru(bpy)_2(dppz)]^{2+}$, 4:1 and 1:1 metal to DNA, respectively, in absence of light and after irradiation. Lanes 7, 8 and 9, 10 show damage pattern for oxidation by $[Ru(bpy)_2(bpy')]^{2+}$, 4:1 and 1:1 metal to DNA, respectively, in absence of light and after irradiation. Lanes 11 and 12 show damage pattern after oxidation by covalently bound $[Ru(bpy')(dppz)(phen)]^{2+}$, in absence of light and after irradiation, respectively. Lanes 13 and 14 show damage pattern by covalently bound $[Ru(bpy)_2(bpy')]^{2+}$, in absence of light and after irradiation, respectively.

CHAPTER 3

Towards Reduction of DNA via the Flash/Quench Technique

3.1 INTRODUCTION

Numerous biochemical, spectroscopic, and electrochemical studies have shown the base stack of DNA can mediate charge transport (CT) reactions (*1-4*). Furthermore, the DNA itself can participate directly in the CT acting as the electron donor (*5*). Of the nucleobases free in solution guanine is the easiest to oxidize (E_0 = 1.3, 1.4, 1.6, and 1.7 V vs. NHE for G, A, C, and T, respectively) (*6, 7*). DNA CT to generate oxidative damage has been demonstrated using a variety of oxidants such as phenanthrenequinone diimine (phi) complexes of Rh(III), polypyridyl complexes of Ru(II), naphthalene diimide, ethidium, and modified anthraquinones (*5, 8-11*). In addition, modified nucleotides such as 5-cyano-benzene deoxyuridine and 4'-pivaloyl deoxythymine have been photolysed to generate hot base and sugar radicals, respectively, that lead to oxidative guanine damage from a remote site (*12, 13*). Use of this family of oxidants results in damage patterns consistent with CT, oxidation of the 5'-G of 5'-GG-3' double guanine sites.

Upon close inspection, one will see that it is specifically *hole* transport (HT) through DNA that is being examined. The molecular orbitals involved in this CT event are the HOMO's of the intervening bases of DNA (Figure 3.1). However, since these molecular orbitals are fully occupied, an electronic hole must be transferred from the oxidant to guanine. If instead of an oxidant a reductant is used, the molecular orbitals involved in the CT event would be the LUMO's of the intervening DNA bases. Since these orbitals are unoccupied, an electron could be transferred directly from the reductant and possibly be trapped on a DNA base. In this manner, *electron* transport (ET) through the π-stack could be examined.

Electrochemical reduction of the nucleobases free in solution has established the trend in reducibility to be T $\approx$ U $\approx$ C > A > G, where E_0 = -1.09, -1.10, -1.10 vs. NHE for

C, T, and U, respectively (*14*); this trend has also been established theoretically (*15*). More detailed calculations of the electron affinities of the bases of DNA as a function of sequence context predict that the strongest electron acceptors are 5'-XCY-3' and 5'-XTY-3' where X and Y are the pyrimidine bases C or T (*16*). In addition, it has been suggested that in the context of double helical DNA the tendency for the cytosine anion radical to be protonated by its complement guanine is more than ten orders of magnitude greater than for protonation of a thymine radical anion by its adenine partner (*15*). Given that the CT event may be coupled with proton transfer this may result in cytosine, not thymine, being the most easily reduced base in DNA. Studies have shown, however, that at room temperature the negative charge created upon γ-pulse radiolysis ultimately ends up as the C6-protonated thymine radical anion (*17*). Furthermore, faster rates of electron injection are observed with thymine-containing ($> 2 \times 10^{12}$ s^{-1}) rather than cytosine-containing (3×10^{11} s^{-1}) oligonucleotides in an end-capped stilbene diether DNA hairpin (*18*). In other words, although in DNA an electron has a better chance of being first trapped at cytosine due to the strong driving force for protonation of the electron adduct, the final burial site of the electron will be thymine where it is trapped by the irreversible protonation of C6.

Recent experiments utilizing photoreductants site-specifically incorporated in oligonucleotides have expanded our knowledge of ET in DNA. Carell and coworkers have shown that thymine dimers can be repaired reductively using a reduced, deprotonated flavin nucleotide as a mimic of the enzyme photolyase (*19*, *20*). HPLC was used to monitor repair of the thymine dimer over 3.4 – 23.8 Å with intervening A – T base pairs; a very weak distance dependence of ET was observed and no dependence on

directionality was observed. Recently, reductive repair of a thymine dimer was achieved following Norrish photocleavage of a modified thymine base (*21*) (Giese Ang.). The yield of dimer repair, as monitored by HPLC, decreased from 14 to 7 to 5% upon introduction of 1-3 intervening A-T base pairs. In assemblies containing two thymine dimers, both dimers were repaired following photoactivation of the modified thymine. Interestingly, the cleavage yield at the distal thymine dimer was twice that at the proximal dimer. The existence of a population of duplexes where repair of the distal, but not proximal, thymine dimer is observed was confirmed by HPLC analysis. Therefore, the authors suggest that the cleavage rate of the thymine dimer following reductive repair is comparable to that of ET through DNA.

Rokita and coworkers have observed DNA strand cleavage at the thymine on the 5'-side of a 5'-bromo-2'-deoxyuridine (BrU) following photoactivation of a *N*,*N*,*N'*,*N'*-tetramethyl-1,5-diaminonapthalene (TMDN) ($E^*_{ox} \approx -2.6$ V vs NHE) analog internally tethered to DNA (*22*). The formation of a uridine-5-yl radical derived from BrU was proposed to induce both the direct and alkaline-dependent strand cleavage observed. This strand cleavage was observed over 3.4 – 20.4 Å. Using the internally tethered TMDN derivative a fourfold suppression of strand cleavage 5' to the BrU residue was observed upon substituting two interving A-T base pairs with G-C base pairs (*23*). This suppression was attributed to the lower ability of cytosine to act as an electron carrier due to preferential protonation of the cytosine anion radical over the thymine anion radical. Competition of proton transfer and ET was confirmed by changing the solvent from H_2O to D_2O. The rate of strand fragmentation as a result of ET through the G-C base pairs was 30% lower in D_2O. Also, in assemblies containing a tethered TMDN derivative and

a BrU residue a change in the orientation of the acceptor and two bridging T residues from 5' to 3' with respect to the donor caused a nine-fold decrease in ET efficiency. Therefore, in this study of ET a 3'→5' directionality preference is observed; previous examinations of HT between *Ap and G demonstrated a 5'→3' directionality preference (*24*). Additionally, time-resolved spectroscopy has been used to monitor the dynamics of electron injection with stilbene diether-capped ($E^*_{ox} \approx -2.3$ V vs NHE) DNA hairpins (*18, 25*) and pyrene ($E^*_{ox} \approx -1.8$ V vs NHE) modified oligonucleotides (*26*).

We are particularly interested in using the flash/quench technique, originally used to explore CT in proteins (*27*), to effect the reduction of DNA (Figure 3.2). Previous studies in our lab have utilized dipyridophenazine (dppz) complexes of ruthenium(II), in combination with the flash/quench technique, to study HT in DNA (*8, 28, 29*). In the oxidative flash/quench technique, an intercalated Ru(II) complex is excited with visible light to yield *Ru(II) which is then quenched with an electron acceptor free in solution (e.g. $[Ru(NH_3)_6]^{3+}$, $[Co(NH_3)_5Cl]^{2+}$, or methyl viologen). This generates a Ru(III) species *in situ* which can oxidize guanines in DNA by HT. When a dppz complex of ruthenium is end-tethered to a DNA duplex and subjected to oxidative flash/quench, neutral guanine radicals have been observed spectroscopically and permanent oxidative damage is obtained biochemically (*8*). Long-range oxidative damage has been demonstrated over 200 Å (*30*) and the HT is sensitive to intervening DNA sequence (*31*) and base stacking perturbations (*32, 33*). With an appropriate Ru(II) intercalator, in combination with the flash/quench technique, we may be able to compare directly HT and ET through the double helix by simply varying the quencher from an electron acceptor to an electron donor.

A reductive flash/quench technique has been developed to explore ET in proteins (*34*). An electron donating quencher p-methoxydimethylaniline (p-MDMA) was used to generate a $[Ru(bpy)_3]^+$ (bpy = 2,2'-bipyridine) species which delivers an electron to the heme center in cytochrome P450 via ET. If possible to apply this technique to DNA there would be numerous questions to ask. Is ET through DNA subject to the same sensitivities in sequence and base stacking perturbations as HT? What is the distance dependence of ET and how do the rates of HT and ET in DNA compare? What is the mechanism of ET through DNA? To develop a reductive flash/quench scheme in DNA there are three requirements: a reductant with ground state reduction potentials capable of reducing a DNA nucleobase, an electron donating quencher, and an assay to observe the reaction products. Here we discuss progress made in all three of these areas.

3.2 METHODS

3.2.1 Metal Complex Synthesis. The ligand dipyrido[3,2-a:2',3'-c]phenazine (dppz), was prepared according to literature protocols (*35, 36*) as was $Ru(phen)_2Cl_2 \cdot 2H_2O$ (*35*). $[Ru(phen)_2(dppz)](PF_6)_2$ was synthesized by heating 1.2 equivalents of dppz with $Ru(bpy)_2Cl_2 \cdot 2H_2O$ at 150 ºC in ethylene glycol for 1 hour. Solid NH_4PF_6 was used to precipitate the orange-red solid which was then washed with H_2O and diethyl ether. The complex was purified on an alumina column equilibrated with dichloromethane and eluted with acetonitrile. The water soluble chloride salt was obtained using a Sephadex QAE-25 ion-exchange resin equilibrated with 0.2 M KCl and eluted with acetonitrile.

3.2.2 Electrochemistry. Ground state oxidation and reduction potentials for the metal complexes were obtained on a Bioanalytical Systems (BAS) Model CV-50W electrochemical analyzer. A glassy carbon working electrode, Ag/AgCl reference electrode and Pt auxillary electrode were used in a single cell sample apparatus. Solutions of racemic metal complex (1mM) in dry acetonitrile (Fluka; stored over molecular sieves) containing 100 mM tetrabutylammonium hexaflourophosphate were degassed with argon prior to use and voltammagrams were collected using 100 mV/s scan rate. $E_{1/2}$ values were taken as the average of the voltage of maximum current for the forward and reverse electrochemical processes. Potentials are reported in volts versus NHE.

3.2.3 Luminescence Spectroscopy. Emission and excitation spectra were obtained on an ISS-K2 spectroflourometer. Emission intensities were determined by integration of the luminescence spectrum and standardized against $[Ru(bpy)_3]^{2+}$ as a calibration for the instrument. Solutions containing 10 μM racemic metal complex and 1 mM nucleotides ct-DNA in 10 mM NaCl, 20 mM sodium phosphate, pH 7.85 were excited at 450 nm and emission was monitored from 500-800 nm. Excitation spectra were obtained by monitoring at the emission maximum while varying excitation wavelength from 250-600 nm. To determine excited state lifetimes, time resolved emission measurements were conducted using a pulsed YAG-OPO laser (λ_{ex} = 470 nm). Laser powers ranged from 3-4 mJ/pulse. To obtain luminescence lifetimes, τ, time-resolved emission data were fit to

$y(t) = 100[C_1\exp(-t/\tau_1) + (1-C_1)\exp(-t/\tau_2)]$ by a nonlinear least-squares method with convolution of the instrument response function using in-house software as described

previously (*37*). Errors in lifetimes and percent contributions are estimated to be ± 10%. All complexes were purified by HPLC prior to luminescence measurement using a Dynamax 300 Å C18 reverse-phase column (Rainin) on a Hewlett-Packard 1100 HPLC (95% 30 mM NH_4OAc/5% acetonitrile to 100% acetonitrile over 60 min). Samples consisted of 10 μM racemic metal complex, 10 mM NaCl, 20 mM sodium phosphate, pH 7.85. For determining excited state lifetimes of metal complexes bound to DNA, 1 mM nucleotides ct-DNA was present. The luminescence traces of the complexes in water were fit to a monoexponential function ($C_1 = 1$).

3.2.4 Oligonucleotide Synthesis. Oligonucleotides were synthesized on an ABI 392 DNA/RNA synthesizer, using standard phosphoramidite chemistry (*38*). DNA was synthesized with a 5'-dimethoxy trityl (DMT) protecting group and was purified by HPLC using a Dynamax 300 Å C18 reverse-phase column (Rainin) on a Hewlett-Packard 1100 HPLC (95% 30 mM NH_4OAc/5% acetonitrile to 84% 30 mM NH_4OAc/16% acetonitrile over 25 min). The DMT group was removed by incubation with 80% glacial acetic acid for 12 min at ambient temperature, and then re-purified by HPLC (100% 30 mM NH_4OAc to 75% 30 mM NH_4OAc/25% acetonitrile over 40 min). Quantification was done on a Beckman DU 7400 Spectrophotometer using the ε_{260} values estimated for single stranded DNA (*39*).

3.2.5 PAGE Assay of DNA Damage. Single oligonucleotide strands were 5'-^{32}P end-labeled using standard protocols (*40*) and annealed to the complementary strand in an aerated buffer of 10 mM NaCl, 20 mM sodium phosphate, pH 7.85. Concentrations of DNA duplex, metal complex, and reductive quencher are indicated in figure captions. The samples were irradiated at 450 nm with a 1000 W Hg/Xe lamp equipped with a

monochromator. Irradiation times varied from 0-60 min. After irradiation, samples were treated with piperidine, base excision repair enzymes, or aniline and dried and electrophoresed through a 20% denaturing polyacrylamide gel. The extent of damage was quantitated by phosphorimagery (ImageQuant).

3.2.6 High Performance Liquid Chromatography. DNA duplexes (10 μM) were annealed in a buffer of 10 mM NaCl, 20 mM sodium phosphate, pH 7.8. Samples were irradiated at 442 nm for 0-60 min in the presence of 20 μM $[Ru(phen)_2(dppz)]^{2+}$, $[Ru(bpy)_2(dpq)]^{2+}$, or $[Ru(bpy)_2(dpqC)]^{2+}$ and 1 M KI or 5 mM p-MDMA. Following irradiation samples were ethanol precipitated to remove the metal complex and quencher and then digested with nuclease P1 and alkaline phosphatase. The nucleoside products were then analyzed by HPLC using a Microsorb MV analytical column where the column temperature was maintained at 40 °C. The mobile phase consisted of 12.5 mM citric acid, 25 mM ammonium acetate, pH 5 and 1-4% methanol over 40 min.

3.2.7 EPR Spectroscopy. EPR spectra were recorded using an X-band Bruker EMX spectrometer equipped with a standard TE_{102} cavity. Magnetic field calibrations were made against a degassed solution of 1% perylene in H_2SO_4. All measurements were made on photolyzed frozen samples at 77 K employing a finger dewar filled with liquid nitrogen designed to fit inside the EPR cavity. Photolysis was carried out by illuminating a 100 μL sample solution contained in quartz tubes (4mm OD) while freezing in an optical dewar filled with liquid nitrogen. The light source used was a 300 W Xe-Arc lamp or HeCd laser (442 nm). UV filters were employed to eliminate light < 320 nm and water to eliminate IR radiation. The samples contained 50 μM $[Ru(phen)_2(dppz)]^{2+}$, 100

μM uracil-containing oligonucleotides, 10 mM NaCl, 20 mM sodium phosphate, pH 7.8, and 2M KI.

3.2.8 Transient Absorption Spectroscopy. DNA duplexes (20 μM) were formed by mixing equal concentrations of complementary strands, and heating to 90 °C followed by slow cooling to room temperature in a buffer of 10 mM NaCl, 20 mM sodium phosphate, pH 7. The samples consisted of 20 μM $[Ru(phen)_2(dppz)]^{2+}$, 20 μM oligonucleotides (sequence shown in Figure 3.11 where U is either uracil or FU) and 1 M KI or 4 mM p-MDMA. Time-resolved emission and transient absorption experiments were carried out on a Nd:YAG laser using an excitation wavelength of 470 nm. The emission of the intercalated ruthenium complexes was monitored at 610 nm. Emission intensities were obtained by integrating the area under the decay curve of the luminescence.

3.3 RESULTS

Exploring ET in DNA using a flash/quench technique has three requirements: a reductant with appropriate redox properties, an electron donating quencher, and an assay for detecting the products of the reaction. These will each be discussed separately.

3.3.1 Reductant. $[Ru(phen)_2(dppz)]^{2+}$ has been utilized extensively to explore HT in DNA owing to its unique luminescence properties (*41*). Its redox properties and strong binding affinity for DNA also make it an ideal component for the oxidative flash/quench scheme. However, with a ground state reduction potential of -0.76 V vs. NHE, $[Ru(phen)_2(dppz)]^{+}$ is not capable of reducing thymine or cytosine. The redox properties of $[Ru(phen)_2(dppz)]^{2+}$ are shown in Table 3.1.

Table 3.1. Redox Properties of $[Ru(phen)_2(dppz)]Cl_2$.[a]

	E_{red} vs. NHE	E_{ox} vs. NHE
$[Ru(phen)_2(dppz)]Cl_2$	-0.76 V	1.55 V
$*[Ru(phen)_2(dppz)]Cl_2$	1.51 V	-0.72 V

[a] Values were obtained for 1 mM $[Ru(phen)_2(dppz)]Cl_2$ in acetonitrile, 100 mM tetrabutylammonium hexafluorophosphate versus Ag/AgCl. Values were corrected to NHE by the addition of 0.197 V.

In an attempt to circumvent this problem, Ru(II) complexes with more favorable ground state reduction potentials, containing derivatives of the dppz ligand, were synthesized and characterized: $[Ru(bpy)_2(dppx)]^{2+}$ (dppx = 7,8-dimethyldipyridophenazine), $[Ru(bpy)_2(dpq)]^{2+}$ (dpq = dipyridoquinoxaline) and $[Ru(bpy)_2(dpqC)]^{2+}$ (dpqC = dipyrido-6,7,8,9-tetrahydrophenazine) (Figure 3.3) (see Chapter 2 for a detailed discussion of the characterization and HT chemistry of this family of ruthenium complexes). After extensive studies with this family of ruthenium complexes, including determination of DNA binding constants, redox properties, excited state lifetimes, and fluorescence properties, it was concluded that although these complexes bind to DNA via an intercalative fashion, and possess favorable redox properties, they bind to DNA with affinities two orders of magnitude lower than their dppz equivalent (*42*). Since tight intercalative binding to DNA is necessary to ensure efficient charge injection into the π-stack, we focused our attention towards designing oligonucleotides containing nucleobases that are easier to reduce than thymine or cytosine; it would then be possible to use the well-characterized $[Ru(phen)_2(dppz)]^{2+}$. Oligonucleotides containing 5-fluoro-uracil (FU), which is reported to have a reduction potential of -0.22 V vs. NHE (*43*), were utilized. With a ground state reduction potential

of -0.76 V vs. NHE, $[Ru(phen)_2(dppz)]^+$ should be able to reduce FU with 0.4 V of driving force.

3.3.2 Reductive Quencher. In an oxidative flash/quench scheme, an electron accepting molecule (i.e. $[Ru(NH_3)_6]^{3+}$, $[Co(NH_3)_5Cl]^{2+}$, or methyl viologen) is used. When considering a reductive flash/quench scheme, an electron donating quencher is needed. In our DNA system, this quencher should be water soluble and preferably positively or neutral in charge to avoid electrostatic repulsion from the negatively charged sugar-phosphate backbone. A variety of molecules have been examined for their ability to reductively quench the luminescence of $*[Ru(phen)_2(dppz)]^{2+}$. The results of steady-state luminescence quenching titrations are shown in Table 3.2 and Stern-Volmer plots in Figure 3.4. Examples of the luminescence titrations for catechol and KI are shown in Figure 3.5.

Table 3.2. Fluorescence Quenching Data for $*[Ru(phen)_2(dppz)]^{2+}$ by Electron Donating Molecules.[a]

Quencher	Amount of Quenching	Concentration of Quencher
catechol	74%	200 mM
p-MDMA	73%	3 mM
cyt c (Fe^{2+})	40% (via *Ru lifetime)	200 μM
KI	90%	2.44 M
$[Ru(NH_3)_6]^{2+}$ [b]	89%	1 mM

[a] Experiments were conducted with 5 μM $Ru(phen)_2(dppz)^{2+}$, 1 mM ct-DNA, 10 mM NaCl, 20 mM sodium phosphate, pH 7.8. [b] Approximately 80% $[Ru(NH_3)_6]^{2+}$ and 20% $[Ru(NH_3)_6]^{3+}$.

Some of these electron donors, although they act as reductive quenchers for $*[Ru(phen)_2(dppz)]^{2+}$, possess other characteristics that lead to complications in product analysis. For instance, oxidized p-MDMA, a product of reductive flash/quench, has a

very large, broad absorbance in the visible region centered around 490 nm (Figure 3.6). This complicates any transient absorption studies where one would look for the Ru^{+} species (λ_{max} = 400, 440 nm). Using cyt c-Fe^{2+} as a reductive quencher complicated gel electrophoresis experiments as a result of extensive crosslinking between the DNA and protein. Contaminating $[Ru(NH_3)_6]^{3+}$ was a problem in experiments utilizing $[Ru(NH_3)_6]^{2+}$. The quencher was synthesized in the laboratory by reduction of $[Ru(NH_3)_6]^{3+}$ with a Hg/Zn amalgam. However, by UV-vis analysis, this procedure yielded approximately 80% $[Ru(NH_3)_6]^{2+}$ and 20% $[Ru(NH_3)_6]^{3+}$. Since $[Ru(NH_3)_6]^{3+}$ is an excellent oxidative quencher, any quenching can not be definitively attributed to $[Ru(NH_3)_6]^{2+}$. Significant quantities of KI were needed to observe efficient quenching; however, control experiments using KCl ensure that the observed quenching is not due to decreased $[Ru(phen)_2(dppz)]^{2+}$ binding in the high salt environment. In fact, slight increases in luminescence were observed at high concentrations of KCl. These increases are attributed to a stiffening of the DNA helix and a resulting increase in quantum yield.

Many additional molecules were explored for their ability to reductively quench $*[Ru(phen)_2(dppz)]^{2+}$ but were not effective quenchers. Some of these molecules are listed below in Table 3.3.

Table 3.3. Unsuccessful Electron Donating Quenchers.

hydroquinone	diethylaniline	dimethyltoluidine
diaminobicyclooctane	tetramethylbenzidine	phenothiazine
triethylamine	wurster's blue	citrate
europium chloride	triethanolamine	

3.3.3 Assay for Reductive DNA Damage.

3.3.3.1 Polyacrylamide Gel Electrophoresis. Products of oxidative DNA flash/quench experiments are readily visualized via denaturing polyacrylamide gel electrophoresis (PAGE) after treatment with piperidine or base excision repair (BER) enzymes. There is evidence that reduction of a DNA base would result in either direct or alkaline labile strand breaks that could be visualized by PAGE. To model the reduction of a nucleobase in DNA, Greenberg and coworkers site-selectively generated a 5,6-dihydrothymid-5-yl radical in single-stranded DNA via Norrish type I photocleavage. Direct strand breaks and alkaline labile lesions were visualized by denaturing PAGE (*44*) and attributed to hydrogen atom abstraction from the C1' and C2' position of the adjacent 5'-nucleotide. However, this strand cleavage was only observed under aerobic conditions; when the experiments were performed in the absence of O_2 no direct strand breaks or alkaline labile lesions were observed. This is consistent with previous proposals involving the formation of reactive oxygen species from nucleobase radicals, which subsequently participate in internucleotidyl hydrogen atom abstraction reactions (Figure 3.7) (*45-49*). In addition to the scheme presented in Figure 3.7, generation of free reactive oxygen species has been proposed and damage cause by this species may be seen at bases surrounding the original electron accepting site (*50*).

Recently, Rokita and coworkers, utilizing an internally tethered TMDN analogue and PAGE, observed direct strand scission and alkaline labile lesions at the adjacent thymine 5'-to a BrU site (*22, 23*). Interestingly, in contrast to the work from Greenberg and coworkers, O_2 was not required for this cleavage; damage was observed after irradiation under both aerobic and anaerobic conditions. Migration of the electron within the DNA duplex was suggested as addition of nitrous oxide (sat.) to scavenge hydrated

electrons had no effect on the damage products. Addition of a hydroxyl radical scavenger also had no effect on the damage products. Taken in combination with the damage observed in single-stranded DNA after site specific generation of a 5,6-dihydrothymid-5-yl radical, these results suggest that reduction of a DNA base does result in direct strand breaks and alkaline labile lesions that can be visualized by denaturing PAGE ; furthermore, the damage products most likely involve strand cleavage not at the reduced base, but rather at the 5'-side of the reduced nucleobase.

Results from denaturing PAGE experiments using $[Ru(phen)_2(dppz)]^{2+}$ and catechol as the reductive quencher are shown in Figure 3.8. The double stranded oligonucleotide contains one FU site which is predicted to be the site easiest to reduce. No direct strand breaks are observed as seen in the samples not treated following irradiation either under aerobic or anaerobic conditions. Following treatment with piperidine, damage is observed at all guanines with no specificity for single or double guanine sites. Following piperidine treatment damage is observed at FU, however, this damage is also present in the dark controls indicating that the damage is not the result of flash/quench chemistry but rather a sensitivity of the site to piperidine treatment. Samples treated with the BER enzyme endo(III) do not display any damage following either aerobic or anaerobic irradiation. Endo(III) recognizes oxidized pyrimidines such as 5-hydroxycytosine and thymine glycol (*51*). Treatment with 10% aniline was also examined as a method to liberate reductive damage products since aniline is used to reveal oxidative damage in RNA. No damage at FU was observed after aniline treatment (data not shown). Importantly, the 5'-GG-3' guanine doublet present in the oligonucleotide serves as an internal control for oxidative damage. The selective damage

at the 5'-G of the 5'-GG-3' guanine doublet consistent with DNA mediated HT is not observed. This indicates that, in fact, no Ru(III) is generated and the quenching is indeed occurring in a reductive fashion.

In addition to catechol, KI was also utilized as a reductive quencher. Initial results from PAGE experiments were quite promising. Following treatment with piperidine, irradiated samples displayed increased amounts of damage above dark controls at both a uracil and FU site over a range of KI concentration (Figure 3.9). This result was seen twice on this oligonucleotide; however, these results were not reproducible. Further changes in the oligonucleotide, metal and quencher concentration, temperature and buffer did not reproduce the results. Figure 3.10 shows an example of a gel where this damage was not reproducible. In this gel damage is observed at both uracil residues in all samples that have been piperidine treated. Dark controls, and even lanes with KCl as a control, contain this damage and there are no observable increases in damage upon irradiation. Lanes which had not been treated with piperidine show no damage, again suggesting that the damage observed is due to the lability of uracil and FU to piperidine treatment. This gel also contains control lanes which utilized $[Ru(NH)_6]^{3+}$ as an oxidative quencher to ensure proper π-stack alignment under the experimental conditions. The characteristic 5'-G of the 5'-GG-3' guanine doublet is observed.

Using PAGE as the method of analysis, $[Ru(phen)_2(dppz)]^{2+}$ was also used in combination with the electron donors p-MDMA, cyt c (Fe^{2+}), and $[Ru(NH_3)_6]^{2+}$; no direct strand breaks or alkaline/BER labile sites were observed. Intercalating metal complexes besides $[Ru(phen)_2(dppz)]^{2+}$ were utilized in a flash/quench scheme in an attempt to reduce the DNA bases. Analysis by PAGE did not yield direct strand breaks or

alkaline/BER sensitive lesions. These metal complexes along with the electron donating quencher, wavelength of photoexcitation, and ground state reduction potential of the metal used are displayed in Table 3.4 below.

Table 3.4. Unsuccesful Reductive Flash/Quench Systems.

Photoreductant	Reductive Quencher	Excitation (nm)	E_{red} vs. NHE
$[Re(Me_2\text{-phen})(CO)_3(im)]Cl$	$K_3Fe(CN)_6$	376	-1.0 V
$[Re(Me_2\text{-phen})(CO)_3(im)]Cl$	$[Ru(NH_3)_6]Cl_2$	376	-1.0 V
$Re(dppz)(CO)_3(im)]Cl$	catechol	364	-0.76 V
$[Ru(bpy)_2(dpq)]Cl_2$	$[Ru(NH_3)_6]Cl_2$	450	-1.04 V
$[Ru(bpy)_2(dpq)]Cl_2$	catechol	450	-1.04 V
$[Ru(bpy)_2(dpqC)]Cl_2$	$[Ru(NH_3)_6]Cl_2$	450	-1.07 V
$[Ru(bpy)_2(dpqC)]Cl_2$	catechol	450	-1.07 V

3.3.3.2 High Performance Liquid Chromatography. HPLC offers an alternative to PAGE analysis and this method was explored as a way to detect reductive DNA damage. Following irradiation of flash/quench samples, nuclease P1 and snake venom phosphodiesterase were used to digest the double stranded oligomer, and the resultant nucleosides were analyzed by HPLC. This assay was utilized to explore the flash/quench reaction between $[Ru(phen)_2(dppz)]^{2+}$, $[Ru(bpy)_2(dpq)]^{2+}$, or $[Ru(bpy)_2(dpqC)]^{2+}$ and KI or p-MDMA as the reductive quencher. The chromatograms were analyzed for the appearance or disappearance of peaks or changes in the absorption properties of existing peaks. These changes were not observed following irradiation of the flash/quench samples at 442 nm for up to 1 h.

3.3.3.3 Electron Paramagnetic Resonance. EPR spectroscopy has been utilized to monitor formation of DNA radicals. Both cytosine and thymine anion radicals have

been observed previously by EPR using solutions of oligonucleotides γ-irradiated and subsequently frozen at 77 K. The cytosine anion radical and thymine radical anion possess nearly identical EPR spectra arising from a single large hyperfine coupling to H6. However, using site specific deuteration to generate [6-^{2}H]-thymidine residues, the EPR spectrum for a mixed sequence DNA was found to result from 85% cytosine anion radical and 15% thymine radical anion (*52*).

Flash/quench experiments utilizing $[Ru(phen)_2(dppz)]^{2+}$ and KI with uracil or FU containing oligonucleotides were conducted. The sample was irradiated with white light while freezing the sample in liquid nitrogen. EPR was then performed at 77 K. The results are shown in Figure 3.11; no signal was observed. These EPR experiments were also repeated using a HeCd laser to irradiate the samples specifically at 442 nm. Again, irradiation was performed as the sample was frozen in liquid nitrogen. No signal was observed.

3.3.3.4 Transient Absorption Spectroscopy. Transient absorption spectroscopy has been utilized to probe reductive flash/quench systems for transient species specifically reduced DNA bases. The samples consisted of 20 μM $[Ru(phen)_2(dppz)]^{2+}$, 20 μM oligonucleotides (sequence shown in Figure 3.11 where U is either uracil or FU) and 1 M KI or 4 mM p-MDMA. Samples were excited at 470 nm and emission was monitored at 400 and 440 nm, two known absorption maxima for $[Ru(phen)_2(dppz)]^{+}$. The absorption spectum of $[Ru(phen)_2(dppz)]^{+}$ was determined in acetonitrile using triethanolamine as a sacrificial reductive quencher (Figure 3.12). Using either KI or p-MDMA the transient spectra for the reductive flash/quench samples were dominated by oxidized quencher. Although observation of oxidized quencher does indicate quenching

of *[Ru(phen)$_2$(dppz)]$^{2+}$, unfortunately the spectra of the oxidized quenchers overlaps the area where we would expect to observe the Ru$^+$ species. There was also no indication of the higher energy absorbing reduced DNA species.

3.4 DISCUSSION

The flash/quench technique has proved to be an incredibly useful technique for examining HT in DNA. The experiments described here aim to apply this technique to study reduction of DNA and ET through the base stack. The Ru(II) complex frequently utilized in oxidative flash/quench, [Ru(phen)$_2$(dppz)]$^+$, does not possess the necessary driving force to reduce the naturally occurring DNA bases, thus base analogs such as FU have been incorporated into oligonucleotides. Although there is a 0.4 V driving force for the reduction of FU by the ruthenium complex, reduced DNA products were not observed by PAGE, HPLC, EPR, or transient absorption spectroscopy. Steady-state luminescence quenching studies indicate *[Ru(phen)$_2$(dppz)]$^{2+}$ is quenched by several electron donating molecules, and there is evidence in the literature of reduction of a uracil derivative leading to strand scission visible by PAGE. Importantly, in these experiments, cleavage was not observed at the reduced base but rather at the 5'-base. The studies by both Greenberg and coworkers and Rokita and coworkers had a thymine positioned 5' to the reduced base. In the studies presented here, an adenine was located 5' to the FU; therefore, the identity of the 5'-nucleotide may play a crucial role in facilitating strand cleavage.

Given that the dppz complex of ruthenium possesses the necessary driving force to reduce FU and DNA strand cleavage has been observed previously using a site-

specifically generated 5,6-dihydrothymid-5-yl radical and a naphthalene derivative, why were we not successful in applying a reductive flash/quench scheme? Recently, it has been demonstrated that back electron transfer (BET) can play a very significant role in determining the yield of charge propagation to a distant site to yield permanent DNA damage products. Perhaps the clearest example is with thionine, a potent photooxidant (~ 2 V vs. NHE) that produces no detectable DNA damage owing to its fast rate of BET (*53*). As another example, in identical DNA duplexes containing different tethered oxidants, different yields of oxidative damage at a distal 5'-GG-3' double guanine site as compared to a proximal 5'-GG-3' site are observed (*54*). These differences in relative oxidative damage are attributed to variations in BET.

It has also been demonstrated that when using a dppz complex of ruthenium, in combination with an oxidative flash/quench technique, a non-productive back reaction with reduced quencher is possible in the case of $[Ru(NH_3)_6]^{3+}$ (*55*). In this instance the ruthenium complex was covalently tethered to the 5'-end of the DNA duplex and back reaction with reduced quencher, $[Ru(NH_3)_6]^{2+}$, was greatest with guanine at the charge injection site. In the case of guanine at the injection site, following injection the charge is fairly localized at that particular site allowing for a back reaction with reduced quencher. In the experiments presented in this Chapter the ruthenium complex is non-covalently bound to DNA. However, it is still feasible to imagine a back reaction with oxidized quencher at the injection site. This back reaction would inhibit charge propagation to yield DNA damage products and may also explain the lack of reaction observed by the various techniques employed.

One potential way to overcome fast BET would be to use a fast trap of reductive damage. The trapping of a DNA base anion radical by H_2O and/or O_2 may be slower than the rate of BET; in this instance, the use of a faster trap may allow the detection of reduction products. A cyclopropylamine-modified guanine (^{CP}G) has been successfully incorporated into DNA and utilized as a fast trap of oxidative damage (*54*). Following long-range CT from a DNA-bound oxidant to generate the ^{CP}G cation radical, the cyclopropyl group undergoes rapid ring opening. Although the rate of ring opening of the cation radical in DNA is unknown, the rate constant for ring opening of the neutral *N*-alkylcyclopropylamine radical is 7×10^{11} s^{-1} (*56*). In comparison, trapping of the guanine cation radical by H_2O and/or O_2 occurs with a rate of 10^4 s^{-1}. Use of this ^{CP}G fast trap has elucidated the role of BET in hindering long-range oxidative damage. For instance, no long-range oxidative damage was observed using tethered thionine as the photooxidant. Previous work utilizing thionine and poly[dGdC] demonstrated a rate of forward CT in the femtosecond regime; similarly, however, the rate of BET is equally rapid. However, ring opening of ^{CP}G was observed following photoactivation of the tethered thionine oxidant underscoring the ability of BET to hinder observation of long-range CT damage.

Recently, a cyclopropylamine-modified cytosine (^{CP}C) has been synthesized (*57*) and may be applicable as a fast trap for excess electrons injected into the double helix. The reduction potential of this modified base is estimated to be lower than cytosine and thymine; therefore, the aforementioned ruthenium complexes may possess the necessary driving force to reduce the modified nucleobase. Future work will include incorporation of the ^{CP}C nucleotide into DNA and monitoring for ring opening following photoactivation of various reductants including dppz complexes of ruthenium.

3.5 REFERENCES

(1) (a) Boon, E. M., and Barton, J. K. (2002) *Curr. Opin. Struct. Biol*. *12*, 320. (b) Delaney, S., and Barton, J. K. (2003) *J. Org. Chem*. *68*, 6475.

(2) Schuster, G. B. (2000) *Acc. Chem. Res. 33*, 253.

(3) Giese, B. (2002) *Ann. Rev. Biochem. 71*, 51.

(4) Lewis, F. D., Letsinger, R. L., and Wasielewski, M. R. (2001) *Acc. Chem. Res*. *34*, 159.

(5) Hall, D. B., Holmlin, R. E., and Barton, J. K. (1996) *Nature 382*, 731.

(6) Steenken, S., and Jovanovic, S. V. (1997) *J. Am. Chem. Soc*. *119*, 617.

(7) Saito, I., Takayama, M., Sugiyama, H., Nakatani, K., Tsuchida, A., and Yamamoto, M. (1995) *J. Am. Chem. Soc*. *117*, 6406.

(8) Stemp, E. D. A., Arkin, M. R., and Barton, J. K. (1997) *J. Am. Chem. Soc*. *119*, 2921.

(9) Núñez, M. E., Noyes, K. T., Gianolio, D., McLaughlin, L. W., and Barton, J. K. (2000) *Biochemistry 39*, 6190.

(10) Hall, D. B., Kelley, S. O., and Barton, J. K. (1998) *Biochemistry 37*, 15933.

(11) Gasper, S. M., and Schuster, G. B. (1997) *J. Am. Chem. Soc*. *119*, 12762.

(12) Nakatani, K., Dohno, C., and Saito, I. (1999) *J. Am. Chem. Soc*. *121*, 10854.

(13) Meggers, E., Kusch, D., Spichty, M., Wille, U., and Giese, B. (1998) *Angew. Chem. Int. Ed*. *37*, 460.

(14) Steenken, S., Telo, J. P., Novais, H. M., and Candeias, L. P. (1992) *J. Am. Chem. Soc*., *114*, 4701.

(15) (a) Wesolowski, S. S., Leininger, M. L., Pentchev, P. N., Scaefer, H. F. (2001) *J. Am. Chem. Soc*., *123*, 4023. (b) Li, X., Cai, Z., Sevilla, M. D. (2002) *J. Phys. Chem. A 106*, 1596. (c) Steenken, S. (1992) *Free Radical Res. Commun. 16*, 349.

(16) Voityuk, A. A., Michel-Beyerle, M.-E., and Roesch, N. (2001) *Chem. Phys. Lett. 342*, 231.

(17) (a) Bernhard, W. A. (1981) *Adv. Radiat. Biol*. *9*, 199. (b) Symons, M. C. R. (1987) *J. Chem. Soc., Faraday Trans*., *83*, 1.

(18) Lewis, F. D., Liu, X., Wu, Y., Miller, S. E., Wasielewski, M. R., Letsinger, R. L., Sanishvii, R., Joachimiak, A., Tereshko, V., and Egli, M. (1999) *J. Am. Chem. Soc. 121*, 9905.

(19) Schwögler, A., Burgdorf, L.T., and Carell, T. (2000) *Angew. Chem. Int. Ed. 39*, 3918.

(20) (a) Breeger, S., Hennecke, U., and Carell, T. (2004) *J. Am. Chem. Soc. 126*, 1302.

(b) Haas, C., Kraeling, K.; Cichon, M., Rahe, N., and Carell, T. (2004) *Angew. Chem. Int. Ed. 43*, 1842.

(21) Giese, B., Carl, B., Carl, T., Carell, T., Behrens, C., Hennecke, U., Schiemann, O., and Feresin, E. (2004) *Angew. Chem. Int. Ed*. 43, 1848.

(22) Ito, T., and Rokita, S. (2003) *J. Am. Chem. Soc. 125*, 11480.

(23) Ito, T., and Rokita, S. (2004) *Angew. Chem. Int. Ed. 43*, 1839.

(24) O'Neill, M. A., and Barton, J. K. (2002) *Proc. Natl. Acad. Sci. U. S. A. 99*, 16543.

(25) Lewis, F. D., Liu, X., Miller, S. E., Hayes, R. T., and Wasieleski, M. R. (2002) *J. Am. Chem. Soc. 124*, 11280.

(26) (a) Manoharan, M., Tivel, D. L., Zhao, M., Nafisi, K., and Netzel, T. (1995) *J. Phys. Chem. 99*, 17461. (b) Amann, N., Pandurski, E.; Fiebig, T., and Wagenknecht, H.-A. (2002) *Angew. Chem. Int. Ed. 41*, 2978.

(27) Chang, I.-J., Gray, H. B., and Winkler, J. R. (1991) *J. Am. Chem. Soc. 113*, 7056.

(28) Wagenknecht, H. A.; Stemp, E. D. A.; Barton, J. K. (2000) *Biochemistry 39*, 5483.

(29) Wagenknecht, H.A.; Rajski, S. R.; Pascaly, M.; Stemp, E. D. A.; Barton, J. K. (2001) *J. Am. Chem. Soc. 123*, 4401.

(30) Núñez, M. E., Hall, D. B., and Barton, J. K. (1999) *Chem. Biol*. *6*, 85.

(31) Williams, T. T., Odom, D. T., and Barton, J. K. (2000) *J. Am. Chem. Soc*. *122*, 9048.

(32) Hall, D. B., and Barton, J. K. (1997) *J. Am. Chem. Soc*. *119*, 5045.

(33) (a) Bhattacharya, P. K., and Barton, J. K. (2001) *J. Am. Chem. Soc*. *123*, 8649. (b) Bhattacharya, P. K., Cha, J., and Barton, J. K. (2002) *Nuc. Acids Res*. *30*, 4740.

(34) Wilker, J. J., Dmochowski, I. J., Dawson, J. H., Winkler, J. R., and Gray, H. B. (1999) *Angew. Chem. Int. Ed. 96*, 12987.

(35) (a) Amouyal, E., Homsi, A., Chambron, J.-C., and Sauvage, J.-P. (1990) *J. Chem. Soc., Dalton Trans*. 1841. (b) Strouse, G. F., Anderson, P. A., Schoonover, J. R., Meyer, T. J., and Keene, F. R. (1992) *Inorg. Chem*. *31*, 3004. (c) Anderson, P. A., Deacon, G. B., Haarman, K. H., Keene, F. R., Meyer, T. J., Reitsma, D. A., Skelton, B. W., Strouse, G. F., Thomas, N. C., and Treadway, J. A. (1995) *Inorg. Chem*. *34*, 6145.

(36) Dupueur, C. M., and Barton, J. K. (1997) *Inorg. Chem*. *36*, 33.

(37) (a) Holmlin, R. E., and Barton, J. K. (1995) *Inorg. Chem*. *34*, 7. (b) Holmlin, R. E., Stemp, E. D. A., and Barton, J. K. (1996) *J. Am. Chem. Soc*. *118*, 5236.

(38) (a) Beaucage, S. L., and Caruthers, M. H. (1981) *Tetrahedron Lett*. *22*, 1859. (b) Goodchild, J. (1990) *Bioconjugate Chem. 1*, 165.

(39) Warshaw, M. M., and Tinoco, I. Jr. (1966) *J. Mol. Biol*. *20*, 29.

(40) Sambrook, J., Fritsch, E. F., and Maniatis, T. (1989) *Molecular Cloning: A Laboratory Manual*, 2nd ed.; Cold Spring Harbor Laboratory: New York.

(41) Friedman, A. E., Chambron, J.-C., Sauvage, J.-P., Turro, N. J., and Barton, J. K. (1990) *J. Am. Chem. Soc*. *112*, 4960.

(42) Delaney, S., Pascaly, M., Bhattacharya, P. K., Han, K., and Barton, J. K. (2002) *Inorg. Chem*. *41*, 1966.

(43) Wang, J. (1987) *Analyst 112*, 247.

(44) Barvian, M. R., and Greenberg, M. M. (1995) *J. Am. Chem. Soc. 117*, 8291.

(45) Deeble, D. J., Schulz, D., and von Sonntag, C. (1986) *Int. J. Radiat. Biol. 49*, 915.

(46) Jones, G. D. D., and O'Neill, P. (1990) *Int. J. Radiat. Biol. 57*, 1123.

(47) Greenberg, M. M. (1998) *Chem. Res. Toxicol. 11*, 1235.

(48) Burrows, C. J., and Muller, J. G. (1998) *Chem. Rev. 98*, 1109.

(49) Pogozelski, W. K., and Tullius, T. D. (1998) *Chem. Rev. 98*, 1089.

(50) Greenberg, M. M., Barvian, M. R., Cook, G. P., Goodman, B. K., Matray, T. J., Tronche, C., and Venkatesan, H. (1997) *J. Am. Chem. Soc. 119*, 1828.

(51) David, S. S., and Williams, S. D. (1998) *Chem. Rev. 98*, 1221.

(52) Cullis, P. M., Evans, P., and Malone, M. E. (1996) *Chem. Comm. 96*, 986.

(53) Dohno, C., Stemp, E. D. A., and Barton, J. K. (2003) *J. Am. Chem. Soc*. *125*, 9586.

(54) Williams, T. T., Dohno, C., Stemp, E. D. A., and Barton, J. K. (2004) Manuscript submitted.

(55) Yoo, J., Delaney, S., Stemp, E. D. A., and Barton, J. K. (2003) *J. Am. Chem. Soc*. *125*, 664.

(56) Musa, O. M., Horner, J. H., Shahin, H., and Newcomb, M. (1996) *J. Am. Chem. Soc. 118*, 3862.

(57) Shao, F. (2004) Unpublished results in our laboratory.

Reductive
Flash/Quench

Oxidative
Flash/Quench

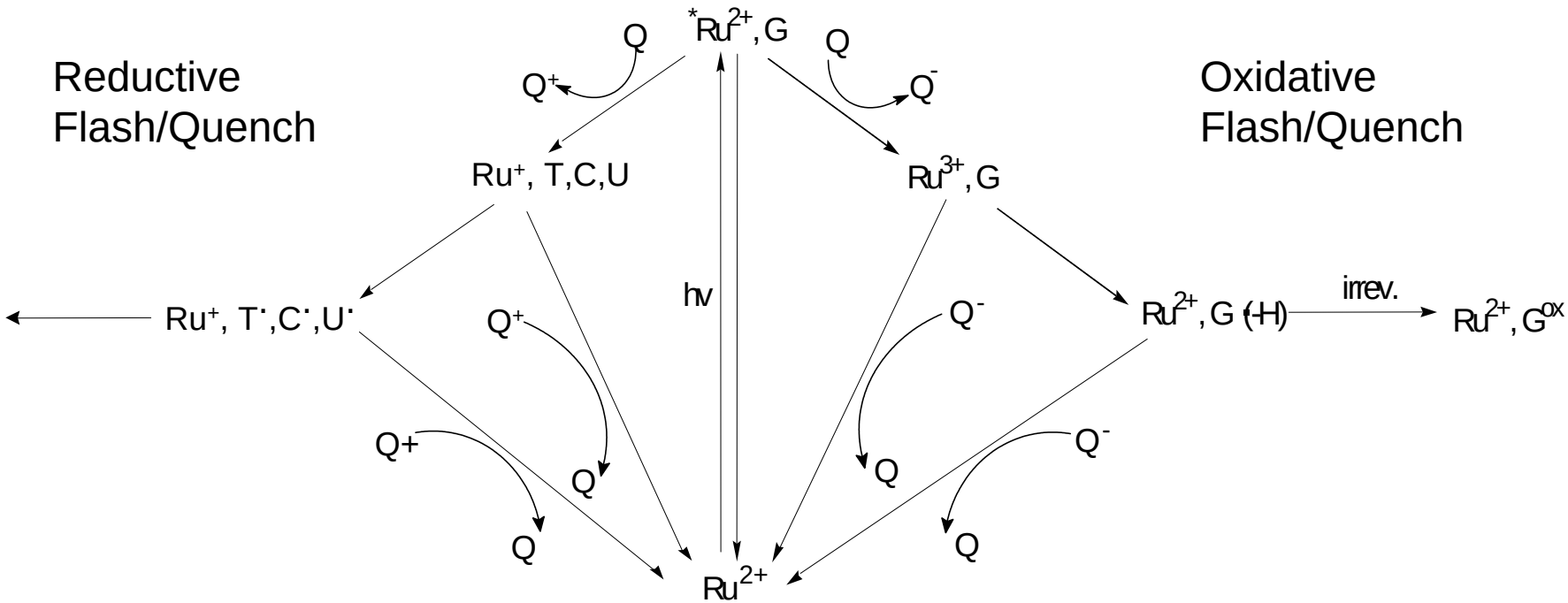

Q = KI, catechol, p-MDMA

Q = $Ru(NH_3)_6^{3+}$, $Co(NH_3)_5Cl^{2+}$, MV^{2+}

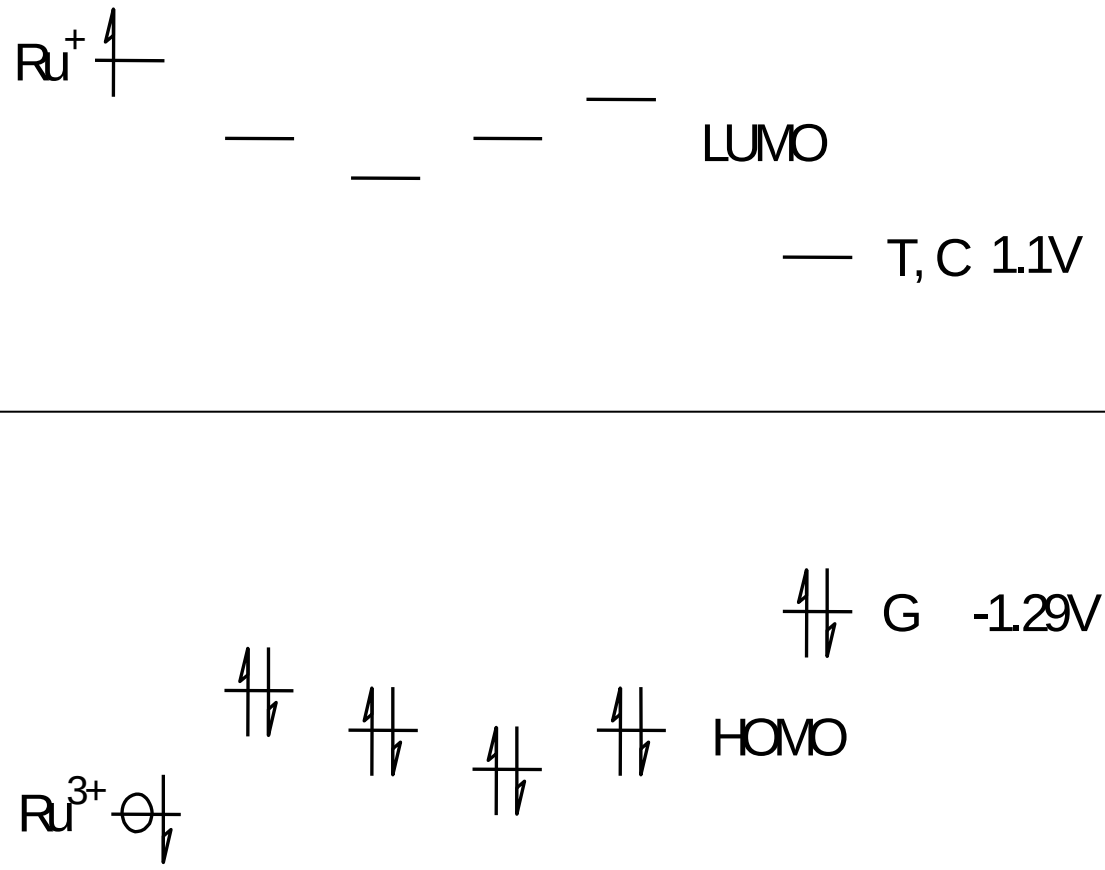

Figure 3.1. Schematic of molecular orbitals involved in DNA mediated CT reactions. Top portion shows the molecular orbitals (LUMO's) involved in ET from a Ru^{+} species to a reducible nucleobase. Since these orbitals are unoccupied, an electron can be directly transferred. The lower portion shows the molecular orbitals (HOMO's) involved in HT from guanine to Ru(III). Since the orbitals are fully occupied, an electronic hole must be transferred.

Figure 3.2. Schematic illustration of oxidative and reductive flash/quench methodology. The cycle is initiated by visible light, which excites the intercalated Ru(II) complex. In oxidative flash/quench, the excited Ru(II) complex, *Ru(II), is then quenched by a nonintercalating electron accepting quencher, Q, such as $[Ru(NH_3)_6]^{3+}$, methyl viologen, or $[Co(NH_3)_5Cl]^{2+}$ to form Ru(III) *in situ*. This species can be reduced back to Ru(II) either through recombination with reduced quencher (Q^-) or by HT to guanine. The oxidized guanine radical can then return to its resting state by reaction with reduced quencher or undergo further reaction to form a family of oxidative products, G_{ox}. It is proposed that the flash/quench technique can also be used with an electron donating molecule to form a Ru^+ species. Once formed, this Ru^+ species may be able to reduce DNA nucleobases with sufficiently low reduction potentials.

Flash/Quench Scheme

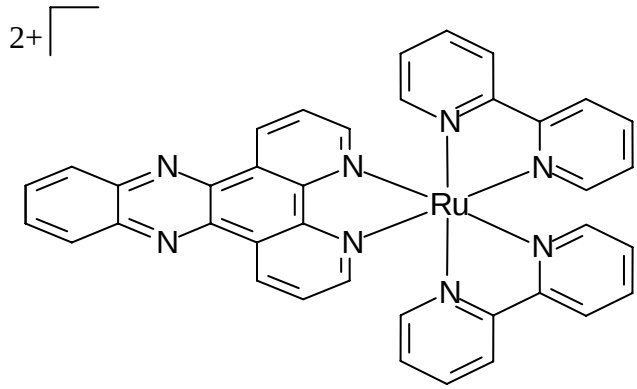

$Ru(bpy)_2(dppz)^{2+}$

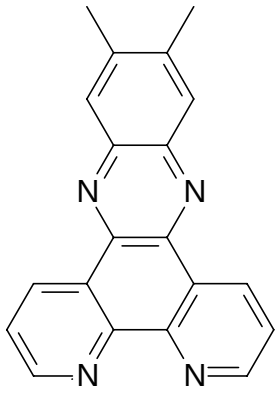

dppx

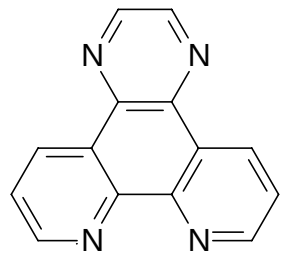

dpq

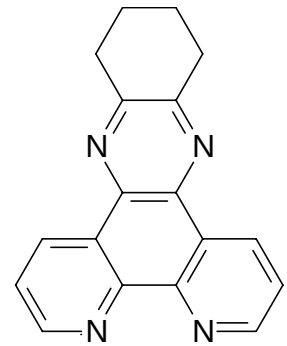

dpqC

Figure 3.3. Shown above is $[Ru(bpy)_2(dppz)]^{2+}$, the parent complex. Below is shown the derivatives of the dppz ligand utilized in these studies: dppx, dpq and dpqC where dppx = 7,8-dimethyldipyridophenazine, dpq = dipyridoquinoxaline and dpqC = dipyrido-6,7,8,9-tetrahydrophenazine.

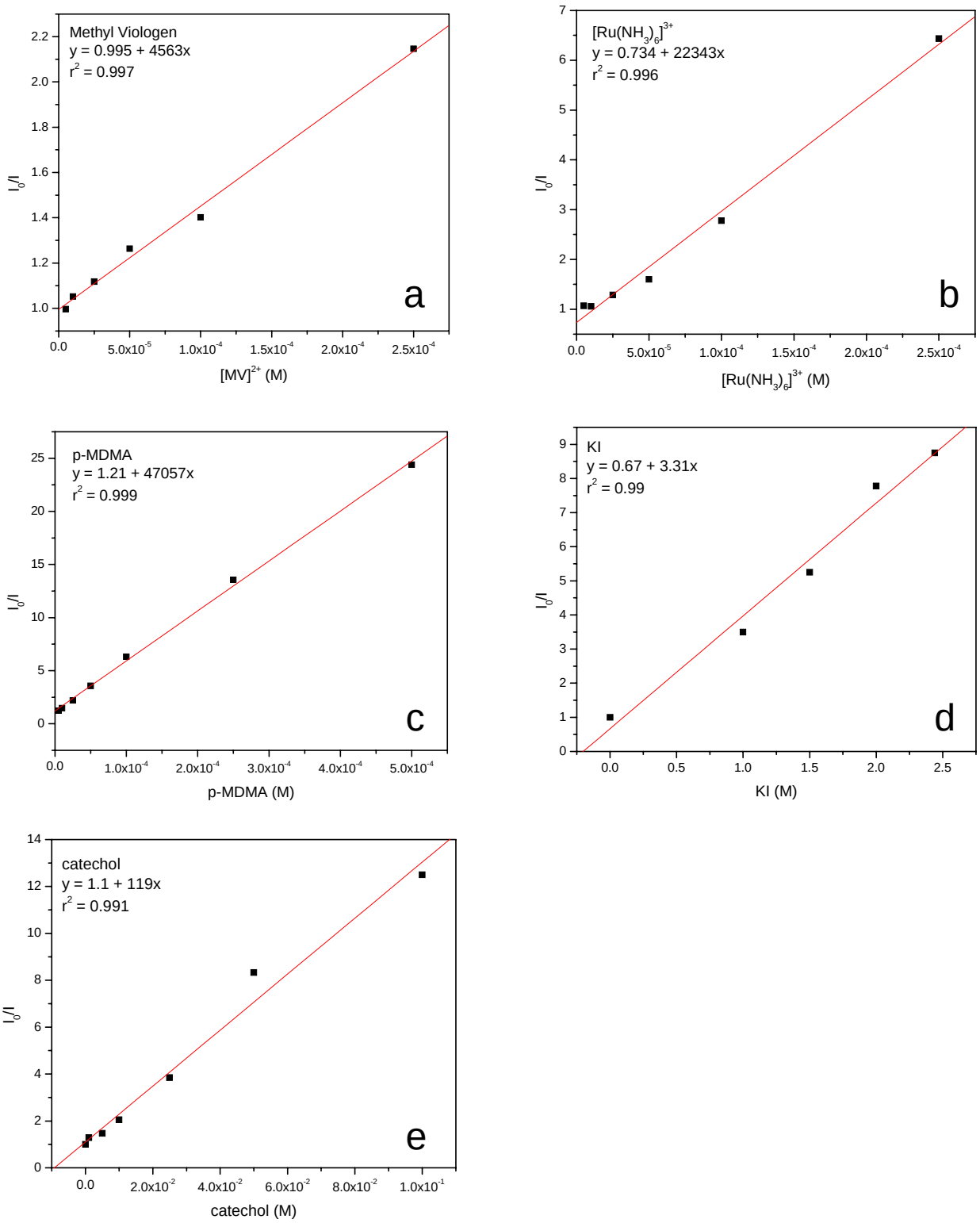

Figure 3.4. Stern-Volmer plots for quenching of 15 μM *$[Ru(phen)_2(dppz)]^{2+}$ using the oxidative quenchers a) methyl viologen and b) $[Ru(NH_3)_6]^{3+}$ and the reductive quenchers c) p-MDMA d) KI and e) catechol.

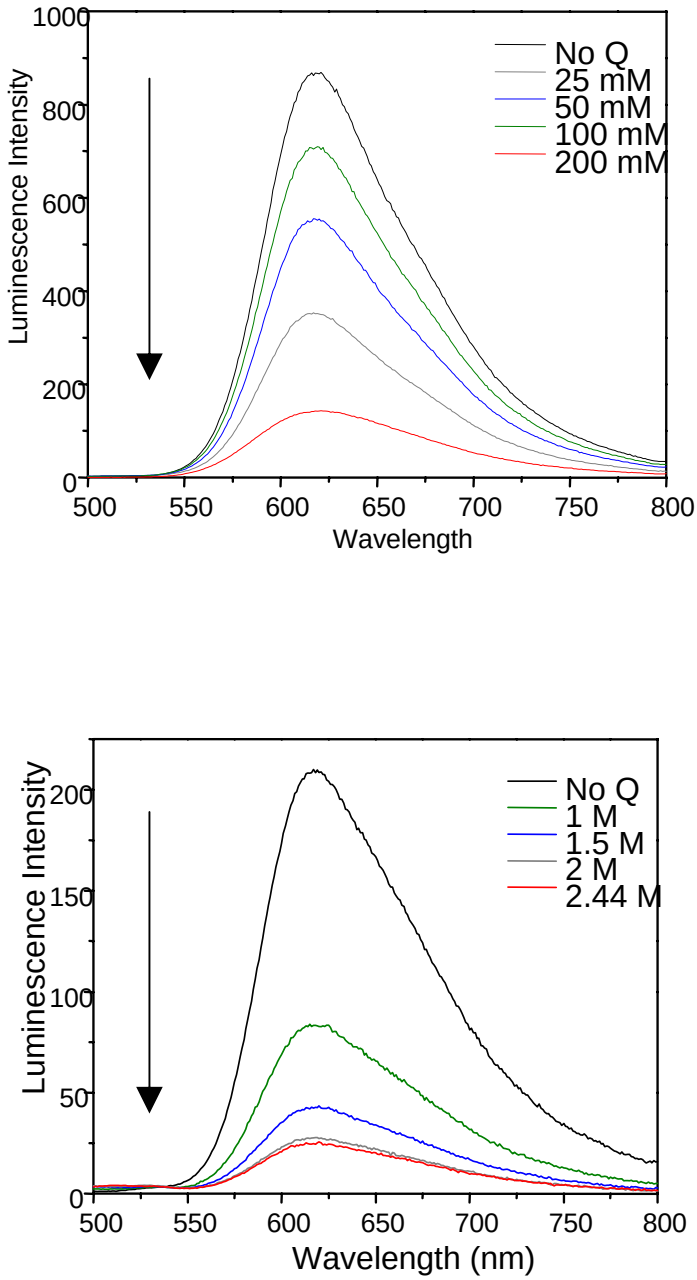

Figure 3.5. Steady-state fluorescence quenching titrations of *$[Ru(phen)_2(dppz)]^{2+}$ in a reductive fashion utilizing catechol as a reductive quencher (top) and KI (bottom). Samples contained 15 µM $[Ru(phen)_2(dppz)]^{2+}$, 1 mM nucleotides ct-DNA, 10 mM NaCl, 20 mM sodium phosphate pH 7.8. Quencher concentrations are indicated in figure legend.

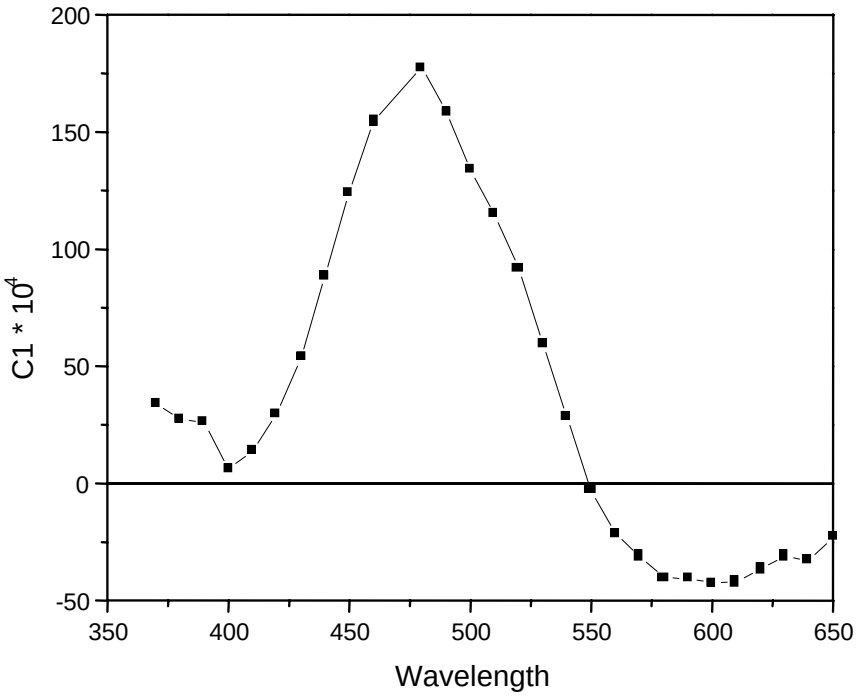

Figure 3.6. Transient absorption spectrum showing oxidized p-MDMA. Sample contained 20 μM $[Ru(phen)_2(dppz)]^{2+}$, 1 mM nucleotides ct-DNA, 4 mM p-MDMA, 10 mM NaCl, 20 mM sodium phosphate pH 7.8.

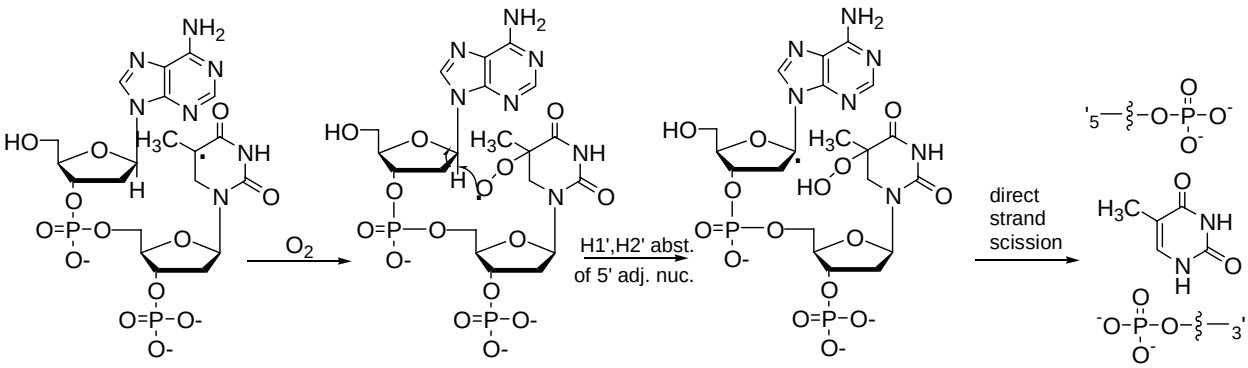

Figure 3.7. Schematic showing formation of reactive oxygen species from nucleobase radicals, which subsequently participate in internucleotidyl hydrogen atom abstraction reactions to yield DNA strand breaks.

5'-GTAGCGACGATACT-3'
3'-CATGGCTGCUATCA-5'*

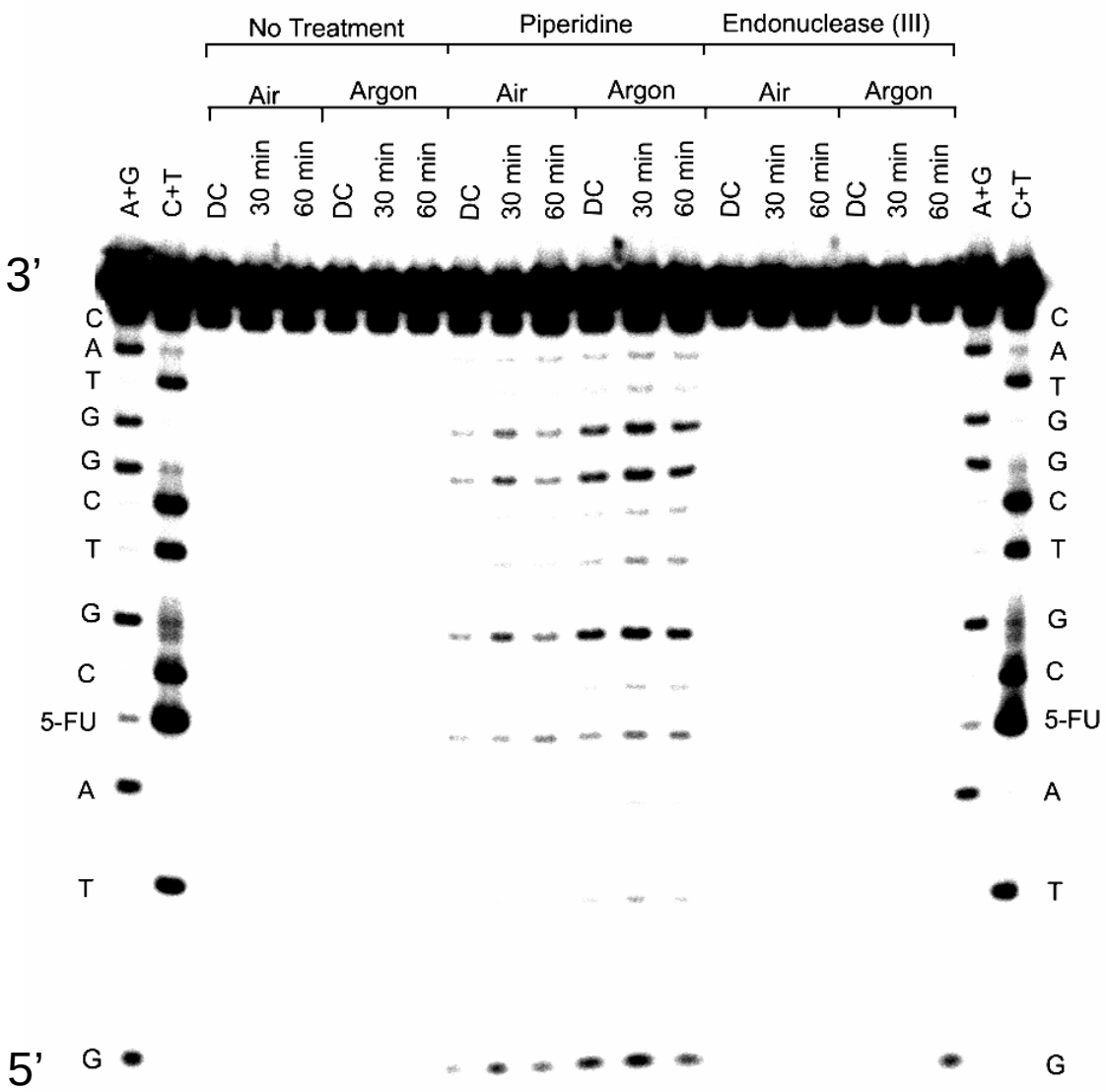

Figure 3.8. Shown above is sequence of oligonucleotides used for electrophoresis experiments where U = FU. Site of ^{32}P labeling is indicated by *. Shown below is the autoradiogram after irradiation of the oligonucleotide in the presence of $Ru(bpy)_2(dppz)^{2+}$ and catechol. Lanes 3-8, 9-14 and 15-20 show damage obtained after no treatment, piperidine and endonuclease(III) treatment, respectively. Lanes 3, 4, 5, 9, 10, 11 and 14, 15, 16 show damage after irradiation in air while lanes 6, 7, 8, 12, 13, 14 and 18, 19, 20 display DNA damage after irradiation under argon. Lanes 3, 6, 9, 12, 15, and 18 display oligonucleotide damage for samples containing $Ru(bpy)_2(dppz)^{2+}$, catechol and DNA, but were not irradiated. Irradiation times (442 nm) are indicated on gel. Samples contain 8 μM oligonucleotide, 16 μM metal, and 1 mM catechol. Lanes 1, 21 and 2, 22 show the damage patterns after Maxam-Gilbert sequencing reactions A+G and C+T, respectively.

5'-GTAGATACGATACG-3'
3'-CATCUATGC$_{FU}$ATGA-5'*

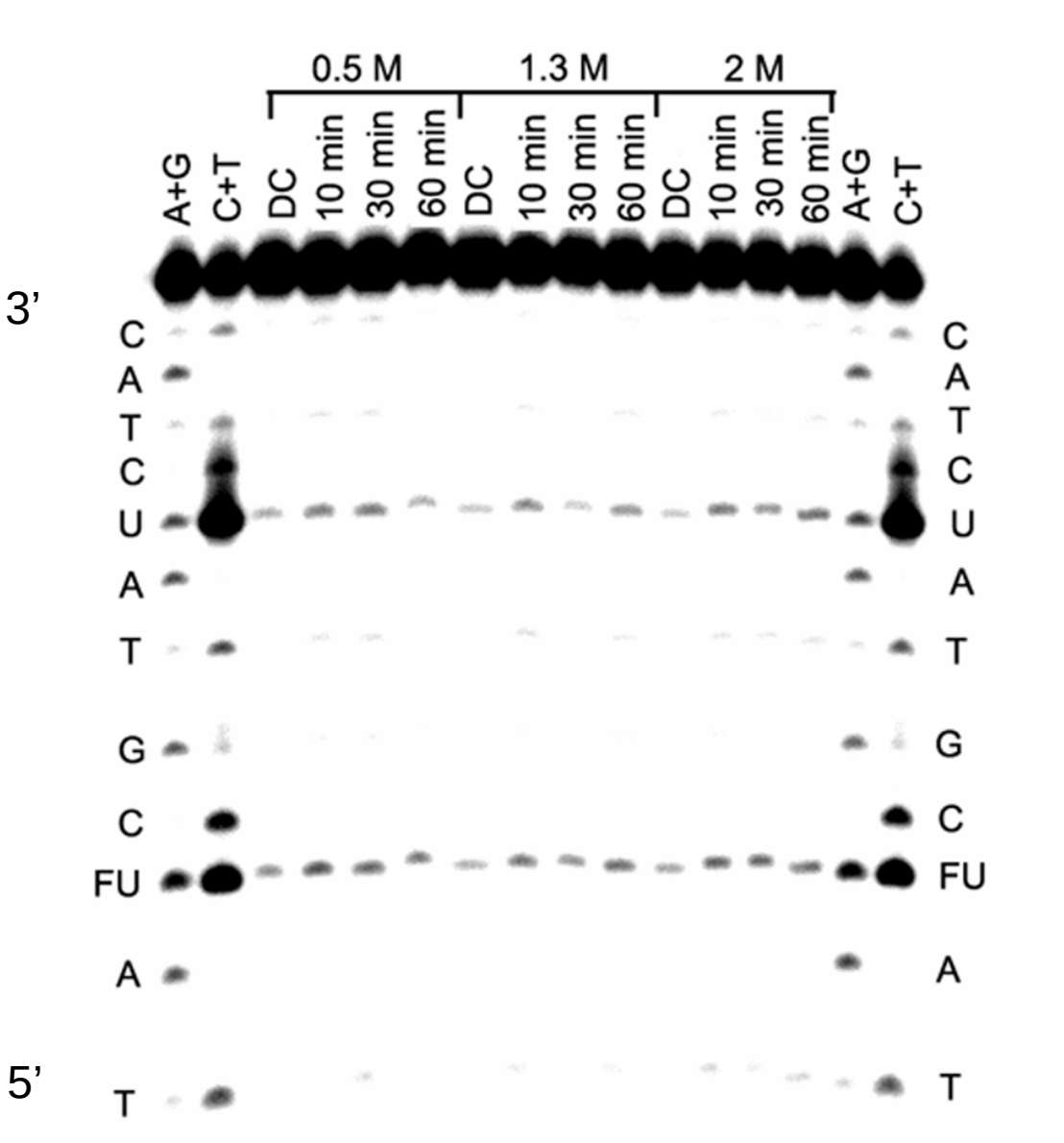

Figure 3.9. Shown above is sequence of oligonucleotides used for electrophoresis experiments. Site of ^{32}P labeling is indicated by *. Shown below is the autoradiogram after irradiation of the oligonucleotide in the presence of $Ru(phen)_2(dppz)^{2+}$ and KI. Lanes 3, 7, and 11 display oligonucleotide damage for samples containing $Ru(phen)_2(dppz)^{2+}$, KI and DNA, but were not irradiated. Lanes 4, 8, 12, and 5, 9, 13 and 6, 10, 14 display oligonucleotide damage after reductive flash/quench irradiation of samples for increasing periods of time: 10, 30 and 60 min, respectively. Samples contain 8 μM oligonucleotide, 16 μM metal. Lanes 3-6, 7-10 and 11-14 utilize 0.5 M, 1.3 M and 2 M KI, respectively. Lanes 1, 15 and 2, 16 show the damage patterns after Maxam-Gilbert sequencing reactions A+G and C+T, respectively.

5'-GTAGATACGATACG-3'
3'-CATCUATGCUATGA-5'*

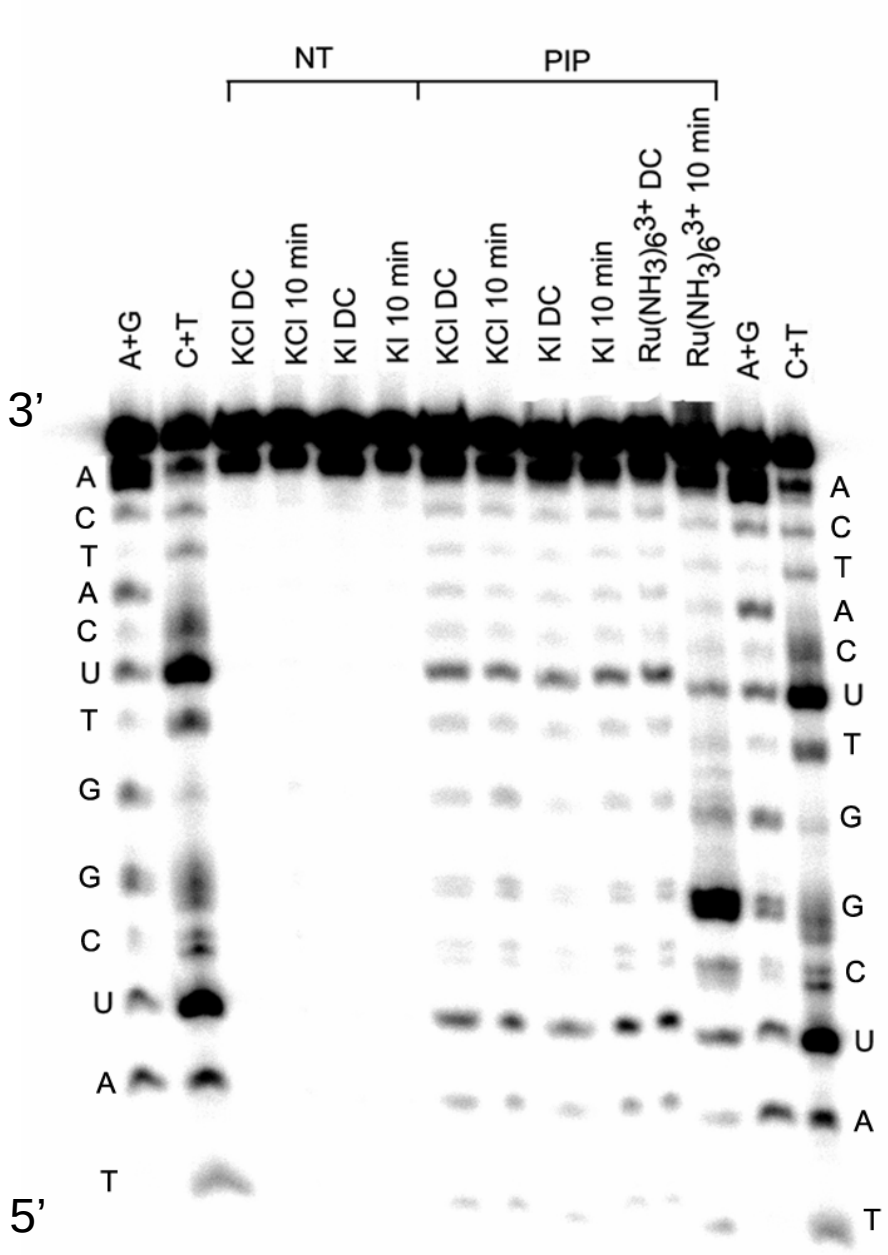

Figure 3.10. Shown above is sequence of oligonucleotides used for electrophoresis experiments. Site of ^{32}P labeling is indicated by *. Shown below is the autoradiogram after irradiation of the oligonucleotide in the presence of $Ru(phen)_2(dppz)^{2+}$ and KI (lanes 5, 6, 9, and 10). Lanes 3, 4, 7, and 8 display oligonucleotide damage for samples containing $Ru(phen)_2(dppz)^{2+}$, KCl and DNA. Lanes 11, 12 display oligonucleotide damage after oxidative flash/quench irradiation of samples utilizing $[Ru(NH_3)_6]^{3+}$ as the oxidative quencher. Samples contain 8 μM oligonucleotide, 16 μM metal and 1 M KCl or KI. Lanes 1, 13 and 2, 14 show the damage patterns after Maxam-Gilbert sequencing reactions A+G and C+T, respectively.

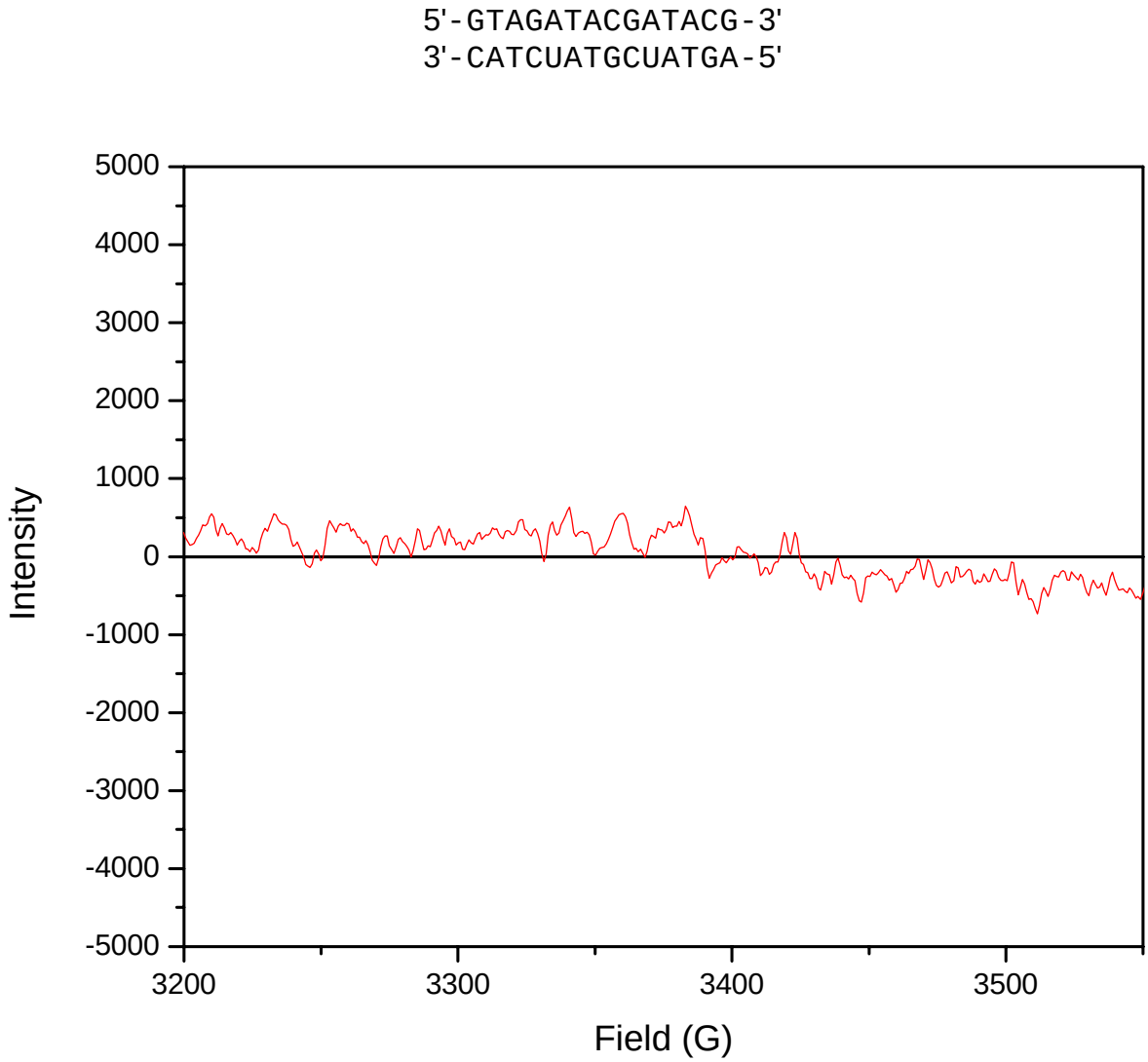

Figure 3.11. Shown above is sequence of oligonucleotides used containing either U or FU at the position marked U. Shown below is EPR spectrum for reductive flash/quench experiments utilizing 50 μM $Ru(phen)_2(dppz)^{2+}$, 100 μM uracil containing oligonucleotides, 10 mM NaCl, 20 mM sodium phosphate, pH 7.8, and 2M KI. The sample was irradiated with white light while freezing the sample in liquid nitrogen. EPR was then performed at 77 K.

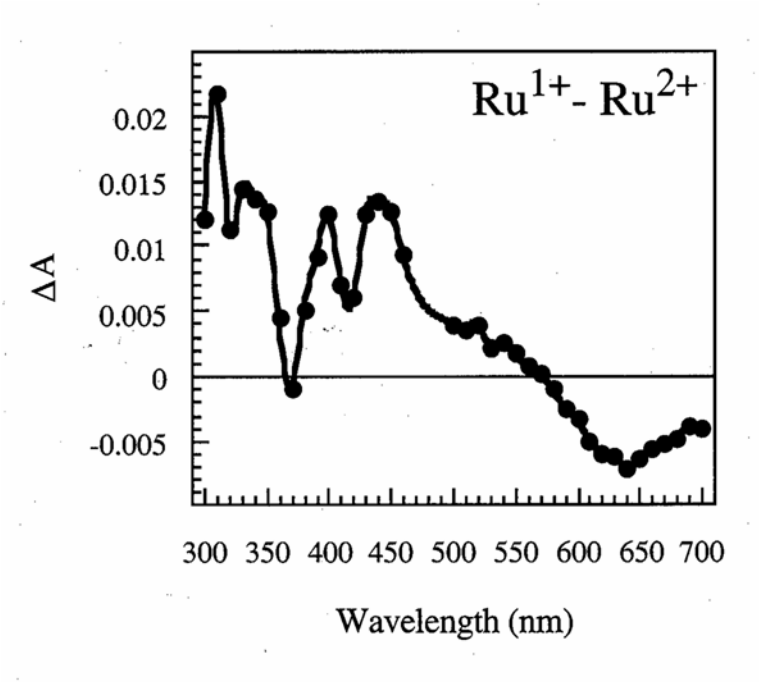

Figure 3.12. Transient absorption spectrum displaying Ru^{+} species obtained using $[Ru(phen)_2(dppz)]^{2+}$ and triethanolamine in acetonitrile with exication at 470 nm. A similar spectrum was obtained using $[Ru(phen)_2(dppz)]^{2+}$ and 7-deazaguanine containing DNA.

CHAPTER 4

Effect of Nucleotide Sequence on Charge Injection and Propagation in DNA

Adapted from:Yoo, J., Delaney, S., Stemp, E. D. A., and Barton, J. K. (2003) *J. Am. Chem. Soc.* 125, 6640.

** Transient absorption experiments were performed by Drs. Jae Yoo and Eric D. A. Stemp.

4.1 INTRODUCTION

DNA charge transport (CT) has been the focus of considerable investigation given its potential importance to cellular mechanisms of oxidative damage, its application in the development of DNA-based sensors, and the general interest in developing a mechanistic understanding of electron transfer chemistry over long distance (*1, 2*). Oxidative damage mediated by double helical DNA has been demonstrated over a distance of 200 Å (*3, 4*) and important to considerations of cellular DNA damage, oxidative damage by CT has been demonstrated in nucleosome core particles (*5*) and in DNA packaged inside nuclei (*6*).

Mechanistically, a mixture of tunneling and hopping has been proposed for DNA CT (*7-10*). Using yield measurements of oxidative DNA damage as a function of intervening sequence, Giese, Jortner, and coworkers offered experimental support for a guanine hopping model (*7, 8*). They observed decreased yields of oxidative damage with increasing separation of the guanine 'stepping stones' by A-T steps. In this guanine hopping model, the charge donor and acceptor molecules are close in energy to the DNA bridge. Charge transiently occupies the bridge orbitals hopping from one low energy guanine site to the next. So long as hopping to the next guanine 'stepping stone' is faster than trapping of the radical charge would be able to propagate through the base stack with a very shallow distance dependence. Contrary to hopping, in a tunneling mechanism the DNA bridge orbitals are energetically higher than the donor and acceptor and the charge tunnels through the bridge without formally occupying it. Based on a purely tunneling mechanism the rates of CT would be exponentially dependant on the donor-acceptor distance and would show a very steep distance dependence.

To explore these mechanistic questions we have prepared DNA assemblies with pendant ruthenium intercalators containing the dipyridophenazine (dppz) ligand as an oxidant to probe DNA CT both spectroscopically and biochemically (*3, 11*). Using the flash/quench technique (Scheme 4.1) (*12*) to generate a ruthenium(III) oxidant *in situ*, these assemblies provide a powerful system for mechanistically delineating long-range DNA CT. An excited state complex, $*Ru^{2+}$, is oxidatively quenched by a non-intercalating electron acceptor (Q) to form Ru^{3+} and reduced quencher, Q^{red}. The Ru^{3+} complex (E_0 ($Ru^{3+/2+}$) = 1.6 V vs. NHE) can back react with Q^{red} or oxidize an electron donor such as guanine or methylindole (E_0 = 1.3, 1.0 V vs. NHE for guanine (*13*) and methylindole (*14*), respectively). The resultant base radical can also back react with Q^{red} or undergo further reactions with H_2O and/or O_2 to form irreversible oxidative products (*15*). In Ru-tethered assemblies containing methylindole as an artificial base, the formation of the methylindole radical cation has been characterized by transient absorption and EPR spectroscopies and the resultant irreversible damage has been monitored biochemically (*14*). CT to form the methylindole radical cation occurs at a rate $\geq 10^7\ s^{-1}$ and is independent of distance over 17-37 Å. Here we present results on a new series of Ru-modified DNA duplexes where the sequence intervening the ruthenium intercalator and methylindole site is varied.

4.2 METHODS

4.2.1 Materials. All chemical reagents and starting materials were purchased from commercial sources and used as received. Phosphoramidites were purchased from Glen Research. The ligands bpy' and dppz were synthesized according to literature

procedures (*16-18*). [Ru(bpy')(dppz)(phen)]Cl_2 was synthesized as described elsewhere (*16, 17*).

4.2.2 Oligonucleotide Synthesis. The oligonucleotides were synthesized on an Applied Biosystems 394 DNA synthesizer using standard phosphoramidite chemistry (*19*). The oligonucleotides were purified by reverse-phase HPLC and characterized by MALDI-TOF mass spectroscopy. The synthesis of ruthenium modified oligonucleotides was carried out with a racemic mixture of [Ru(bpy')(dppz)(phen)]Cl_2 using solid phase synthetic methodology described elsewhere (*20*). Purification of the ruthenium modified DNA by reverse-phase HPLC yields four isomers, which were characterized by UV-vis spectroscopy and MALDI-TOF mass spectrometry. A mixture of all four diastereomers was used for the laser spectroscopy and biochemical experiments.

4.2.3 Assay of Oxidized Products. Unmetalated oligonucleotide strands were 5'-^{32}P-end-labeled using standard procedures (*21*). DNA duplexes were formed by mixing equal concentrations of complementary strands in 50 mM NaCl, 15 mM sodium phosphate, pH 7 and heating to 90 °C followed by slow cooling to 20 °C. DNA duplexes (5 μM) were irradiated at room temperature in the presence of 125 μM either $[Ru(NH_3)_6]^{3+}$ or $[Co(NH_3)_5Cl]^{2+}$ using a HeCd laser (~ 13 mW at 442 nm). After irradiation, all samples were treated with 10% (v/v) piperidine at 90 °C for 30 min, dried, and subjected to electrophoresis through a 20% denaturing polyacrylamide gel. The levels of damage were quantitated using phosphorimagery (Imagequant).

4.2.4 Laser Spectroscopy. DNA duplexes (20 μM) were formed by mixing equal concentrations of complementary strands, and heating to 90 °C followed by slow cooling to room temperature in a buffer of 10 mM NaCl, 10 mM potassium phosphate,

pH 7. The $[Ru(NH_3)_6]^{3+}$ quencher concentration was 300 μM. Time-resolved emission and transient absorption experiments were carried out on a Nd:YAG laser using an excitation wavelength of 470 nm. The emission of the intercalated ruthenium complexes was monitored at 610 nm. Emission intensities were obtained by integrating the area under the decay curve of the luminescence.

4.3 RESULTS AND DISCUSSION

4.3.1 Ruthenium-DNA Assemblies. The DNA assemblies utilized in this work are shown in Figure 4.1. Each assembly includes a 4-methylindole nucleoside (M) embedded between two G bases for greater stability as well as $[Ru(bpy')(dppz)(phen)]^{2+}$ tethered to the 5' end of the oligomer; this tethered complex intercalates (*11*) 2-3 base pairs from the end of the duplex. The Ru-M distance of 30.8 Å is constant across the series. Sequences contain either a G or inosine (I) at the hole injection site with the intervening sequence to the G**M**G oxidation site varied as all A's, all T's, or containing an intervening AA mismatch. Luminescence decays (τ_1 = 80 ns, τ_2 = 280 ns) and quenching yields (~85%) are equivalent in all duplexes, reflecting the minimal perturbation of the I substitution. Analogous assemblies containing GGG in place of G**M**G were also synthesized for biochemical experiments.

4.3.2 Transient Absorption Spectroscopy on Methylindole Containing Assemblies. Figure 4.2 shows transient absorption data monitored at 600 nm after laser excitation at 470 nm for assemblies **Ru-I-A-M** and **Ru-I-A-M-mis**. For assembly **Ru-I-A-M**, the data at 600 nm clearly show the rise of a positive signal consistent with the formation of the methylindole radical cation. Associated with the rise of this positive

signal at 600 nm is the loss of a negative signal at 440 nm (Figure 4.3), reflecting the conversion of Ru^{3+} to Ru^{2+}. These rates are both $\geq 10^7$ s^{-1} and show that oxidation to form the methylindole radical cation 31 Å away is indistinguishable from Ru^{3+} reduction. Importantly, in **Ru-I-A-M**, there are no guanines intervening or at the site of hole injection, yet CT is rapid.

Significantly, the transient at 600 nm for **Ru-I-A-M-mis**, which contains an AA mismatch intervening the Ru and methylindole, indicates negligible formation of the methylindole radical cation. Notably, in this assembly, despite the lack of formation of product radical, the transient at 440 nm (Figure 4.3) is consistent with rapid hole injection. This observation of an attenuated yield in radical formation in the mismatch-containing assembly is wholly consistent with the diminished yields of CT products in mismatched DNAs observed by gel analysis (*22*) or by electrochemistry (*23*). Therefore, the intervening mismatch clearly inhibits radical formation.

Diminished radical formation is also evident with guanine substitution at the site of hole injection. In Figure 4.3, the transients on a longer timescale for **Ru-I-A-M** are compared to those for **Ru-G-A-M** as well as **Ru-I-A-M-mis**. Here the expectation might have been that hole injection into the bridge would be less efficient for **Ru-I-A-M** than **Ru-G-A-M** because of the higher oxidation potential of I (1.5 V vs. NHE) at the injection site. We observe rapid formation of the radical in both cases. Nonetheless, the 600 nm signal is noticeably larger for **Ru-I-A-M** than that for **Ru-G-A-M** at long time ($\geq$ 2 μs). Similar differences in radical yield are evident with T's intervening (data not shown). In fact, substitution at the injection site may have a more pronounced effect on radical yield than well-matched sequence variations in the intervening bridge. At 440 nm we also see

a component with a slow rate (4×10^4 s^{-1}) of Ru^{2+} recovery, reflecting unreacted Ru^{3+}, and as expected, this signal correlates inversely with the extent of methylindole radical formation at 600 nm.

4.3.3 Oxidative DNA Damage Products Observed by Gel Electrophoresis. We can account for the differences seen in **Ru-I** versus **Ru-G** assemblies based upon the extent of radical delocalization and its effects on subsequent reaction with Q^{red}. To test this notion, product analysis was carried out by DNA damage quantitation using two different quenchers on analogous assemblies to **Ru-I-A-M** and **Ru-G-A-M** where a GGG was substituted for G**M**G (Figure 4.4). The reactivity of GGG sites to long-range CT has been well-characterized and were therefore used in these studies. Using $[Ru(NH_3)_6]^{3+}$ as Q, more irreversible oxidative damage was observed at the GGG site in duplex **Ru-I-A-G** compared to duplex **Ru-G-A-G**, consistent with our spectroscopic measurements of radical yield. However, reaction of the DNA radical with the diffusive quencher at the site of hole injection can be minimized using a sacrificial quencher such as $[Co(NH_3)_5Cl]^{2+}$, which is unstable in its reduced form. Indeed, the damage yield at the GGG site with $[Co(NH_3)_5Cl]^{2+}$ is comparable for **Ru-I-A-G** and **Ru-G-A-G**. Thus the yield of oxidative damage in a remote DNA site is modulated sensitively by reactivity at the injection site. It is noteworthy that a sensitivity in long-range oxidative damage to the sequence near hole injection was seen also with capped anthraquinone photooxidants (*4*).

4.3.4 Sensitivity of DNA Sequence at Charge Injection Site. Scheme 4.2 illustrates our model to account for the observed data. After flash/quench, in assembly **Ru-G-A-M**, we expect hole injection to be centered on the guanine; for **Ru-I-A-M**, hole injection may be more delocalized since the –IAAAAAA- bridging bases all have similar

oxidation potentials. For both DNA radicals, two pathways are then available: hole migration to form the lowest energy methylindole radical, or reaction with the Q^{red}. For **Ru-I-A-M-mis**, CT to form the methylindole radical is disrupted, so the hole remains localized proximal to the injection site, and only reaction with Q^{red} is available. It is reasonable that more efficient reaction with the reduced quencher is likely with the hole localized in the proximity of the original quenching. Thus, for **Ru-G-A-M**, reaction with Q^{red} is more favorable than for **Ru-I-A-M**, where the hole is more delocalized. This difference is necessarily tempered by the stability of Q^{red}, with the sacrificial cobalt quencher, reaction to form the lowest energy methylindole radical is equally favored for both assemblies. Given the possibility of reaction with Q^{red}, however, the presence of guanine at the injection site does not serve to facilitate CT but instead diminishes net product yield.

In summary, the kinetics and yield of methylindole radical formation as a function of DNA sequence were studied by laser spectroscopy and biochemical methods. Remarkably, hole injection and subsequent formation of the methylindole radical cation was observed at a distance of over 30 Å at rates $\geq 10^7\ s^{-1}$ in assemblies with no intervening guanines. Considering these data and previous studies in our lab which examined CT as a function of intervening sequence it is difficult to rationalize a pure guanine hopping model of DNA CT. However, as identified here, also critical to yield of CT is the sequence at the injection site since this sequence determines initial hole localization and hence the probability of hole propagation. Indeed, here the presence of a guanine site serves to increase hole localization and diminish CT through the base pair stack.

4.4 REFERENCES

1. (a) Nunez, M. E., and Barton, J. K. (2000) *Curr. Opin. Chem. Biol. 4*, 199. (b) Boon, E. M., and Barton, J. K. (2002) *Curr. Opin. Struct. Biol. 12*, 320. (c) Delaney, S., and Barton, J. K. (2003) *J. Org. Chem. 68*, 6475.

2. (a) Lewis, F. D., Letsinger, R. L., and Wasielewski, M. R. (2001) *Acc. Chem. Res. 34*, 159. (b) Schuster, G. B. (2000) *Acc. Chem. Res. 33*, 253. (c) Giese, B. (2000) *Acc. Chem. Res. 33*, 631.

3. (a) Nunez, M. E., Hall, D. B., and Barton, J. K. (1999) *Chem. Biol. 6*, 85. (b) Hall, D. B., Holmlin, R. E., and Barton, J. K. (1996) *Nature 382*, 731.

4. Ly, D., Sanii, L., and Schuster, G. B. (1999) *J. Am. Chem. Soc. 121*, 9400.

5. Núñez, M. E., Noyes, K. T., and Barton, J. K. (2002) *Chem. Biol. 9*, 403.

6. Núñez, M. E., Holmquist, G. P., and Barton, J. K. (2001) *Biochemistry 40*, 12465.

7. (a) Giese, B., Amaudrut, J., Köhler, A.-K., Spormann, M., and Wessely, S. (2001) *Nature 412*, 318. (b) Giese, B., and Spichty, M. (2000) *Chem. Phys. Chem. 1*, 195.

8. (a) Bixon, M., and Jortner, J. (2001) *J. Am. Chem. Soc*. *123*, 12556. (b) Grozema, F. C., Berlin, Y. A., and Siebbeles, L. D. A. (2000) *J. Am. Chem. Soc*. *122*, 10903.

9. Henderson, P. T., Jones, D., Hampikian, G., Kan, Y., and Schuster, G. B. (1999) *Proc. Natl. Acad. Sci*. *U. S. A. 96*, 8353.

10. (a) Wan, C., Fiebig, T., Kelley, S. O., Treadway, C. R., Barton, J. K., and Zewail, A. H. (1999) *Proc. Natl. Acad. Sci*. *U. S. A. 96*, 6014. (b) Wan, C., Fiebig, T., Schiemann, O., Barton, J. K., and Zewail, A. H. (2000) *Proc. Natl. Acad. Sci*. *U. S. A. 97*, 14052.

11. (a) Arkin, M. R., Stemp, E. D. A., and Coates Pulver, S. (1997) *Chem. Biol. 4*, 389. (b) Wagenknect, H. A., Stemp, E. D. A., and Barton, J. K. (2000) *J. Am. Chem. Soc*. *122*, 1.

12. Stemp, E. D. A., Arkin, M. R., and Barton, J. K. (1997) *J. Am. Chem. Soc*. *119*, 2921.

13. Steenken, S., and Jovanovic, S. V. (1997) *J. Am. Chem. Soc*. *119*, 617.

14. Pascaly, M., Yoo, J., and Barton, J. K. (2002) *J. Am. Chem. Soc*. *124*, 9083.

15. Burrows, C. J., and Muller, J. G. (1998) *Chem. Rev*. *98*, 1109.

16. Della Ciena, L., Hamachi, I., and Meyer, T. J. (1989) *J. Org. Chem*. *54*, 1731.

17. Dupueur, C. M., and Barton, J. K. (1997) *Inorg. Chem*. *36*, 33.

18. (a) Amouyal, E., Homsi, A., Chambron, J.-C., and Sauvage, J.-P. (1990) *J. Chem. Soc., Dalton Trans*. 1841. (b) Strouse, G. F., Anderson, P. A., Schoonover, J. R., Meyer, T. J., and Keene, F. R. (1992) *Inorg. Chem*. *31*, 3004. (c) Anderson, P. A., Deacon, G. B., Haarman, K. H., Keene, F. R., Meyer, T. J., Reitsma, D. A., Skelton, B. W., Strouse, G. F., Thomas, N. C., and Treadway, J. A. (1995) *Inorg. Chem*. *34*, 6145.

19. (a) Beaucage, S. L., and Caruthers, M. H. (1981) *Tet. Lett*. *22*, 1859. (b) Goodchild, J. (1990) *Bioconj. Chem*. *1*, 165.

20. Holmlin, R. E., Dandliker, P. J., and Barton, J. K. (1999) *Bioconj. Chem*. *10*, 1122.

21. Sambrook, J., Fritsch, E. F., and Maniatis, T. (1989) *Molecular Cloning: A Laboratory Manual*, 2nd ed.; Cold Spring Harbor Laboratory: New York.

22. (a) Bhattacharya, P. K., and Barton, J. K. (2001) *J. Am. Chem. Soc*. *123*, 8649. (b)

Bhattacharya, P. K., Cha, J., and Barton, J. K. (2002) *Nuc. Acids Res*. *30*, 4740.

23. Boon, E. M., Ceres, D. M., Drummond, T. G., Hill, M. G., and Barton, J. K. (2000) *Nat. Biotech. 18*, 1096.

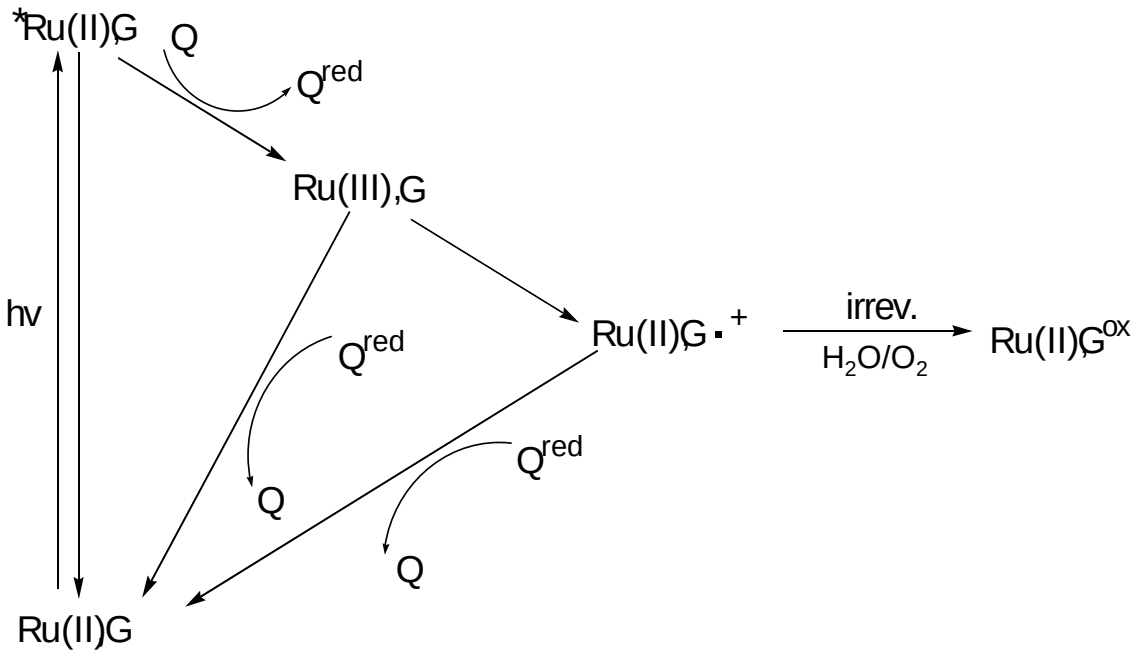

Scheme 4.1. Schematic representation of the flash/quench technique. The intercalating Ru(II) oxidant is excited with visible light to yield *Ru(II). This excited state is quenched with an electron accepting molecule diffusing in solution such as $[Ru(NH_3)_6]^{3+}$, $[Co(NH_3)_5Cl]^{2+}$, or methyl viologen. This quenching reaction yields reduced quencher (Q_{red}) and a Ru(III) oxidant which can oxidize guanine from a distance.

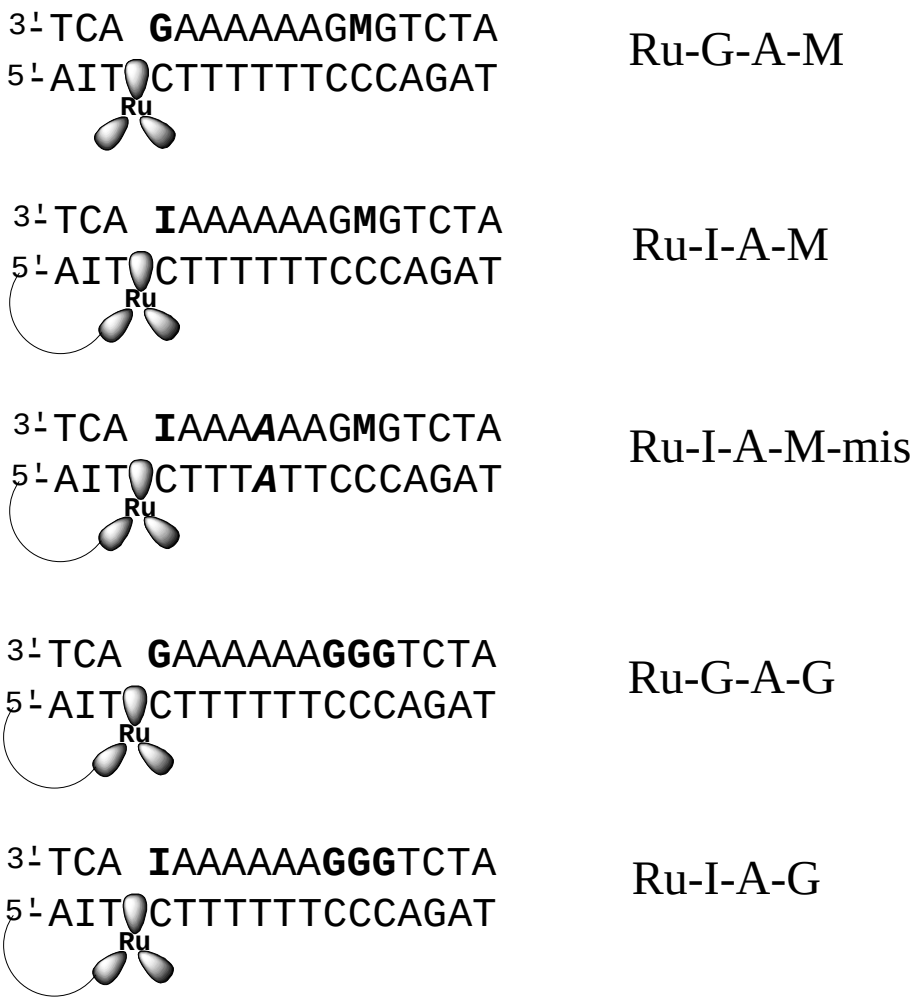

Figure 4.1. Schematic illustrations of the DNA assemblies used in this study. Ru = $[Ru(bpy')(dppz)(phen)]^{2+}$, I = inosine nucleotide, and M = methylindole nucleotide.

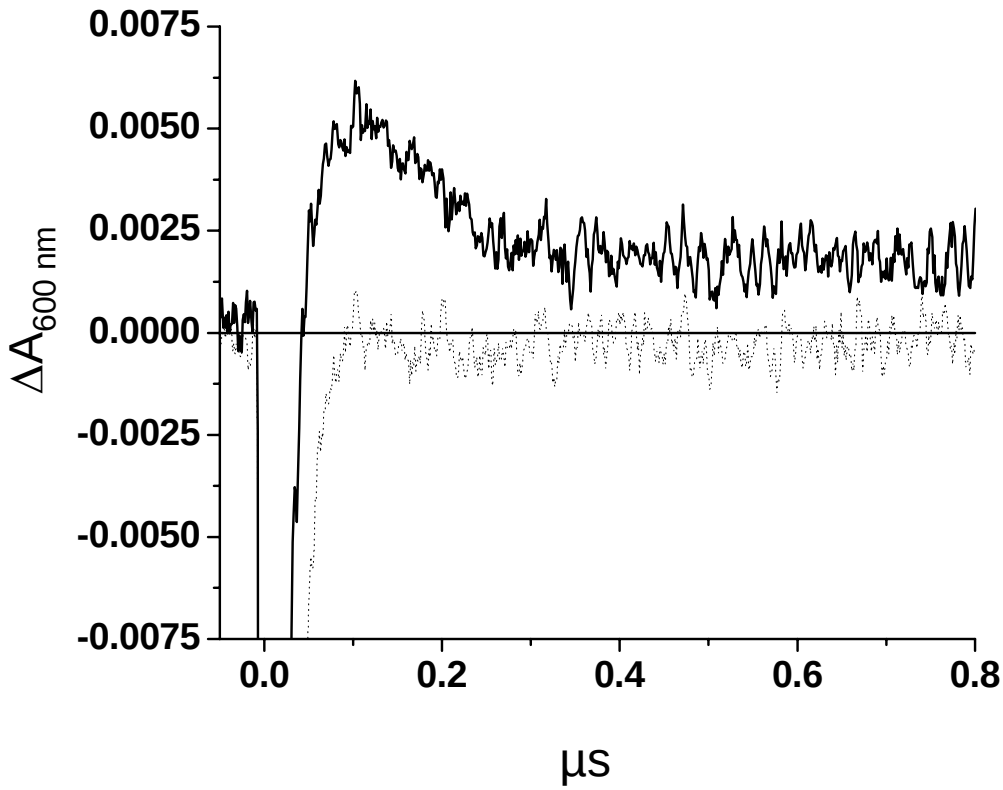

Figure 4.2. Time-resolved transient absorption traces for Ru-I-A-M (solid) and Ru-I-A-M-mis (dotted) measured at 600 nm. Samples contained 20 mM Ru-DNA conjugate, 300 mM $[Ru(NH_3)_6]^{3+}$, 10 mM NaCl, and 10 mM potassium phosphate, pH = 7, λ_{exc}=470 nm. A large initial negative spike is due to emission from residual $*Ru^{2+}$.

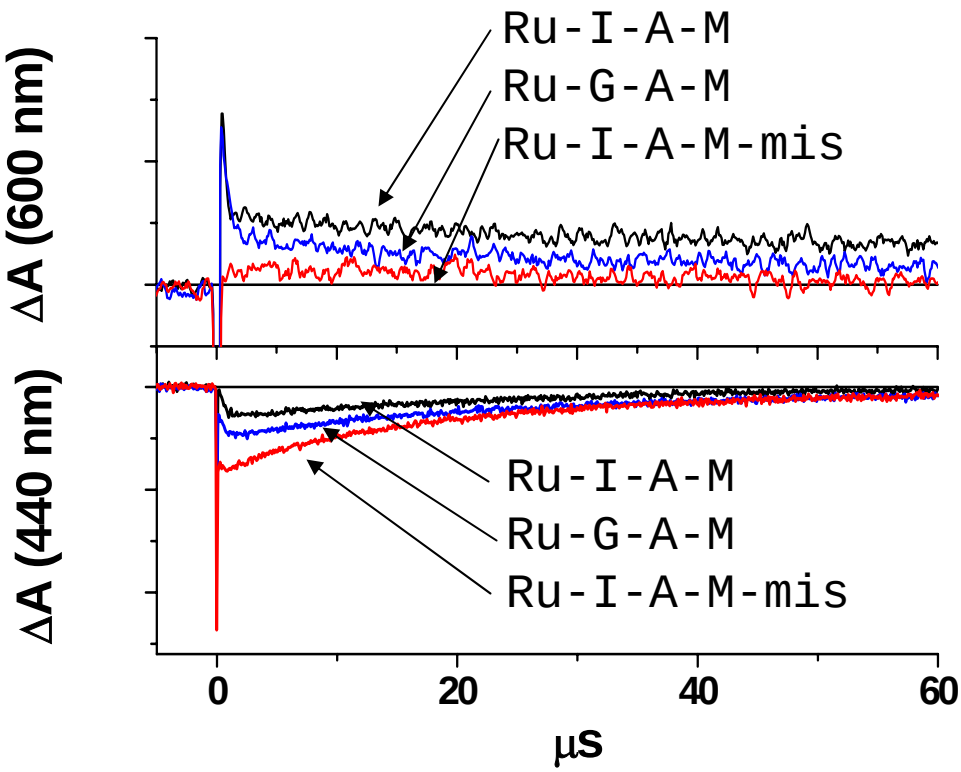

Figure 4.3. Time-resolved transient absorption traces for Ru-I-A-M, Ru-G-A-M, and Ru-I-A-M-mis measured at 600 nm (top) and 440 nm (bottom). Samples contained 20 mM Ru-DNA conjugate, 300 μM $[Ru(NH_3)_6]^{3+}$, 10 mM NaCl, and 10 mM potassium phosphate, pH = 7, λ_{exc}= 470 nm.

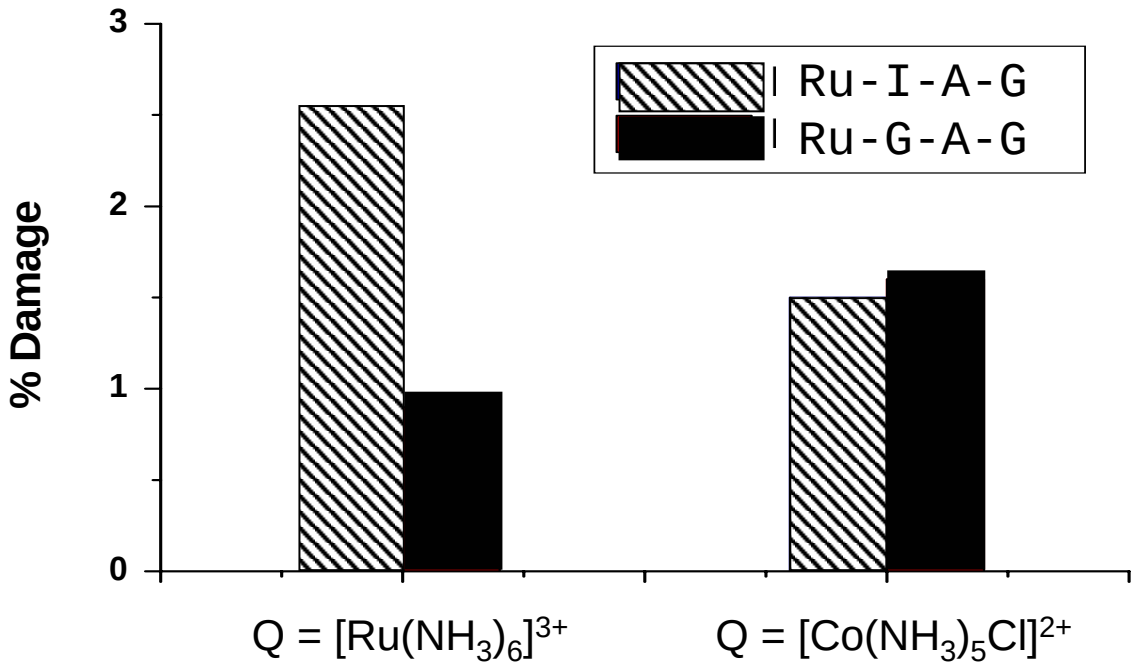

Figure 4.4. Quantitation of damage yields at the 5'-GGG-3' site in assemblies Ru-I-A-G and Ru-G-A-G as a function of different quenchers after 5 min of irradiation using λ_{exc} = 440 nm. Samples contained 5 μM Ru-DNA, 125 μM $[Ru(NH_3)_6]^{3+}$, 50 mM NaCl, and 15 mM sodium phosphate, pH = 7.

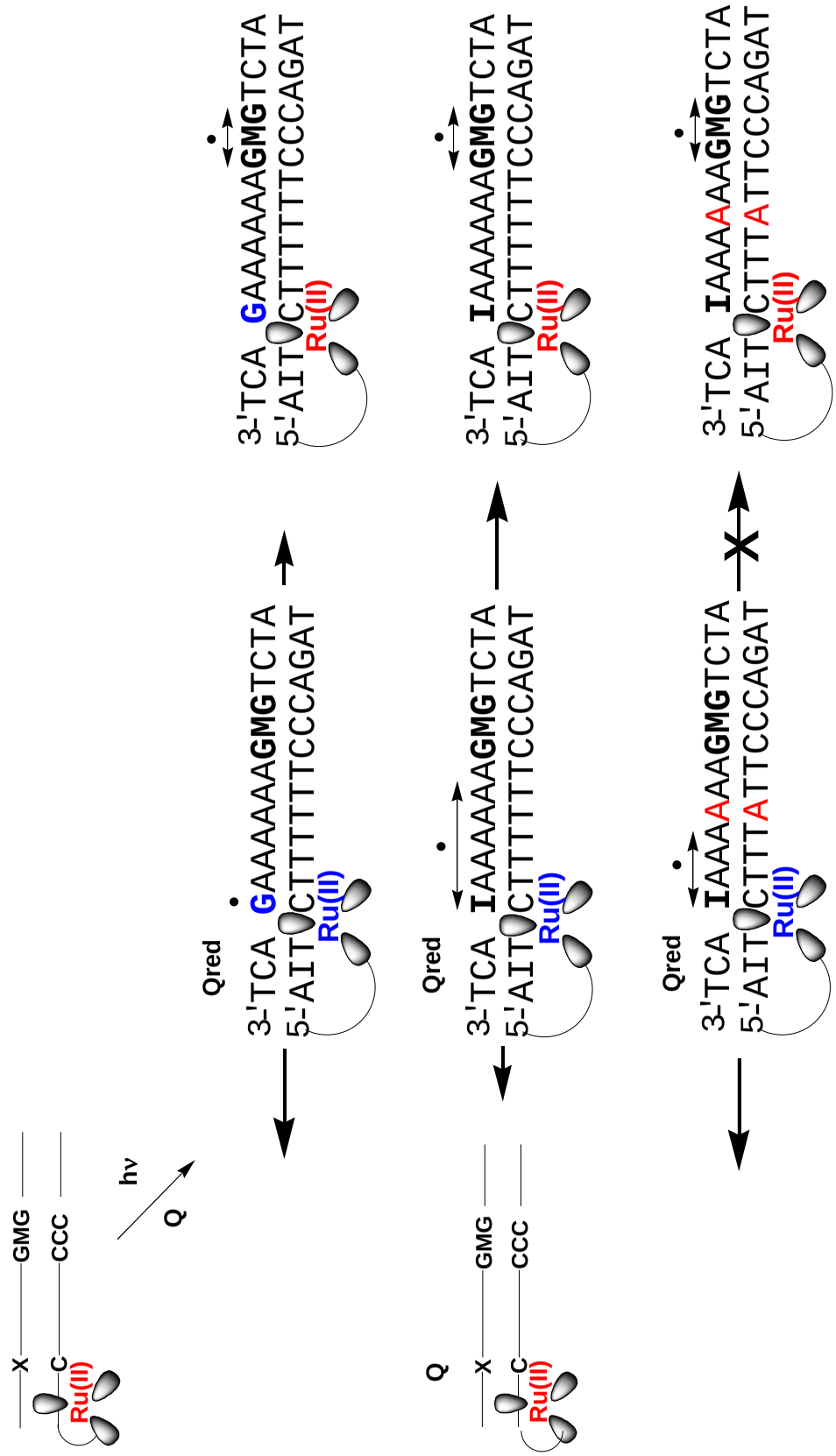

Scheme 4.2. Proposed model for hole injection and subsequent reactivity in the Ru-DNA assemblies.

CHAPTER 5

Charge Equilibration between Two Distinct Sites in Double Helical DNA

Adapted from: Delaney, S., Yoo, J., Stemp, E. D. A., and Barton, J. K. (2004) Manuscript submitted.

** Transient absorption experiments were performed by Drs. Jae Yoo and Eric D. A. Stemp.

5.1 INTRODUCTION

Numerous spectroscopic and biochemical experiments have shown that the base stack of DNA can mediate charge transport (CT) reactions (*1-4*). Chemically well-defined assemblies, consisting of DNA duplexes with covalently bound oxidants, have been particularly useful in exploring the effects of base stacking perturbations (*5-8*), intervening DNA sequence (*9, 10*), and donor-acceptor distance (*11-13*) on CT. Long-range oxidative DNA damage has been demonstrated over a distance of 200 Å (*14, 15*). Indeed DNA either packaged in nucleosome core particles (*16*) or inside the cell nucleus (*17*) has been found to be susceptible to long-range oxidative damage.

DNA-mediated CT from a distance to generate oxidative damage was first demonstrated in an assembly containing a tethered, intercalating phenanthrenequinone diimine (phi) complex of Rh(III) (*18*). In this assembly, photoinduced oxidative damage of the 5'-G of 5'-GG-3' sites was observed; this damage pattern is considered the hallmark of CT and long-range oxidative damage has now been confirmed using a variety of pendant oxidants (*19-23*). Hence, the focus of research has shifted from whether or not DNA CT occurs at all to mechanistically how does charge migrate through DNA. Utilizing yield measurements of oxidative DNA damage as a function of intervening sequence, Giese, Jortner, and coworkers offered experimental support for a model involving a mixture of hopping and tunneling (*24, 25*). Also based on oxidative yield determinations, Schuster and coworkers have proposed phonon-assisted polaron hopping between guanine bases (*26*). In this model the formation of polarons, localized structural distortions of DNA that stabilize the cation radical, allows for charge delocalization over regions of sequence; propagation of these polarons through the helix is aided by phonons.

In addition to biochemical experiments to determine yields of oxidative damage, experiments using some oxidants permit spectroscopic analysis to determine rates of CT or to monitor CT radical intermediates. These studies can be especially useful in addressing the mechanistic considerations of DNA CT. Using rigid stilbene-modified hairpins, Lewis and coworkers observed a steep distance dependence of CT rates by monitoring formation of the stilbene radical anion (*13*). Recent work by Kawai, Majima, and coworkers examined the yields of the charge-separated state in DNA hairpins modified to contain a naphthalene diimide (NDI) acceptor and a phenothiazine donor (*12*). By monitoring the formation and decay of the NDI radical anion, the yield of the charge-separated state was slightly dependent on the number of intervening A-T base pairs; however, the rate of charge recombination was found to be strongly dependent upon the number of intervening A-T steps. The authors propose an adenine hopping model to account for these and other previous experimental observations. Using photoexcited 2-aminopurine (*Ap), a fluorescent nucleobase analog, our laboratory found that rates of intrastrand base-base CT between *Ap and G were ~10^{10} s^{-1} (*27*). Very recent experiments, also monitoring quenching of *Ap, have shown that base dynamics play a significant role in modulating propagation of charge through DNA (*28, 29*). In these systems, higher yields of CT are observed with increasing temperature; these higher temperatures provide increased base fluctuations which in turn allow access to more CT-active conformations.

DNA assemblies containing dipyridophenazine (dppz) complexes of Ru(II) have been particularly useful for probing CT, because they allow both for spectroscopic studies to monitor formation of DNA radicals on a short time scale and for biochemical

analysis to determine the yield of oxidative damage occurring on a longer time scale. With these ruthenium complexes, a flash/quench technique is typically utilized (Figure 5.1) (*30*, *31*). The cycle is initiated by visible light, which excites the intercalated Ru(II) complex. This excited Ru(II) complex, *Ru(II), is then quenched by a nonintercalating electron acceptor, Q, such as $[Ru(NH_3)_6]^{3+}$ or $[Co(NH_3)_5Cl]^{2+}$, so as to form Ru(III) *in situ*. It is this Ru(III) species that can oxidize guanines from a distance. The oxidized guanine radical can then undergo further reaction with H_2O and/or O_2 to form a family of oxidative products, G_{ox} (*32*). The flash/quench technique, coupled with transient absorption spectroscopy, has been applied effectively in characterizing the resultant neutral guanine radical in duplex DNA; deprotonation of the cation radical must occur faster than the 10^{-7} s time scale of the experiment (*31*). We have also utilized flash/quench experiments in characterizing radical products in peptide/DNA assemblies (*33*) and a protein/DNA complex (*7*).

Assemblies containing 4-methylindole (M) as the electron donor as well as a tethered Ru intercalator were constructed to explore long-range DNA CT spectroscopically and biochemically (*34*). The methylindole moiety is particularly amenable as an artificial base in these studies because of its relatively low oxidation potential (1 V vs. NHE) and the strong absorptivity at 600 nm of its cation radical. Formation of the M cation radical over 17-37 Å away from the tethered intercalating oxidant occurs with a rate $\geq 10^7$ s^{-1} and is found to be coincident with quenching of the ruthenium excited state to form the Ru(III) oxidant; CT is not rate limiting. Furthermore, in these assemblies, where the intervening DNA bridge was composed solely of A-T base

pairs, efficient CT is observed over 37 Å with no intervening guanines. Thus, a model of charge hopping strictly among guanines seems unlikely.

We have found that DNA CT is exquisitely sensitive to DNA base pair stacking, both statically and dynamically. Based on spectroscopic and biochemical experiments using Ru and Rh intercalating oxidants, along with the temperature dependent base-base CT chemistry (*28, 29*), we have proposed a model (*29*) for CT involving conformationally gated charge hopping among DNA domains. Domains over which charge may be delocalized are defined by sequence and dynamics; a domain size of ~ 4 base pairs has been characterized in assemblies containing repetitive tracts of adenines. CT among these DNA domains is conformationally gated: increased base dynamics permits access to CT-active configurations and hence facilitates CT.

Recently, additional assemblies containing a pendant Ru oxidant and M as the charge donor were constructed to examine spectroscopically the effects of sequence at the injection site on charge propagation to yield oxidative damage (*35*). Sequences contained either a G or inosine (I) at the injection site, where I is ~ 200 mV harder to oxidize than G. Interestingly, despite the higher oxidation potential, a larger signal at 600 nm, indicative of a higher cation radical yield, is observed for sequences containing I at the injection site. Biochemical analyses suggest these differences depend upon the extent of radical delocalization at the injection site by allowing (with G) or inhibiting (with I) a non-productive back reaction with reduced quencher.

Recent photophysical experiments have also demonstrated that back electron transfer (BET) can play a significant role in diminishing the yield of charge propagation out to a distant site (*36, 37*). If BET with the reduced DNA-bound photooxidant is faster

than trapping of the guanine radical by H_2O and/or O_2, fast BET can prevent formation of a permanent guanine lesion. Perhaps the clearest example is with thionine, a potent photooxidant (~ 2 V vs. NHE) that produces no detectable DNA damage owing to its fast rate of BET (*38*). As another example, in identical DNA duplexes containing different tethered oxidants, different yields of oxidative damage at a distal 5'-GG-3' double guanine site as compared to a proximal 5'-GG-3' site are observed (*39*). These differences in relative oxidative damage are attributed to variations in BET.

The consequences of rapid BET demonstrate that in DNA reverse CT must be as carefully considered as in studies of forward CT. Given radical migration in both directions through DNA, yields of oxidative damage will necessarily reflect some extent of charge equilibration prior to radical localization and trapping. To explore this issue, we have prepared duplexes containing a tethered dppz complex of Ru(II), the nucleoside analogue methylindole, and a second radical trap, a GGG site; the two trapping sites have been varied in position with and without an intervening stacking perturbation to limit migration between these low potential sites. Using these assemblies, here we report results demonstrating charge equilibration across the DNA duplex.

5.2 METHODS

5.2.1 Materials. All chemical reagents and starting materials were purchased from commercial sources and used as received. Phosphoramidites were purchased from Glen Research. The ligands bpy' and dppz were synthesized according to literature procedures (*40-42*). $[Ru(bpy')(dppz)(phen)]Cl_2$ was synthesized as described elsewhere (*41*, *42*).

5.2.2 DNA Synthesis. The oligonucleotides were synthesized on an Applied Biosystems 394 DNA synthesizer using standard phosphoramidite chemistry (*43*). The oligonucleotides were purified by reverse-phase HPLC and characterized by MALDI-TOF mass spectroscopy. The synthesis of ruthenium modified oligonucleotides was carried out with a racemic mixture of [Ru(bpy')(dppz)(phen)]Cl_2 using solid phase synthetic methodology described elsewhere (*44*). Purification of the ruthenium modified DNA by reverse-phase HPLC yields four isomers, which were characterized by UV-vis spectroscopy and MALDI-TOF mass spectrometry. A mixture of all four diastereomers was used for the laser spectroscopy and biochemical experiments.

5.2.3 Assay of Oxidized Products. Unmetalated oligonucleotide strands were labeled at the 5' end with ^{32}P using standard procedures (*45*). DNA duplexes were formed by mixing equal concentrations of complementary strands in 50 mM NaCl, 15 mM sodium phosphate, pH 7 and heating to 90 °C followed by slow cooling to 20 °C over 120 min. DNA duplexes (5 μM) and bulge-containing assemblies (1 μM) were irradiated at room temperature in the presence of $[Co(NH_3)_5Cl]^{2+}$ (125 μM) using a HeCd laser (~ 13 mW at 442 nm). For the intermolecular control experiments, equimolar amounts of non-^{32}P-labeled ruthenium assemblies were mixed with their corresponding ^{32}P-labeled assembly which did not contain tethered ruthenium, and irradiated for 60 min in the absence of quencher. Importantly, for the intermolecular control experiments the inosine at the ruthenium binding site was replaced by guanine to make this site susceptible to oxidation by singlet oxygen. Additionally, in the intermolecular control experiments, the methylindole was replaced with guanine yielding two GGG sites. After irradiation, all samples were treated with 10% (v/v) piperidine at 90 °C for 30 min, dried,

and subjected to electrophoresis through a 20% denaturing polyacrylamide gel. The levels of damage were quantitated using phosphorimagery (Imagequant).

5.2.4 Laser Spectroscopy. DNA duplexes (20 μM) were formed by mixing equal concentrations of complementary strands, and heating to 90 °C followed by slow cooling to room temperature in a buffer of 10 mM NaCl, 10 mM potassium phosphate, pH 7. The $[Ru(NH_3)_6]^{3+}$ quencher concentration was 300 μM. Time-resolved emission and transient absorption experiments were carried out on a Nd:YAG laser using an excitation wavelength of 470 nm. The emission of the intercalated ruthenium complexes was monitored at 610 nm. Emission intensities were obtained by integrating the area under the decay curve of the luminescence.

5.3 RESULTS

5.3.1 Ruthenium-DNA Assemblies. The ruthenium-DNA assemblies used in this study are shown in Figure 5.2. Each DNA assembly contains a 5'-tethered $[Ru(bpy')(dppz)(phen)]^{2+}$ and a methylindole flanked on either side by guanines to afford stability. **Ru-GMG** is the control assembly containing only one site of low oxidation potential, the GMG site. **Ru-GGG-GMG** contains a GGG positioned between the ruthenium binding site and the GMG site, while **Ru-GMG-GGG** has the GGG positioned distal to the ruthenium binding site. **Ru-mis-GMG** contains an A-A mismatch intervening the ruthenium and the methylindole. **Ru-GMG-blg-GGG** contains a 5'-ATA-3' bulge between the proximal GMG and distal GGG sites. In all cases, inosine is incorporated near the ruthenium binding site to allow for maximal charge injection and propagation (*35*).

5.3.2 Charge Transport Chemistry Is an Intraduplex Reaction. To initiate CT chemistry using dppz complexes of ruthenium the flash/quench technique is utilized (*31*). However, when these same ruthenium complexes are excited in the absence of quencher, *Ru(II) sensitizes the formation of singlet oxygen. Since singlet oxygen reacts preferentially with guanines (*46*) within diffusional reach, this chemistry can be used to mark the binding site of the oxidant. To confirm the intraduplex nature of the CT chemistry described here, we irradiated an unlabeled ruthenium-modified duplex in the presence of a ^{32}P-end-labeled duplex containing no ruthenium. If interduplex associations occur, damage will be observed on the ^{32}P-end-labeled duplex even though this assembly does not contain ruthenium. Importantly, in these intermolecular controls the inosine at the ruthenium binding site is replaced with guanine to allow susceptibility to singlet oxygen damage. Furthermore, for these control experiments the GMG site is replaced with GGG owing to the well-characterized reactivity of the GGG site. Over a concentration range of 0.5 – 20 μM, the ^{32}P-end-labeled duplexes show no damage. Shown in Figure 5.3 is a representative gel for the **Ru-GMG-GGG** assembly. This lack of reaction indicates that over this concentration range all CT chemistry is intraduplex and the assemblies do not form higher order aggregates.

Similar results are obtained for the bulge-containing assembly at low concentrations (0.5 – 5 μM). No damage is observed at concentrations of 5 μM or lower in the assemblies that do not contain ruthenium; thus, under these conditions the assemblies do not aggregate and the CT is intraduplex. However, at 20 μM, the bulge-containing assembly does yield singlet oxygen damage even though it does not contain tethered ruthenium (Figure 5.3). Therefore, at this high concentration interduplex

interactions do occur. In this case, the singlet oxygen damage is observed predominately at the guanines in both GGG sites located on either side of the bulge. The metallointercalator binds most likely at the bulge itself. However, compared to guanine, adenine and thymine are far less susceptible to damage by singlet oxygen and therefore damage is not observed immediately at the bulge. A small amount of damage is also observed at the single guanine at the injection site.

Due to the interduplex associations observed at 20 μM, experiments utilizing the bulge-containing assembly were conducted only at low concentration (1 μM) where no damage is detectable. This interduplex reaction observed at 20 μM clearly results from a species present in equilibrium with the free ruthenium-modified duplex and the ^{32}P-end-labeled duplex. The high sensitivity of phosphorimagery, in combination with guanine damage due to singlet oxygen sensitization by the DNA-bound ruthenium intercalator, provides critical information regarding the binding site of the oxidant. As demonstrated in the control experiments described here, it is therefore quite straightforward to identify and confirm conditions under which solely an intraduplex CT reaction occurs. Some percentage of aggregation of DNA duplexes would instead yield detectable damage. Under the conditions utilized for transient absorption and biochemical experiments, no aggregation is observed and all CT reactions are intraduplex.

5.3.3 Oxidative Damage Products Observed by Gel Electrophoresis.

Oxidative damage assays were carried out using denaturing polyacrylamide gel electrophoresis (PAGE), which allows for quantitation of DNA damage products resulting from flash/quench experiments. The PAGE results reveal the damage pattern for the assemblies **Ru-GMG**, **Ru-GGG-GMG**, and **Ru-GMG-GGG** (Figure 5.4). In

these assemblies there are two oxidatively sensitive sites, GMG and GGG, which upon one-electron oxidation yield different damage products. Damage at guanine is expected to include 8-oxo-guanine, formamidopyrimidine, oxazalone, and imidazalone (*32*); damage at methylindole also produces a piperidine-sensitive lesion, but the final products have not been characterized.

In all assemblies examined, damage at the methylindole-containing site is predominant. For **Ru-GGG-GMG** and **Ru-GMG-GGG**, damage is also observed at the low energy GGG site. The PAGE results for the 5'-ATA-3' bulge-containing assembly **Ru-GMG-blg-GGG** are shown in Figure 5.5. Again, the predominant damage site is the methylindole, however, damage is also observed at the low energy GGG site. The ratio of damage at the distal GGG site compared to the proximal GMG site is 0.4 ± 0.1 for **Ru-GMG-blg-GGG**. In contrast, a ratio of 0.8 ± 0.1 is observed for the assembly lacking a bulge. This decrease in damage out to the distal GGG site for **Ru-GMG-blg-GGG** is consistent with earlier studies where intervening base stacking perturbations, such as the 5'-ATA-3' base bulge, were found to inhibit CT and the resultant long-range oxidative damage (*5, 6*).

For all assemblies, the amount of damage at the M site after 60 min of irradiation was quantitated with respect to the parent band, and corrected for damage observed in the absence of irradiation (Figure 6A). Here the greatest amount of methylindole damage is observed for **Ru-GMG**. The assemblies containing an additional low energy site, **Ru-GMG-GGG** and **Ru-GGG-GMG**, show approximately 40% less oxidative damage at the methylindole than the control assembly. However, upon insertion of a base bulge, a partial restoration of damage at the methylindole, approximately 50% compared to **Ru-**

GMG, is observed. As seen in Figure 5.5, damage at the guanine bases flanking the methylindole site is also observed. These guanines were incorporated specifically to provide stability at the methylindole site due to base stacking. However, this stacking may also render the guanines more susceptible to oxidative damage. Importantly, if the damage at these flanking guanine sites is quantitated and included with the damage observed at the methylindole, a pattern similar to that in Figure 5.6A is obtained (Figure 5.6B).

5.3.4 Emission and Transient Absorption Spectroscopy on Ruthenium-Modified Assemblies. Time-resolved luminescence measurements at 610 nm indicate that the excited-state ruthenium complex, *[Ru(bpy')(dppz)(phen)]$^{2+}$, decays biexponentially with τ_1 = 71 ns (76%) and τ_2 = 279 ns (26%) for **Ru-GMG** (Table 5.1). Similar values are obtained for all assemblies examined. These values are consistent with those reported earlier for dppz complexes of Ru(II) bound to DNA (*47*). Upon addition of 15 equivalents of $[Ru(NH_3)_6]^{3+}$, the luminescence is quenched by 80% in all assemblies.

Figure 5.7 shows the transient absorption spectra monitored at 600 nm after laser excitation of **Ru-GMG**, **Ru-GGG-GMG**, **Ru-GMG-GGG**, or **Ru-mis-GMG** in the presence of $[Ru(NH_3)_6]^{3+}$. Previous transient absorption and EPR studies provide evidence for formation of the methylindole cation radical which absorbs in this region (*34*). The transient signals for all assemblies are initially negative, which is attributed to emission from residual *Ru(II) generated in the flash/quench technique. For **Ru-GMG**, a large positive signal at 600 nm, consistent with formation of the methylindole radical, is observed. Positive signals of roughly equal height are also observed at 600 nm for **Ru-**

GGG-GMG and **Ru-GMG-GGG**, but they are considerably smaller than that for **Ru-GMG**. Although these signals are small, they are significant and clearly represent a positive signal compared to that obtained with the mismatch containing assembly. In **Ru-mis-GMG**, which contains an AA mismatch intervening the ruthenium oxidant and methylindole, no significant positive signal is observed. This attenuated yield in radical formation is consistent with decreased yields of CT products observed previously in mismatch-containing DNA (*6*, *34*).

The rise of the traces at 600 nm (< 0.2 μs) was fit to a monoexponential function, indicating that the formation of the transient occurs with a rate of $\sim 4 \times 10^7$ s^{-1} for all three assemblies (Table 5.1). This rate is consistent with those obtained previously for formation of the methylindole cation radical via CT from a bound ruthenium oxidant (*34*, *35*). This value is comparable to the time scale of the quenched emission of the ruthenium complex bound to DNA, and is approaching the instrument response. For all assemblies, the return to the Ru(II) ground state is also observed by monitoring the bleach of the MLCT band at 440 nm. The disappearance of the negative signal at 440 nm, reflecting the conversion from *Ru(II) to Ru(III), is concomitant with the rise of the positive signal at 600 nm. Hence, the rate of formation of Ru(III) and the base radical are coincident so that the rate of CT is greater than or equal to these values.

Also evident in Figure 5.7 is the difference in the decay rate of the positive signal at 600 nm for **Ru-GMG**, **Ru-GGG-GMG**, and **Ru-GMG-GGG**. The radical formed in **Ru-GMG** appears to contain two components, one of which decays significantly faster than those formed in **Ru-GGG-GMG** and **Ru-GMG-GGG**. Indeed, fitting the first part of the decay of the 600 nm signal to a monoexponential function reveals a rate ~ 10^6 s^{-1}

for **Ru-GMG**, whereas no significant decay is observed for the long-lived component nor for **Ru-GGG-GMG** and **Ru-GMG-GGG** over 50 μs. This long-lived species may reflect generation of guanine radical; the transient assigned to the neutral guanine radical was found to decay on the order of 10^4 s^{-1} in analogous ruthenium-tethered duplexes (*31*). The finding of oxidative damage at the guanine bases flanking M in the biochemical experiments supports this formation of guanine radical in **Ru-GMG** as well as in **Ru-GGG-GMG** and **Ru-GMG-GGG**. The neutral guanine radical does absorb at 600 nm but with an extinction coefficient 3.5 fold lower than that for the methylindole cation radical (*48-50*).

5.4 DISCUSSION

5.4.1 Singlet Oxygen Chemistry to Confirm an Intraduplex Charge Transport Reaction.

The ruthenium photochemistry (*31*) is valuable not only in initiating charge injection into the DNA base pair stack, but also in providing a reaction to mark the intercalator position along the DNA duplex. If the ruthenium-tethered DNA assemblies are irradiated in the absence of quencher, *Ru(II) sensitizes the formation of singlet oxygen. This singlet oxygen reacts preferentially with guanines within its sphere of diffusion to generate piperidine-sensitive damage products that can be visualized by PAGE (*46*). In so doing, this singlet oxygen chemistry marks the binding site for the Ru intercalator.

It has been suggested that duplexes containing a tethered ruthenium or rhodium oxidant may aggregate (*8*, *51*). In appropriately designed control experiments utilizing a mixture of unlabeled ruthenium-tethered duplexes and ^{32}P-end-labeled duplexes

containing no ruthenium, any interduplex association can be detected. No damage is observed on the ^{32}P-end-labeled duplex lacking the pendant intercalator. Hence, the data presented here clearly show that at concentrations $\leq$ 20 μM, the duplex assemblies do not aggregate. Thus, all CT chemistry is intraduplex. Interestingly, for these assays of intermolecularity, the bulge-containing DNA assembly serves as a useful positive control; in this assembly, a small amount of interduplex reaction is detectable at 20 μM, consistent with higher binding of the dppz complex at the bulged site. All CT experiments with the bulge-containing assembly were therefore conducted at 1 μM, more than one order of magnitude below the concentration where interduplex reaction is detected.

The application of ruthenium and rhodium intercalators to studies of DNA-mediated CT offers complementary chemistry to establish that reactions being explored are indeed intraduplex. With studies being conducted to probe CT over distances as long as 200 Å, these control experiments become exceedingly important. Analogous experiments with other pendant oxidants are rarely conducted. Indeed, only in the cases of the rhodium and ruthenium intercalating oxidants have the intraduplex characteristics of the reaction been unambiguously demonstrated.

5.4.2 Formation of DNA Charge Transport Intermediates. Using the ruthenium-tethered assemblies, the formation of base radicals at a distant site is monitored directly by transient absorption spectroscopy. Here we have explored how other low guanine energy sites may compete with methylindole cation radical formation.

Clearly it is not surprising that in **Ru-GGG-GMG,** the presence of the GGG site diminishes the yield of methylindole cation radical. Following charge injection, the hole

has two low energy sites for localization in **Ru-GGG-GMG** but only one in **Ru-GMG**. The oxidation potential of M is estimated to be 1.0 V vs. NHE (*34*) however the potential measured was irreversible. In separate experiments the oxidation potential of a 5'-GGG-3' site has been estimated to be in the range 1.0 (*52*)-1.2 (*53*) V vs. NHE. Thus, these sites are expected to be similar energetically. As seen in Figure 5.7, the presence of a GGG site does indeed affect the methylindole cation radical yield but not the rate. The signal at 600 nm of **Ru-GMG** is seen to have two components likely to be the methylindole cation radical and the neutral guanine radical. The signal at 600 nm is considerably smaller for **Ru-GGG-GMG** and **Ru-GMG-GGG** reflecting a greater contribution from the more weakly absorbing guanine radical. However, the rise of the signal at 600 nm occurs with a rate of 10^7 s^{-1} for all assemblies. This lack of sensitivity of the rate of radical formation is consistent with earlier studies demonstrating that CT is not rate limiting over this distance range (*34*).

Perhaps most interesting are our observations that the relative orientations of the GGG and GMG sites do not affect methylindole cation radical formation. The transient absorption signals at 600 nm and the rates of formation for **Ru-GGG-GMG** and **Ru-GMG-GGG** are essentially identical. Lewis and coworkers have suggested a hopping rate of 10^6 s^{-1} among guanine sites (*54*). If such a rate were operative here, one would expect to see differences in the transient profiles for these two assemblies on the microsecond time scale. Instead, the insensitivity to orientation that we observe supports a faster diffusive hopping mechanism.

The transient absorption data also provide insight into the different reactivity of the two sites. In **Ru-GMG**, which contains only one low potential site, the rate of

methylindole cation radical decay is ~ 10^6 s^{-1}. The rate of decay of the neutral guanine radical in similar DNA assemblies is much slower, ~ 10^4 s^{-1}(*31*). The differing rates of decay for the two radicals likely reflect their differing protonation states as well as the differing access of water and oxygen for trapping. There is little hydrogen bonding of M to the complementary C (*55*) and reduction of the neutral guanine radical requires a proton transfer, whereas reduction of the methylindole cation radical can be accomplished by a simple electron transfer. The transient signals obtained for assemblies containing both the GMG and GGG sites, **Ru-GGG-GMG** and **Ru-GMG-GGG**, are consistent with decay profiles for assemblies containing either GMG or GGG. For these assemblies the signal heights are smaller, as expected from the smaller extinction coefficient for neutral guanine radical as compared to methylindole cation radical (*48-50*). Moreover, the signals do not decay appreciably over the 50 μs time window, consistent with our earlier measurements of guanine radical decay in flash/quench experiments.

5.4.3 Competition between Two Oxidatively Sensitive Sites in DNA. The biochemical experiments confirm the competition between the methylindole and GGG sites, irrespective of orientation, and provide quantitative information regarding the yield of oxidized products at both sites. The damage yield at methylindole is lower by approximately 40% in **Ru-GGG-GMG** and **Ru-GMG-GGG** assemblies compared to the amount observed in **Ru-GMG**. Again these data support the idea that the GGG site is effective in competing for the migrating hole and provides an additional trapping site.

Thus by both biochemical and spectroscopic analysis, switching the orientation of the GMG and GGG does not affect the yield of CT products. Both forward and back CT

occur through the DNA base pair stack so as to provide equilibration across the duplex on a time scale that is fast compared to localization at a particular site(s).

Further evidence of charge equilibration results from incorporating an intervening base-stacking perturbation and monitoring the fate of the injected hole. Upon insertion of a 5'-ATA-3' base bulge, a 50% decrease in CT to the distal GGG site is observed as compared to the non-bulge-containing assembly. A decrease in CT to a distal site has been observed previously with base mismatches (*6*), nonaromatic protein side chains (*7*), and a variety of base bulges (*5*). In fact, using a tethered rhodium oxidant, insertion of a 5'-ATA-3' base bulge resulted in a 75% decrease in CT to a distal GG site. Differences in CT yield through this particular bulge may result from differing sequence contexts and/or oxidant used.

Most interestingly, with the decrease in CT to the distal GGG site as a result of the base bulge, an increase in oxidative damage at methylindole relative to **Ru-GMG-GGG** is observed. Thus we can consider this increase as a recovery in oxidative damage compared to the control assembly containing no GGG site. The recovery, however, is not complete. The intervening 5'-ATA-3' base bulge does not eliminate CT to the distal GGG site, it decreases damage at the distal site by 50%. Thus we find also a 50% recovery of methylindole damage upon insertion of the base bulge. These data suggest that the 50% of radicals that do not initially traverse the bulge to reach the GGG site instead return to the proximal methylindole site to yield oxidative damage. These experiments do not exclude the possibility of a charge migrating through the bulge in both forward and reverse directions to return to the methylindole site. In both instances,

however, equilibration across the duplex is achieved before trapping at an individual site(s).

Scheme 5.1 illustrates our model to account for the transient absorption and biochemical data. Following flash/quench and hole injection, charge propagation occurs in a forward direction with a rate k_f. In **Ru-GMG**, **Ru-GGG-GMG**, and **Ru-GMG-GGG**, the hole can sample the entire length of the duplex before returning with a rate k_r. In **Ru-GMG-blg-GGG**, the bulge presents a barrier to CT and most of the injected charge can only sample the region of the helix proximal to the ruthenium oxidant. Charge that might have been trapped at the distal GGG site in the absence of a bulge instead returns to the methylindole and is trapped as oxidative damage. Some charge may be trapped during forward propagation, however, there is certainly a portion of charges that are trapped after initially sampling the entire duplex. For **Ru-mis-GMG**, a base mismatch prevents charge propagation to yield the methylindole cation radical and the charge equilibrates only over the region of the duplex proximal to the ruthenium.

5.4.4 Kinetic and Themodynamic Traps of Charge Transport Damage. When examining oxidative damage at two sites in a DNA duplex, it is important to consider the respective kinetic and thermodynamic trapping abilities of the distinct sites. If one site presents a very deep thermodynamic well damage may be funneled exclusively to this site. If on the other hand, one site is a fast kinetic trap of oxidative damage, the second site may not be sampled. In order to observe competition between two different sites in DNA, neither site can behave as an absolute kinetic or thermodynamic trap.

In the data presented here both biochemical and spectroscopic analysis reveal comparable amounts of oxidative damage at the methylindole site in **Ru-GMG-GGG**

and **Ru-GGG-GMG**, regardless of orientation of the two oxidative traps. This lack of dependence on orientation of the trapping sites is in contrast to previous biochemical studies using an internally tethered anthraquinone oxidant (*15*). An intervening 8-oxo-G was found to reduce significantly the yield of oxidative damage at a distal GG site. However, when 8-oxo-G was not intervening and instead positioned distal to the GG site, the 8-oxo-G was not nearly as efficient in competing for and trapping oxidative damage. This contrasting behavior may result from differences in oxidation potential for methylindole and 8-oxo-G. The oxidation potential of methylindole is considerably higher than 8-oxo-G (E_0 = 0.6 – 0.8 V) (*56*). Additionally, based on calculations, the ionization potential of a GGG site is 0.2 eV lower than a GG site (*51*).

There is also precedence for a kinetic factor in the trapping of oxidative damage at two distinct sites in DNA. Selective and exclusive oxidation at a 7-deaza-guanine (^{Z}G) base in DNA was observed in the presence of a GGG site using a cyanobenzophenone-substituted 2'-deoxyuridine oxidant (*10*), despite the fact that theoretical calculations predict the ionization potential of ^{Z}G is 0.38 eV higher than GGG. A kinetic factor was suggested to explain the observed oxidative damage at only ^{Z}G. Oxidative damage was not examined in an assembly where the ^{Z}G and GGG sites were switched in orientation relative to the oxidant.

Another example of a kinetic trap for oxidizing equivalents in duplex DNA is a thymine dimer. The repair of this DNA lesion, which forms as a result of a [2 + 2] photocycloaddition between adjacent thymine bases, can be triggered by one-electron oxidation with a standard oxidation potential of approximately + 2.0 V (*57*, *58*). Thermodynamically, the thymine dimer is considerably more uphill to oxidize than a 5'-

GG-3' site. Furthermore, the radicals formed at the two sites have distinctively different lifetimes; the neutral guanine radical has a lifetime of 10^4 s^{-1} whereas the thymine dimer cation radical is estimated to have a lifetime of 10^9 s^{-1} (*59*). Nonetheless, when both a thymine dimer and a 5'-GG-3' site are present in a rhodium tethered duplex, both repair of the dimer and oxidation of the 5'-GG-3' site are observed (*60*). While the 5'-GG-3' site provides a thermodynamic trap, the dimer provides a kinetic trap resulting in competition between the two sites. Critical to these studies was the use of a high energy rhodium photooxidant (E_0 ($Rh^{3+*/2+}$) ~ 2 V vs. NHE). When analogous experiments were conducted with a ruthenium oxidant (E_0 ($Ru^{3+/2+}$) ~ 1.6 V vs. NHE) in combination with the flash/quench technique oxidative damage only at the 5'-GG-3' site was observed. Dppz complexes of Ru(III) are less potent oxidants and cannot trigger the repair of a thymine dimer lesion.

Importantly, by selecting appropriate sites, namely GMG and GGG, that are comparable energetically and kinetically, we can observe charge equilibration over the DNA duplex. Charge migration leads to a sampling of the entire duplex on a time scale that is fast compared to localization and trapping. Charge transport through DNA can not be considered statically with conclusions based upon measurements of yield. Instead, the reaction must be viewed dynamically with rates of CT across the duplex in both forward and reverse directions being considered.

5.5 REFERENCES

(1) (a) Boon, E. M., and Barton, J. K. (2002) *Curr. Opin. Struct. Biol*. *12*, 320. (b) Delaney, S., and Barton, J. K. (2003) *J. Org. Chem. 68*, 6475.

(2) Schuster, G. B. (2000) *Acc. Chem. Res. 33*, 253.

(3) Giese, B. (2002) *Ann. Rev. Biochem. 71*, 51.

(4) Lewis, F. D., Letsinger, R. L., and Wasielewski, M. R. (2001) *Acc. Chem. Res. 34*, 159.

(5) Hall, D. B., and Barton, J. K. (1997) *J. Am. Chem. Soc*. *119*, 5045.

(6) (a) Bhattacharya, P. K., and Barton, J. K. (2001) *J. Am. Chem. Soc*. *123*, 8649. (b) Bhattacharya, P. K., Cha, J., and Barton, J. K. (2002) *Nuc. Acids Res*. *30*, 4740.

(7) Wagenknecht, H.-A., Rajski, S. R., Pascaly, M., Stemp, E. D. A., and Barton, J. K. (2001) *J. Am. Chem. Soc. 123*, 4401.

(8) (a) Schlientz, N. W., and Schuster, G. B. (2003) *J. Am. Chem. Soc*. *125*, 15432. (b) Schlientz, N. W., and Schuster, G. B. (2004) *J. Am. Chem. Soc*. *126*, 1921.

(9) Williams, T. T., Odom, D. T., and Barton, J. K. (2000) *J. Am. Chem. Soc*. *122*, 9048.

(10) Nakatani, K., Dohno, C., and Saito, I. (2000) *J. Am. Chem. Soc*. *122*, 5893.

(11) Furrer, E., and Giese, B. (2003) *Helv. Chim. Acta. 86*, 3632.

(12) (a) Kawai, K., Takada, T., Tojo, S., and Majima, T. (2004) *J. Am. Chem. Soc*. *126*, 1125. (b) Kawai, K., Takada, T., Nagai, T., Cai, X. C., Sugimoto, A., Fujitsuka, M., and Majima, T. (2003) *J. Am. Chem. Soc*. *125*, 16198. (c) Takada, T., Kawai, K., Tojo, S., and Majima, T. (2003) *J. Phys. Chem. B 107*, 14052.

(13) (a) Lewis, F. D., Liu, J. Q., Weigel, W., Rettig, W., Kurnikov, I. V., and Beratan, D. N. (2002) *Proc. Natl. Acad. Sci. U. S. A. 99*, 12536. (b) Lewis, F. D., Liu, X. Y., Miller, S. E., Hayes, R. T., and Wasielewski, M. R. (2002) *J. Am. Chem. Soc*. *124*, 14020. (c) Lewis, F. D., Zuo, X. B., Liu, J. Q., Hayes, R. T., and Wasielewski, M. R. (2002) *J. Am. Chem. Soc*. *124*, 4568.

(14) Núñez, M. E., Hall, D. B., and Barton, J. K. (1999) *Chem. Biol*. *6*, 85.

(15) Ly, D., Sanii, L., and Schuster, G. B. (1999) *J. Am. Chem. Soc*. *121*, 9400.

(16) Núñez, M. E., Noyes, K. T., and Barton, J. K. (2002) *Chem. Biol*. *9*, 403.

(17) Núñez, M. E., Holmquist, G. P., and Barton, J. K. (2001) *Biochemistry 40*, 12465.

(18) Hall, D. B., Holmlin, R. E., and Barton, J. K. (1996) *Nature 382*, 731.

(19) Núñez, M. E., Noyes, K. T., Gianolio, D., McLaughlin, L. W., and Barton, J. K. (2000) *Biochemistry 39*, 6190.

(20) Hall, D. B., Kelley, S. O., and Barton, J. K. (1998) *Biochemistry 37*, 15933.

(21) Gasper, S. M., and Schuster, G. B. (1997) *J. Am. Chem. Soc*. *119*, 12762.

(22) Nakatani, K., Dohno, C., and Saito, I. (1999) *J. Am. Chem. Soc*. *121*, 10854.

(23) Meggers, E., Kusch, D., Spichty, M., Wille, U., and Giese, B. (1998) *Angew. Chem., Int. Ed*. *37*, 460.

(24) (a) Bixon, M., Giese, B., Wessely, S., Langenbacher, T., Michel-Beyerle, M. E., and Jortner, J. (1999) *Proc. Nat. Acad. Sci. U. S. A. 96*, 11713. (b) Giese, B., Wessely, S., Spormann, M., Lindemann, U., Meggers, E., and Michel-Beyerle, M. E. (1999) *Angew. Chem. Int. Ed*. *38*, 996.

(25) Kendrick, T., and Giese, B. (2002) *Chem. Comm*. *18*, 2016.

(26) Henderson, P. T., Jones, D., Hampikian, G., Kan, Y., and Schuster, G. B. (1999) *Proc. Nat. Acad. Sci. U. S. A. 96*, 8353.

(27) Kelley, S. O., and Barton, J. K. (1999) *Science 283*, 375.

(28) O'Neill, M. A., Becker, H.-C., Wan, C., Barton, J. K., and Zewail, A. H. (2003) *Angew. Chem,.Int. Ed*. *42*, 5896.

(29) O'Neill, M. A., and Barton, J. K. (2004) Manuscript submitted.

(30) Chang, I.-J., Gray, H. B., and Winkler, J. R. (1991) *J. Am. Chem. Soc*. *113*, 7056.

(31) Stemp, E. D. A., Arkin, M. R., and Barton, J. K. (1997) *J. Am. Chem. Soc*. *119*, 2921.

(32) Burrows, C. J., and Muller, J. G. (1998) *Chem. Rev*. *98*, 1109.

(33) Wagenknecht, H. A., Stemp, E. D. A., and Barton, J. K. (2000) *Biochemistry 39*, 5483.

(34) Pascaly, M., Yoo, J., and Barton, J. K. (2002) *J. Am. Chem. Soc*. *124*, 9083.

(35) Yoo, J., Delaney, S., Stemp, E. D. A., and Barton, J. K. (2003) *J. Am. Chem. Soc*. *125*, 664.

(36) Dohno, C., Stemp, E. D. A., and Barton, J. K. (2003) *J. Am. Chem. Soc*. *125*, 9586.

(37) O'Neill, M. A., Dohno, C., and Barton, J. K. (2004) *J. Am. Chem. Soc*. *126*, 1316.

(38) Reid, G. D., Whittaker, D. J., Day, M. A., Creely, C. M., Tuite, E. M., Kelly, J. M., and Beddard, G. S. (2001) *J. Am. Chem. Soc*. *123*, 6953.

(39) Williams, T. T., Dohno, C., Stemp, E. D. A., and Barton, J. K. (2004) Manuscript submitted.

(40) Della Ciena, L., Hamachi, I., and Meyer, T. J. (1989) *J. Org. Chem*. *54*, 1731.

(41) Dupueur, C. M., and Barton, J. K. (1997) *Inorg. Chem*. *36*, 33.

(42) (a) Amouyal, E., Homsi, A., Chambron, J.-C., and Sauvage, J.-P. (1990) *J. Chem. Soc., Dalton Trans*. 1841. (b) Strouse, G. F., Anderson, P. A., Schoonover, J. R., Meyer, T. J., and Keene, F. R. (1992) *Inorg. Chem*. *31*, 3004. (c) Anderson, P. A., Deacon, G. B., Haarman, K. H., Keene, F. R., Meyer, T. J., Reitsma, D. A., Skelton, B. W., Strouse, G. F., Thomas, N. C., and Treadway, J. A. (1995) *Inorg. Chem*. *34*, 6145.

(43) (a) Beaucage, S. L., and Caruthers, M. H. (1981) *Tetrahedron Lett*. *22*, 1859. (b) Goodchild, J. (1990) *Bioconj. Chem*. *1*, 165.

(44) Holmlin, R. E., Dandliker, P. J., and Barton, J. K. (1999) *Bioconj. Chem*. *10*, 1122.

(45) Sambrook, J., Fritsch, E. F., and Maniatis, T. (1989) *Molecular Cloning: A Laboratory Manual*, 2nd ed.; Cold Spring Harbor Laboratory: New York.

(46) Rougee, M., and Bensasson, R. V. (1986) *C. R. Acad. Sci. Ser. II 302*, 1223.

(47) (a) Delaney, S., Pascaly, M., Bhattacharya, P., Koun, H., and Barton, J. K. (2002) *Inorg. Chem*. *41*, 1966. (b) Lincoln, P., Broo, A., and Norden, B. (1996) *J. Am. Chem. Soc*. *118*, 2644.

(48) Candeias, L. P., and Steenken, S. (1989) *J. Am. Chem. Soc*. *111*, 1094.

(49) Steenken, S., and Jovanovic, S. V. (1997) *J. Am. Chem. Soc*. *119*, 617.

(50) Solar, S., Getoff, N., Surdar, P. S., Armstrong, D. A., and Gingh, A. (1991) *J. Phys. Chem*. *95*, 3639.

(51) Fahlman, R. P., Sharma, R. D., and Sen, D. (2002) *J. Am. Chem. Soc*. *124*, 12477.

(52) (a) Saito, I., Takayama, M., Sugiyama, H., Nakatani, K., Tsuchida, A., and Yamamoto, M. *J. Am. Chem. Soc*. **1995**, *117*, 6406. (b) Prat, F., Houk, K. N., and Foote, C. S. *J. Am. Chem. Soc*. **1998**, *120*, 845.

(53) Lewis, F. D., Liu, X., Liu, J., Hayes, R. T., and Wasielewski, M. R. (2000) *J. Am. Chem. Soc. 122*, 12037.

(54) Lewis, F. D., Liu, X., Liu, J., Miller, S. E., Hayes, R. T., and Wasielewski, M. R. (2000) *Nature 406*, 51.

(55) (a) Guckian, K. M., Morales, J. C., and Kool, E. T. (1998) *J. Org. Chem*. *63*, 9652. (b) Kool, E. T. (2001) *Annu. Rev. Biophys. Biomol. Struct. 30*, 1.

(56) (a) Berger, M., Anselmino, C., Mouret, J.-F., and Cadet, J. (1990) *J. Liq. Chromatogr*. *13*, 929. (b) Goyal, R. N., and Dryhurst, G. (1992) *J. Electroanal. Chem*. *135*, 75. (c) Yanagawa, H., Ogawa, Y., and Ueno, M. (1992) *J. Biol. Chem*. *267*, 13320.

(57) Heelis, P. F., Deeble, D. J., Kim. S.-T., and Sancar, A. (1992) *Int. J. Radiat. Biol*. *62*, 137.

(58) Pac, C., Kubo, J., Tetsuro, M., and Sakurai, H. (1982) *Photchem. Photobiol*. *36*, 273.

(59) Kemmink, J., Eker, A. P. M., and Kaptein, R. (1986) *Photochem. Photobiol*. *44*, 137.

(60) Dandliker, P. J., Nunez, M. E., and Barton, J. K. (1998) *Biochemistry 37*, 6491.

Table 5.1. Kinetic data for [Ru(bpy')(dppz)(phen)]$^{2+}$ and the Methylindole Radical (M_{rad})[a]

	Ru-GMG	**Ru-GMG-GGG**	**Ru-GGG-GMG**	**Ru-mis-GMG**
luminescence lifetime of *[Ru]$^{2+}$-DNA [b]	τ_1=71 ns (76%) τ_2=279 ns (26%)	τ_1=68 ns (76%) τ_2=227 ns (26%)	τ_1=72 ns (79%) τ_2=269 ns (26%)	τ_1=80 ns (74%) τ_2=280 ns (29%)
M_{rad} formation[c,e]	4×10^7 s^{-1}	4×10^7 s^{-1}	4×10^7 s^{-1}	N/A
M_{rad} decay[c,d]	1×10^6 s^{-1}	*f*	*f*	N/A

[a] All samples contained 20 μM Ru-duplex, 10 mM NaCl, 10 mM potassium phosphate, pH 7. [b] The luminescence traces were fit to a biexponential function by nonlinear least-squares method with convolution of the instrument response function. Uncertainties in values are ± 10%. [c] Samples contained 15 equivalents of $[Ru(NH_3)_6]^{3+}$. [d] The transient absorption decay at 600 nm corresponding to the M_{rad} was fit to a monoexponential function by nonlinear least-squares method. Uncertainties in values are ± 10%. [e] The rise of the signal at 600 nm was fit to a monoexponential function by nonlinear least-squares method. Considering bandwidth used and region fit, these values represent lower limits. [f] No significant decay observed over 50 μs.

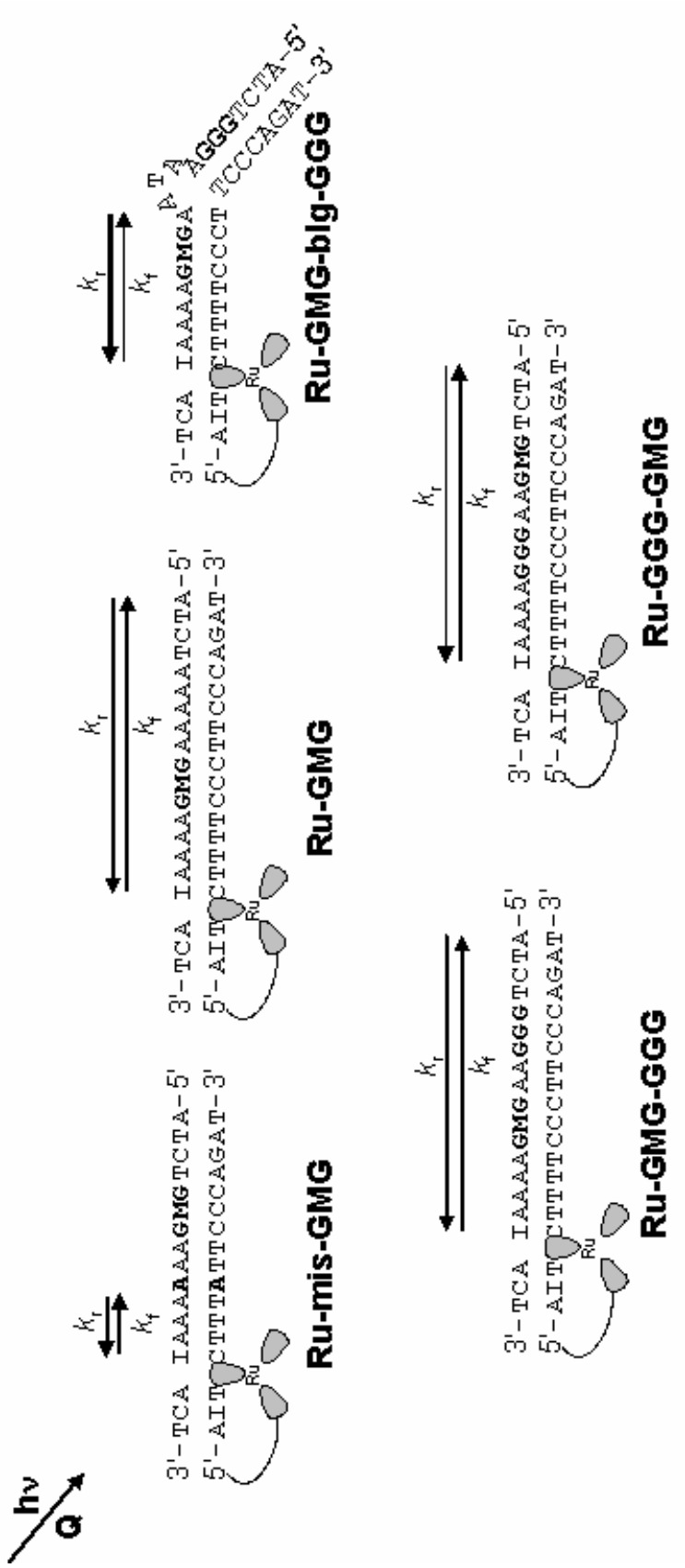

Scheme 5.1. Proposed model of charge equilibration in DNA CT.

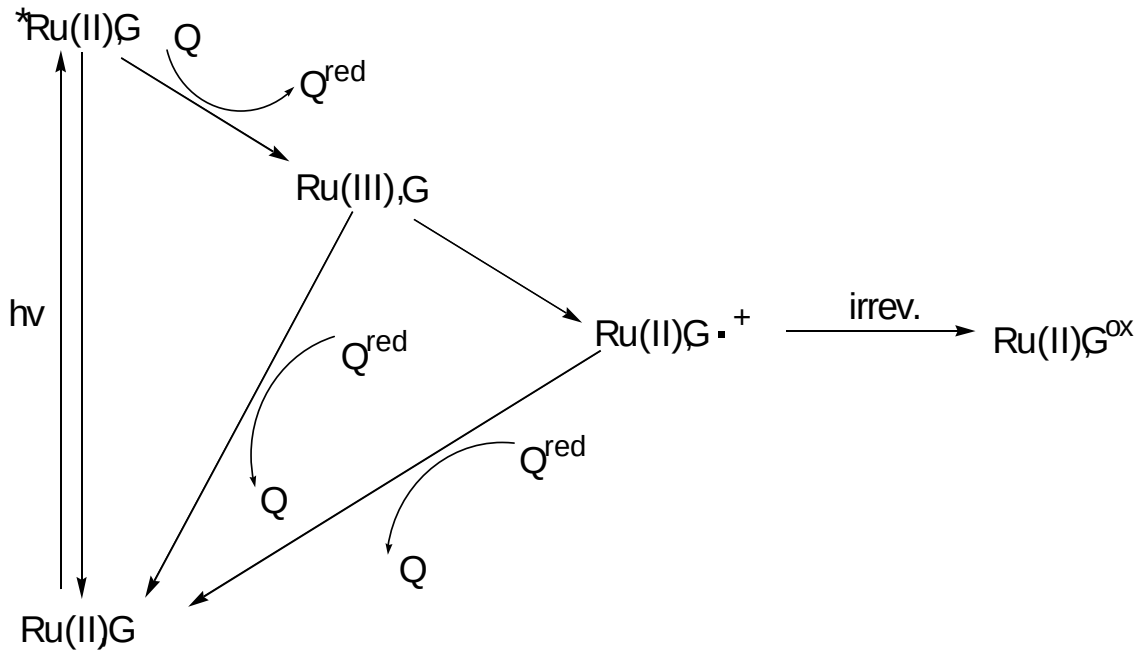

Figure 5.1. Schematic of the flash/quench technique. The intercalating Ru(II) oxidant is excited with visible light to yield *Ru(II). This excited state is quenched with an electron accepting molecule diffusing in solution such as $[Ru(NH_3)_6]^{3+}$, $[Co(NH_3)_5Cl]^{2+}$, or methyl viologen. This quenching reaction yields reduced quencher (Q_{red}) and a Ru(III) oxidant which can oxidize guanine from a distance.

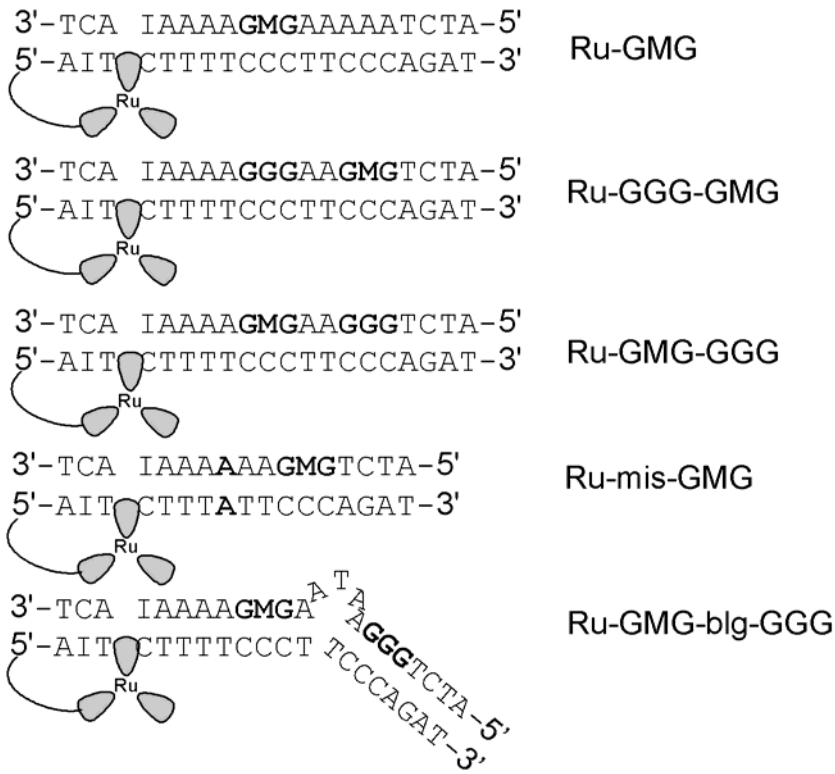

Figure 5.2. Schematic illustrations of the DNA assemblies used in this study. Ru = [Ru(bpy')(dppz)(phen)]2+, I = inosine nucleotide, and M = methylindole nucleotide.

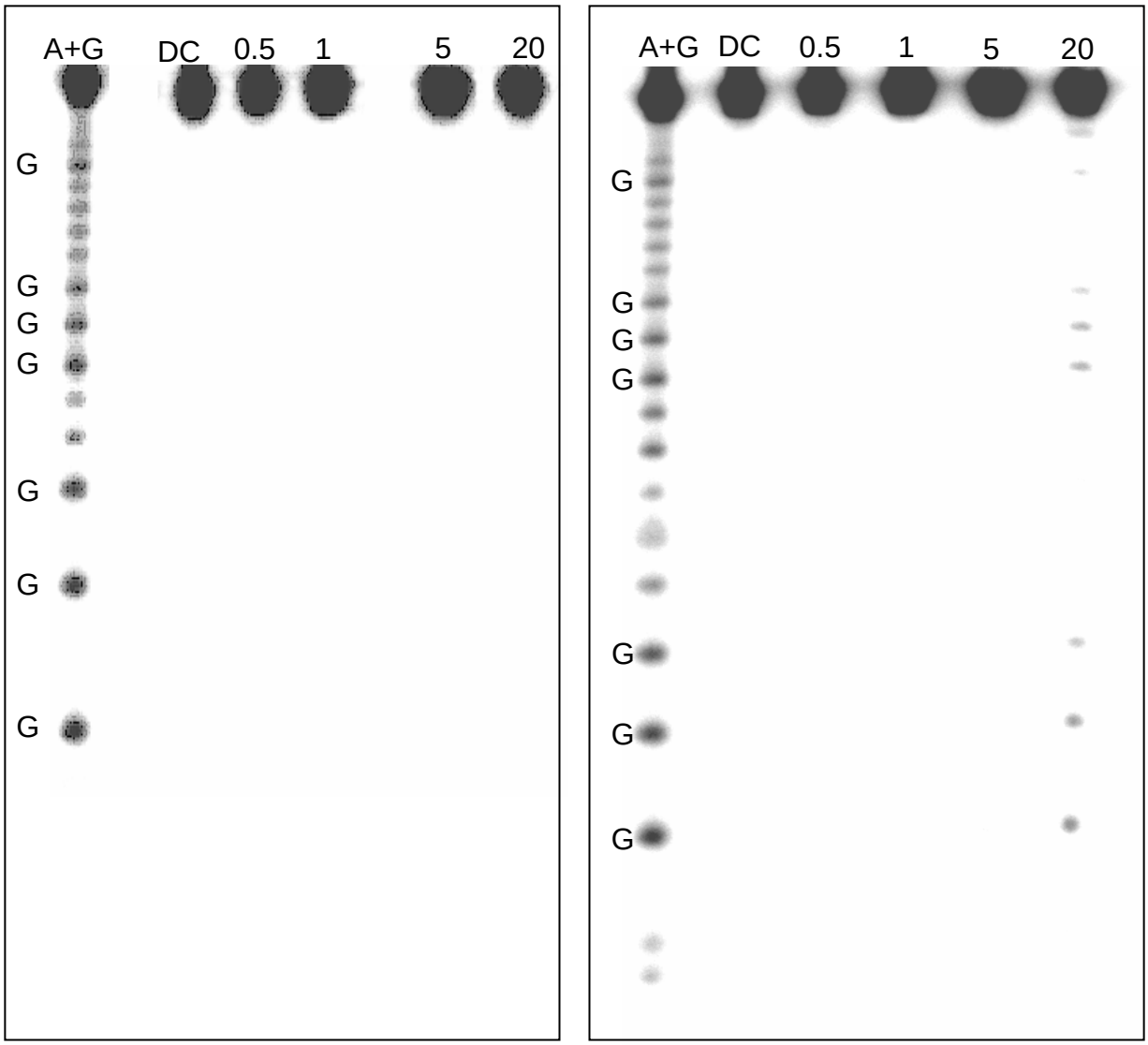

Figure 5.3. PAGE after irradiation of **Ru-GMG-GGG** (left) and bulge-containing duplex **Ru-GMG-blg-GGG** (right) in the absence of quencher. Samples contained equimolar amounts of nonlabeled duplex containing the ruthenium oxidant and ^{32}P-labeled duplexes without ruthenium. Lane 1 shows the Maxam-Gilbert sequencing reaction A+G. Lane 2 shows damage of 5 μM duplex in the absence of light. Lanes 3, 4, 5, and 6 display damage after 60 min of irradiation of 0.5, 1, 5, and 20 μM Ru-DNA, respectively. All samples contained 15 mM sodium phosphate, pH 7 with 50 mM NaCl.

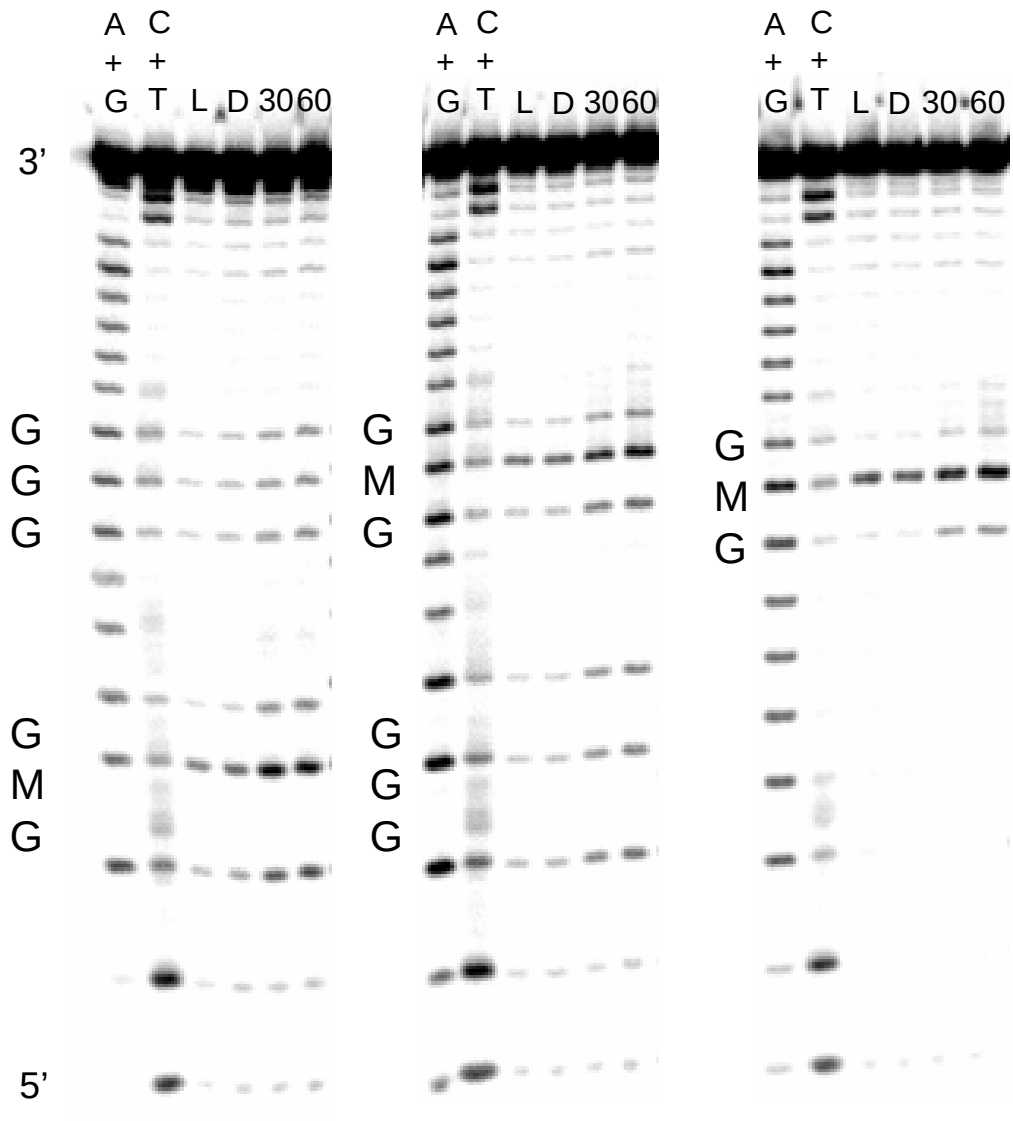

Figure 5.4. PAGE results following irradiation of **Ru-GGG-GMG** (left), **Ru-GMG-GGG** (center), and **Ru-GMG** (right) in the presence of quencher. For each assembly, lanes 1 and 2 represent the Maxam-Gilbert sequencing reactions A + G and C + T, respectively. Lane 3 is a light control irradiated for 30 min in the absence of quencher. Lanes 4, 5, and 6 show oxidative damage after 0, 30, and 60 min of irradiation, respectively. Samples consisted of 5 μM duplex, 15 mM sodium phosphate, pH 7, 50 mM NaCl, 125 μM $[Co(NH_3)_5Cl]^{2+}$.

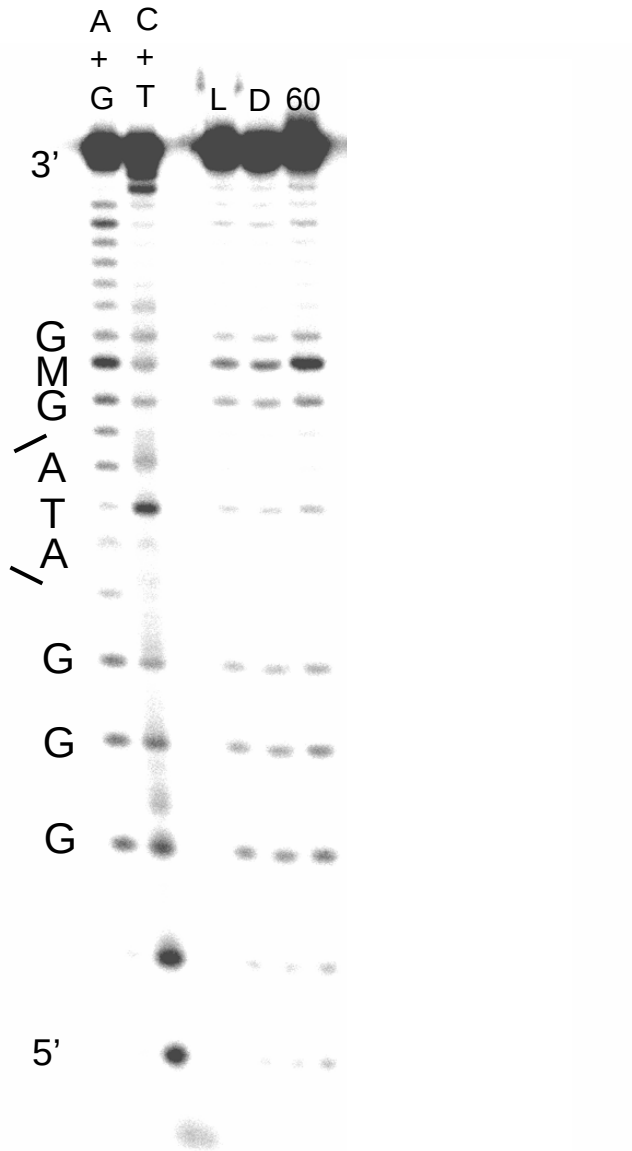

Figure 5.5. PAGE results following irradiation of **Ru-GMG-blg-GGG** in the presence of quencher. Lanes 1 and 2 represent the Maxam-Gilbert sequencing reactions A + G and C + T, respectively. Lane 3 is a light control irradiated for 30 min in the absence of quencher. Lanes 4 and 5 show oxidative damage after 0 and 60 min of irradiation, respectively. Samples consisted of 1 μM duplex, 15 mM sodium phosphate, pH 7, 50 mM NaCl, 125 μM $[Co(NH3)_5Cl]^{2+}$.

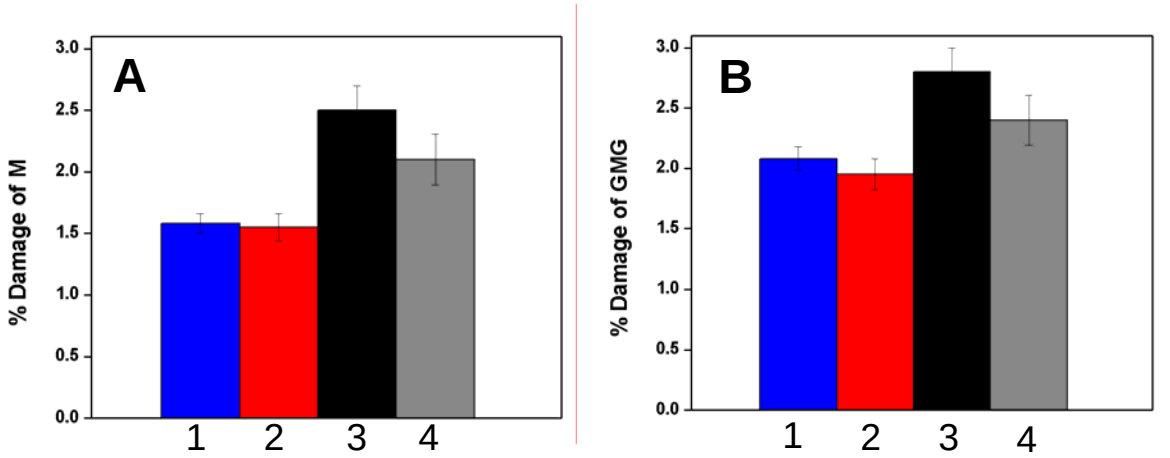

Figure 5.6. Quantitation of damage observed by PAGE at A) methylindole alone or B) methylindole and flanking guanines as compared to parent band for **Ru-GGG-GMG** (1), **Ru-GMG-GGG** (2), **Ru-GMG** (3), and **Ru-GMG-blg-GGG** (4).

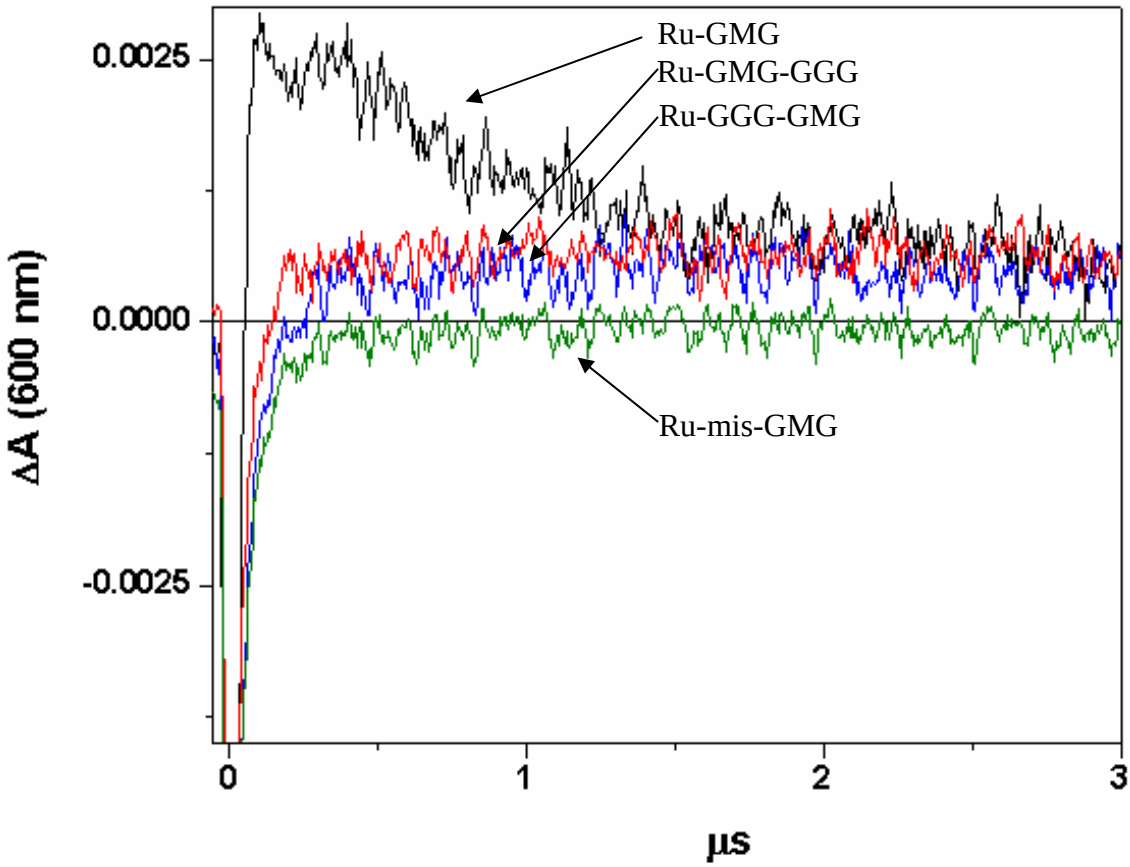

Figure 5.7. Time-resolved transient absorption traces at 600 nm for **Ru-GMG** (black), **Ru-GGG-GMG** (blue), **Ru-GMG-GGG** (red), and **Ru-mis-GMG** (green). The samples contained 20 μM Ru-duplex, 300 μM $[Ru(NH_3)_6]^{3+}$, 10 mM NaCl, 10 mM potassium phosphate, pH 7.

CHAPTER 6

Charge Transport in DNA Duplex/Quadruplex Conjugates

Adapted from: Delaney, S., and Barton, J. K. (2003) *Biochemistry 42*, 14159.

6.1 INTRODUCTION

DNA quadruplexes have received a wealth of attention in the recent literature (*1-4*). These structures have gained notoriety as inhibitors of telomerase (*5*), the enzyme that provides cancerous cells immortality, and quadruplex formation has recently been implicated as a transcriptional repressor element (*6*). The unique structure of guanine quadruplexes consists of stacked tetrads where each tetrad, as shown in Figure 6.1, is a planar array of four Hoogsteen-bonded guanines (*7*). The formation of guanine quadruplexes is stabilized by the presence of monovalent cations (e.g. K^+, Na^+) positioned in the center of the structure and coordinated by the electron-rich carbonyl oxygens (*8, 9*). Quadruplexes can form in an intramolecular fashion from a single strand, from two DNA hairpins, or from four individual strands. Depending on the strand orientation, both parallel and antiparallel quadruplexes are possible (*10*).

DNA quadruplexes have been proposed to form at telomeres (*7, 11*), the repetitive DNA sequence located at the ends of linear chromosomes. Human telomeric-DNA is composed of approximately 10 kb of double stranded $(5'\text{-TTAGGG-}3')_n$ repeats (*12*). The extreme 3'-end is a 200-300 base single stranded overhang of the guanine containing strand (*13*). These guanine-rich single stranded overhangs have been shown *in vitro* to form guanine quadruplexes (*10*). Of particular relevance to the studies described here, it has been proposed that these guanine-rich telomeric regions may serve as hot spots for oxidative DNA damage within the genome (*14*).

Oxidative damage to DNA has been shown to arise not only as a result of reaction of DNA with an impinging oxidant but also as a result of reaction from a distance through DNA charge transport (CT) from a remotely bound oxidant (*15-18*). The base

stack of B-DNA has been shown to mediate CT over a distance of 200 Å (*19*, *20*). By triplex targeting of a photooxidant to long DNA restriction fragments, the typical distance regime for long-range oxidative damage to DNA by CT was shown to be ~ 60 base pairs (*21*). DNA packaged within a nucleosome core particle is also subject to oxidative damage from a distance (*22*). Moreover, long-range oxidative damage to DNA has been demonstrated within *Hela* cell nuclei (*23*). Thus, oxidative damage to DNA from a distance through DNA CT chemistry provides a feasible mechanism for the generation of cellular base lesions and now requires consideration as a mechanism for DNA damage within the cell.

In that context, it has been suggested that telomeric regions of DNA, rich in guanine-containing repetitive sequences and hot spots for oxidative damage, might provide regions to which oxidizing equivalents are funneled through long-range CT. Heller has proposed a means of cathodic DNA protection similar to the way in which Zn^{2+} protects steel (*24*). The number of 5'-GGG-3' triple guanine sites was shown statistically to be elevated in the regions flanking protein-coding exons, and thus it was suggested that charges injected into DNA might be funneled to these sacrificial guanine-rich introns or to the non-protein coding sequences of guanine-rich telomeric-DNA. Our studies of the distance regime for long-range oxidative damage indicate that funneling of all damage to telomeres is unlikely, and electrochemical studies of oxidative damage in quadruplexes have suggested that the structure is not more reactive to accessible oxidants than duplex DNA (*25*). It is of interest, nonetheless, to establish whether telomeric regions and the quadruplex structures proposed to form within telomeres might represent

domains for long-range CT. Here we describe long-range CT to quadruplex structures to effect oxidative DNA damage.

6.2 METHODS

6.2.1 Oligonucleotide Synthesis and Formation of DNA Duplex/Quadruplex Conjugates. Oligonucleotides were synthesized on an ABI 392 DNA/RNA synthesizer, using standard phosphoramidite chemistry (*26*). DNA was purified by HPLC using a Dynamax 300 Å C18 reverse-phase column (Rainin) (100% 30 mM NH_4OAc to 85% 30 mM NH_4OAc/15% acetonitrile over 30 min). Quantification was done on a Beckman DU 7400 Spectrophotometer using the ε_{260} values estimated for single stranded DNA (*27*). The $[Rh(phi)_2bpy']^{3+}$ (phi = phenanthrenequinone diimine, bpy' = 4'-methylbipyridine-4-butyric acid) tethered oligonucleotides were prepared as described previously (*28*) and were purified by HPLC on a Dynamax 300 Å C18 reverse-phase column (85% 30 mM NH_4OAc/15% acetonitrile to 75% 30 mM NH_4OAc/25% acetonitrile over 40 min). The rhodium-conjugated oligonucleotides were characterized by mass spectrometry (MALDI) and quantitated by UV-vis using an extinction coefficient of ε_{350} = 23,600 $M^{-1}cm^{-1}$. To form the DNA duplex/quadruplex conjugate, equimolar concentrations of the quadruplex forming strand and the 10 base complement were annealed in 10 mM potassium phosphate, pH 7 with 100 mM KCl. Samples were heated to 90 °C and slowly cooled to room temperature.

6.2.2 Circular Dichroism Measurements. CD spectra were obtained on an AVIV CD spectrometer at room temperature. Unmetallated oligonucleotides were utilized for all CD measurements to avoid a signal from the rhodium photooxidant. The

conjugate concentration was 2.5 μM, duplex was 4 μM, and quadruplex forming strand alone was 4 μM, and all were in 10 mM potassium phosphate, pH 7 with 100 mM KCl. The melting profile of the conjugate (2.5 μM) was obtained by slowly lowering the temperature (0.5 °C/min) from 85 to 25 °C and monitoring the ellipticity at 285 nm. Melting and annealing profiles of **G4** were monitored at 295 nm. The melting temperature value represents the midpoint of the transition as obtained by fitting the melting profile with a sigmoidal expression.

6.2.3 Dimethyl Sulfate Protection Assay. The quadruplex forming single strand was 5'-^{32}P-end-labeled using standard protocols and the conjugate was annealed at a concentration of 4 μM. The duplex control was also annealed at a concentration of 4 μM. The assemblies were treated with 10% (v/v) DMS for 10 min at ambient temperature; reactions were stopped by adding quenching buffer (1 M β-mercaptoethanol, 1.5 M sodium acetate, pH 7). Samples were ethanol precipitated and treated with 10% piperidine (v/v) at 90 °C for 30 min, dried, and electrophoresed through a 20% denaturing polyacrylamide gel. The extent of methylation was visualized by phosphorimagery (ImageQuant).

6.2.4 Native Gel Electrophoresis. The quadruplex forming single strand was 5'-^{32}P-end-labeled using standard protocols and the conjugate was annealed at a concentration of 4 μM in 10 mM potassium phosphate, pH 7 with 100 mM KCl. Samples were electrophoresed at 4 °C and 10 W for ~ 12 hours through a 12% nondenaturing gel containing 100 mM KCl in the gel matrix, running buffer (0.5X TBE), and loading dye. The products were visualized by phosphorimagery (ImageQuant).

6.2.5 Assay of Oxidative DNA Damage. The quadruplex forming single strand was 5'-^{32}P-end-labeled as above and the conjugates were annealed at a concentration of 4 μM. Experiments utilizing noncovalently bound photooxidant contained either 4 or 40 μM $[Rh(phi)_2bpy']^{3+}$. For the rhodium photocleavage experiments, samples were irradiated at 313 nm with a 1000 W Hg/Xe lamp equipped with a monochromator, and dried following irradiation. For the CT experiments, samples were irradiated at 365 nm, treated with 10% (v/v) piperidine at 90 °C for 30 min, dried, and all samples were electrophoresed through a 20% denaturing polyacrylamide gel. The extent of damage was visualized by phosphorimagery (ImageQuant).

6.3 RESULTS

6.3.1 Design of Duplex/Quadruplex Assemblies. DNA conjugates containing adjacent duplex and guanine quadruplex structures were designed as shown in Figure 6.1. First, we examined oxidative damage in a duplex/quadruplex conjugate (**DQ-1**) using noncovalently bound $[Rh(phi)_2bpy']^{3+}$. The rhodium photooxidant is particularly useful owing to its well-characterized photochemistry with DNA. Upon high energy irradiation (λ = 313 nm), this rhodium complex promotes direct strand cleavage owing to hydrogen atom abstraction from the sugar ring closest to the intercalation site; this reaction marks the site of binding by the photooxidant (*29*). When irradiated at lower energy (λ = 365 nm), the rhodium complex promotes guanine oxidation at sites remote from the photooxidant via DNA CT (*30*); with piperidine treatment, irreversible oxidative damage is revealed.

In designing **DQ-1**, a 10 base pair duplex region was selected to provide a suitable binding site for the photooxidant and to contain a 5'-GG-3' guanine doublet, while the 22 bases of the single stranded overhang should form an intramolecular guanine quadruplex. A crystal structure of this 22 base single strand in the presence of K^+ indicates formation of a parallel quadruplex (*31*), while an NMR solution structure in the presence of Na^+ indicates formation of an antiparallel quadruplex (*32*). Circular dichroism studies show the formation of an antiparallel quadruplex in the presence of either K^+ or Na^+ (*33*).

An assembly analogous to **DQ-1** contains the rhodium photooxidant covalently tethered to the end of the duplex (**DQ-2**). In a third assembly, **DQ-3**, which also includes covalently tethered rhodium photooxidant, a single base pair has been changed to yield a 5'-GA-3' in the duplex region. These three conjugates allow us to probe CT between the two distinct regions, duplex and quadruplex. Additionally, in the conjugates containing a covalently bound rhodium photooxidant, CT through duplex/quadruplex junctions can be examined.

6.3.2 Characterization of DNA Duplex/Quadruplex Conjugates by Circular Dichroism. Antiparallel and parallel guanine quadruplexes possess characteristic and distinct circular dichroism spectra. Antiparallel quadruplexes are characterized by maxima at 290 nm and minima at 260 nm; parallel quadruplexes possess maxima at 260 nm and minima at 240 nm (*34*). In order to fully characterize a single DNA conjugate by CD, three assemblies were examined; the first contains only the quadruplex forming strand with no 10 base complement; the second assembly consists of the 10 base pair duplex with no 22 base overhang; the third assembly is the duplex/quadruplex conjugate.

Figure 6.2 shows the circular dichroism spectra for the quadruplex forming strand alone of **DQ-1** (closed circles), 10 base pair duplex of **DQ-1** alone (closed triangles), and **DQ-1** (open circles). For the quadruplex-forming strand, a maximum at 290 nm in addition to a minimum at 260 nm is observed indicating the formation of an antiparallel quadruplex. The minimum at 240 nm likely results from the 10 bases not involved in quadruplex formation, as this minimum is present even at denaturing temperatures (data not shown). The CD spectrum of **DQ-1** has a maximum at 290 nm indicative of antiparallel quadruplex formation, in addition to a broad minimum centered around 250 nm, similar to that of the 10 base pair duplex alone.

6.3.3 Protection from Dimethyl Sulfate to Determine Guanine Quadruplex Formation. In double helical DNA, the N-7 of guanine is susceptible to methylation by DMS. However, as seen in Figure 6.1, the N-7 of guanine in a tetrad is involved in hydrogen bonding and is therefore protected from methylation. Methylation by DMS was examined in the duplex/quadruplex conjugates in addition to control assemblies in which the quadruplex forming strand was base paired to its complement, resulting in a 32 base pair duplex. As seen in Figure 6.3 for the **DQ-3** duplex control, all guanines in the duplex are methylated, as expected. However, in **DQ-3** methylation is only observed in the 10 base pair duplex (the first guanine proximal to the duplex, although involved in quadruplex formation, may be transiently accessible by DMS as methylation is observed). The remaining guanines are protected from methylation, consistent with guanine quadruplex formation. Similar methylation patterns were obtained for **DQ-1** and **DQ-2** (Figure 6.4).

6.3.4 Structural Analysis by Native Gel Electrophoresis. After electrophoresis through a nondenaturing gel, all three duplex/quadruplex conjugates **DQ-1**, **DQ-2**, and **DQ-3** migrate as single bands, representing a unique structure containing an intramolecular guanine quadruplex (Figure 6.5). The observance of only one band indicates the presence of a single species, not multiple species or species containing more than one global conformation. Importantly, since slower moving bands are not observed, the conjugates do not aggregate under the conditions used for the CT experiments.

6.3.5 Melting Temperature Studies of the Duplex/Quadruplex Conjugates. The melting temperature profile of **DQ-1**, monitored at 285 nm by CD, is shown in Figure 6.6. A single transition is observed. These data were fit to a sigmoidal curve and the inflection point yields a melting temperature of 60.8 °C for **DQ-1**. Previous studies of this quadruplex forming sequence, performed under comparable salt conditions, revealed little hysteresis between the annealing and melting curves (*35*). Importantly, the melting temperature is independent of concentration indicative of an intramolecular quadruplex (*35*). Melting temperature experiments were performed for the 10 base pair duplex and quadruplex forming strand alone yielding melting temperatures of 58.6 °C and 59.0 °C, respectively (Figure 6.7). Due to the similarities in melting temperatures, it is not surprising that only one melting transition is observed for **DQ-1**. In fact, the temperature range over which the transition occurs is the same for the quadruplex forming strand alone as for the duplex/quadruplex conjugate.

6.3.6 Charge Transport Chemistry in DNA Duplex/Quadruplex Conjugates. Figure 6.8 shows the denaturing PAGE of **DQ-1** after photoactivation of the noncovalently bound rhodium intercalator. In the 313 lane, where direct strand cleavage

by the rhodium complex is assayed, damage is observed exclusively in the duplex portion of the conjugate, particularly the two bases adjacent to the quadruplex. These sites may be more accessible to rhodium binding due to proximity of the quadruplex or duplex fraying. Since the rhodium photooxidant cannot promote direct strand scission on single stranded DNA, the damage observed after irradiation at 313 nm provides evidence that the 10 base pair duplex is indeed forming. Interestingly, with irradiation at 313 nm, no damage is observed in the quadruplex portion of the conjugate. It is noteworthy that when present in excess, this rhodium photooxidant can promote direct strand cleavage within the quadruplex region. At equimolar concentrations, however the oxidant appears to bind preferentially to the duplex rather than quadruplex DNA. Upon irradiation of **DQ-1** at 365 nm in the presence of rhodium photooxidant, damage is observed only in the quadruplex region. Specifically, damage is observed almost exclusively at the 5'-G and 3'-G of each 5'-GGG-3' guanine triplet comprising the quadruplex. There is very little damage detected at the center G's of the triplets or within the duplex region.

In order to explore CT in duplex/quadruplex conjugates where the location of photooxidant binding and, therefore, radical injection are defined, **DQ-2** and **DQ-3** containing the duplex-tethered rhodium intercalator, were utilized. Figure 6.9A shows the denaturing PAGE of both **DQ-2** and **DQ-3** after photoactivation of the rhodium intercalator. In the 313 lanes, reflecting direct reaction by the rhodium complex, damage is observed only at the end of the duplex, as expected for our covalently tethered photooxidant. Importantly, this establishes the duplex end as the site of radical injection. Furthermore, the observation of direct strand scission assures duplex formation, as discussed earlier. After irradiation of **DQ-2** and **DQ-3** at 365 nm, damage is observed at

guanines in the quadruplex portion. As we had observed with **DQ-1**, for all of the 5'-GGG-3' triple guanine sites comprising the quadruplex regions, damage is observed almost exclusively at the 3'- and 5'-G's; there is little damage at the center guanine of each triplet. It is noteworthy that little damage is observed in the duplex region, which includes a guanine doublet site. Histograms of the oxidative damage observed after 120 min of irradiation at 365 nm for **DQ-2** and **DQ-3** are shown in Figure 6.9B. Due to poor resolution on the gel compared to other triple guanine sites, the 5'-GGG-3' at the 3'-end of the sequence appears as only two peaks in the histogram; these two peaks correspond to the 3' and 5'-G's.

Schematics summarizing the CT damage in the duplex/quadruplex conjugates as well as in the rhodium-tethered assembly containing the same duplex sequence studied previously (*19*), are shown in Figure 6.10 (oxidatively damaged sites are bolded). The duplex assembly was damaged at both 5'-G's of the 5'-GG-3' guanine doublets. In all three duplex/quadruplex conjugates, irrespective of rhodium binding site or presence of a guanine doublet, the two outer tetrads are oxidatively damaged while the center guanines of the 5'-GGG-3' guanine triplets, which form the center tetrad, are not damaged; little significant damage occurs within the duplex region of the duplex/quadruplex conjugates.

6.3.7 Characterization of and Charge Transport Chemistry in a Guanine Quadruplex Containing Four Stacked Tetrads. The charge transport chemistry and oxidative DNA damage in a guanine quadruplex containing four, as opposed to three, stacked tetrads was also examined. The 28 base oligonucleotide comprising **G4 (**d[$G_4T_4G_4T_4G_4T_4G_4$]) contains repeating units of the *Oxytricha nova* telomeric-sequence. In the presence of 100 mM KCl the 28 base oligonucleotide folds in an intramolecular

fashion to form a guanine quadruplex with four stacked tetrads, as initially observed by ^{1}H-NMR (Figure 6.11) (*36*). The circular dichroism spectrum shown in Figure 6.12 confirms the formation of an antiparallel quadruplex due to the characteristic maximum at 290 nm and minimum at 260 nm. This quadruplex is extremely stable as shown in the temperature dependent CD profiles with melting and annealing temperatures of 94.8 °C and 85.5 °C, respectively (Figure 6.13). This hysteresis occurs because the heating and cooling curves are not in thermodynamic equilibrium. This could reflect a slow rate of association or a slow rate of dissociation. Since the folding of **G4** is intramolecular, the hysteresis is most likely due to slow dissociation; in fact, the rate of dissociation of intermolecular quadruplexes is known to be very slow (~ 10^{-7} min^{-1}) (*37, 38*).

Charge transport in **G4** was first examined using noncovalently bound $[Rh(phi)_2bpy']^{3+}$ with equimolar amounts of DNA and oxidant. Figure 6.14 shows the denaturing PAGE of **G4** after photoactivation of the noncovalently bound rhodium intercalator. In the 313 lane, where binding of the rhodium complex is assayed, damage is observed at G4, G20, G25, and G26 where G20 is the predominate site of damage. These sites mainly form the bottom tetrad of the quadruplex, positioned next to the lateral loops. The rhodium complex most likely binds in the lateral loop formed by the four thymine bases T21-T24, but since the rhodium photooxidant cannot promote direct strand scission on single stranded DNA, damage is only observed at the adjacent guanines which form the quadruplex. There is not significant damage observed at G9, which forms the forth corner of the bottom tetrad, suggesting that binding of the rhodium complex to one lateral loop (T21-T24) is favored over the other. Figure 6.15 shows the denaturing PAGE of **G4** after photoactivation of the rhodium intercalator present in 10-

fold excess over DNA. Irradiation to identify oxidant binding sites reveals a damage pattern similar to that observed with equimolar DNA and oxidant, as observed in the 313 lane; however, the intensity of damage is increased. There is again significant damage at G20, G25, and G26. Some damage is observed at G4. As was observed with equimolar DNA and oxidant, the complex does appear to prefer binding at the T21-T24 lateral loop as opposed to the T5-T8 lateral loop. Interestingly, in the case of excess rhodium complex, following photoactivation at 313 nm, strand cleavage is observed at the thymines comprising the T21-T24 loop. This is surprising as rhodium photocleavage has not been observed on single stranded DNA; however, it is important to note that the effect on the structure of the quadruplex of a 10-fold excess of rhodium intercalator is not known.

Upon irradiation of **G4** at 365 nm, in the presence of either equimolar or 10 fold excess rhodium oxidant, oxidative damage is observed mostly in the T21-T24 lateral thymine loop and at G20 and G25 which are located adjacent to the lateral loop. A schematic summarizing oxidative damage in **G4** is shown in Figure 6.16. Oxidative damage is observed at other sites in **G4**, but the damage is minor compared to at the T21-T24 loop and at G20 and G25.

6.4 DISCUSSION

6.4.1 Characterization of Duplex/Quadruplex Conjugates. In order to explore CT in a DNA structure proposed to be biologically important for oxidative damage, DNA conjugates containing adjacent duplex and guanine quadruplex regions were designed. Circular dichroism is a valuable tool for monitoring the formation of antiparallel guanine

quadruplex structures in solution due to distinctive signals at 260 and 290 nm. In combination with a DMS protection assay, native gel electrophoresis, and high energy irradiation of the rhodium photooxidant, we were able to characterize the formation of both the duplex and quadruplex regions of the conjugate assemblies. The melting temperature studies provide a measure of stability of the DNA conjugates; with melting temperatures of ~ 60 °C these assemblies are quite robust.

In assemblies containing a tethered photooxidant, radical injection occurs in the duplex region and must be funneled to the quadruplex region to yield damage. Irradiation at 313 nm marks the site of rhodium binding through direct strand scission, and under the conditions utilized for CT experiments, this direct strand cleavage occurs exclusively within the duplex region; only at much higher concentrations is some cleavage detectable within the quadruplex. Thus at the concentrations utilized, CT to yield damage within the quadruplex must originate within the duplex region. The reaction is therefore within an individual assembly and does not involve inter-assembly interactions. Native gel electrophoresis also supports this intra-assembly reaction, in that no evidence of aggregation or multimer formation is detected.

6.4.2 Long-Range Charge Transport in Duplex/Quadruplex Conjugates. The schematics in Figure 6.1 illustrate the base stack of the duplexes aligning with the stacked tetrads of the quadruplexes. This alignment was originally unanticipated and required experimental support. In fact, molecular modeling of a DNA conjugate containing the same 22 base quadruplex-forming overhang and dT_{12}:dA_{12} as the duplex sequence revealed very little base-base overlap between the duplex and folded quadruplex regions (*39*). In this scenario, CT from a duplex-bound photooxidant to the bases of the

quadruplex would not be possible since a continual array of π-orbitals is requisite. CT in DNA is exquisitely sensitive to base stacking and dynamics; insertion of a π-stacking perturbation such as a base bulge, mismatch, or non-aromatic moiety can turn off CT (*40-42*). The observation of CT to the quadruplexes of the conjugates designed here indicates that sufficient base-base overlap does exist at the duplex/quadruplex junction. We also explored CT in conjugates containing a three base 5'-ATA-3' linker between the duplex and quadruplex regions. The amount of oxidative damage in the quadruplex regions of these conjugates was very small, suggesting that a linker region provides too much flexibility at the duplex/quadruplex junction, resulting in poor base stacking overlap and therefore inefficient CT. In the absence of the linker, however, sufficient interaction between the two regions provide a route for CT. Indeed, in all three conjugates examined, similar damage patterns are obtained, suggesting that the guanine quadruplex serves as the trap for the oxidizing equivalents, regardless of the site of radical injection. Hence, in these assemblies, it is clear that radicals generated in the duplex/quadruplex conjugate are preferentially trapped in the folded quadruplex. If instead, deeper traps were to exist within the duplex region, possibly they would provide effective competition for damage.

6.4.3 Quadruplexes Display a Unique Oxidative Damage Pattern. The pattern of damage within the quadruplex is also easily distinguished from that for a 5'-GGG-3' triplet within duplex DNA. One explanation for the damage pattern observed, specifically the lack of damage at the center tetrad, is that the stacking overlap of guanines in a quadruplex results in lowered oxidation potentials for the 5'- and 3'-guanines. Stacking of guanines in double helical DNA has been shown, both

experimentally and theoretically, to lead to lowered oxidation potentials. For instance, 6-31G* single-point calculations predict the ionization potential for a single non-stacked guanine base to be 7.75 eV, while that of a guanine doublet, triplet, and quadruplet in duplex DNA to be 7.28, 7.07, and 6.98 eV, respectively (*43, 44*). Furthermore, similar calculations predict the HOMO of these guanine sequences stacked as in a duplex are localized on the 5'-G. Previous experiments demonstrated that after photoactivation of an intercalating oxidant, oxidative damage is observed exclusively at the 5'-G of 5'-GG-3' guanine doublets (*30*).

In order to ascertain if stacking of the bases in the quadruplex results in varying oxidation potentials for the guanines, 6-31G* single-point calculations analogous to those performed on the stacked bases of duplex DNA were performed. Preliminary calculations on the stacked guanines arranged in the geometry of an antiparallel quadruplex do not indicate a higher oxidation potential for the guanines comprising the center tetrad. This is consistent with experimental work reported by Thorp and coworkers (*25*). Using electrochemical generation of a $[Ru(bpy)_3]^{3+}$ oxidant to test for competitive damage based on oxidation potential, only minor differences in the amount of oxidation of an oligonucleotide in duplex versus quadruplex form were observed. This is in contrast to a 12-fold difference in guanine oxidation for an oligonucleotide containing single G's versus 5'-GG-3' guanine doublets.

If the pattern of damage within the guanine triplets of the quadruplex structure does not reflect a variation in oxidation potential based upon guanine stacking, a more likely explanation for the oxidative damage pattern observed relates to differential trapping of the guanine radical. It has been established that long-range CT results in the

formation of guanine cation and neutral radicals which then react irreversibly with H_2O and O_2 to form oxidative products that include 8-oxo-guanine, formamidopyrimidine, oxazalone, and imidazalone derivates visualized by gel electrophoresis (*45*). Access to diffusible molecular oxygen may be limited in the core of the quadruplex leading to a decreased efficiency of radical trapping at the center tetrad. This reduced access would lead to the damage pattern we observe.

To further test this hypothesis, we examined oxidative DNA damage in a quadruplex containing four stacked tetrads. If radical trapping is less efficient in the core of the quadruplex, a quadruplex of four stacked tetrads may have less damage in the center two tetrads while the external two tetrads would be oxidatively damaged. Unfortunately, the rhodium oxidant binds preferentially at one of the lateral loops in **G4**, which are one base larger than those in the duplex/quadruplex conjugates, and we only observe oxidative damage directly adjacent to the loop structures. Perhaps the presence of the duplex region in the conjugates prevented the rhodium intercalator from binding in this manner, in addition to providing a means of introducing a radical into the stacked guanine tetrads.

These quadruplex structures may be physiologically relevant with respect to oxidative damage within the cell. Recently, Hurley and coworkers have shown *in vivo* that the purine-rich strand of the nuclease hypersensitivity element III_1 can form intramolecular guanine quadruplexes; addition of a quadruplex-stabilizing cationic porphyrin stabilizes the quadruplex, which in turn serves as a transcriptional repressor element (*6*). These quadruplex structures may also exist at telomeres, although obtaining *in vivo* evidence has been more elusive. Intriguingly, the results provided here suggest

that DNA quadruplexes could, in fact, serve as traps of oxidative damage in the genome. Since trapping of charges in the guanine doublets of the duplex region, a known thermodynamic trap of electronic holes in DNA, was not found to be competitive with trapping within the folded quadruplex, the quadruplexes must provide a more effective trap.

Finally, the results obtained in this work may also aid in elucidating the DNA sequences that form guanine quadruplexes *in vivo*. The 5'-GGG-3' guanine triplets composing the guanine quadruplexes show an oxidative damage pattern of 5'-G ~ 3'-G >> center-G after CT from a rhodium photooxidant. In contrast, the oxidative damage pattern observed at 5'-GGG-3' guanine triplets in duplex DNA packaged within nuclei after incubation and photoactivation of a rhodium intercalator is 5'-G > center-G > 3'-G (*23*); this is the damage pattern typically observed after long-range CT in duplex DNA. Therefore, by observing CT damage patterns in different regions of the genome, one may be able to distinguish purine rich sequences that *in vivo* form quadruplex structures. Hence studies of long-range oxidative DNA damage *in vivo* by CT may provide a tool to assess quadruplex formation.

6.5 REFERENCES

(1) Mergny, J. L., and Helene, C. (1998) *Nat. Med. 12*, 1366.

(2) Parkinson, G. N., Lee, M. P. H., and Neidle, S. (2002) *Nature 417*, 876.

(3) Neidle, S., and Read, M. A. (2001) *Biopolymers 56*, 209.

(4) Patel, D. J., Bouaziz, S., Kettani, A., and Wang, Y. (1999) in *Oxford Handbook of Nucleic Acid Structure* (Neidle, S., Ed.) pp 398, Oxford University Press, Oxford.

(5) Rezler, E. M., Bearss, D. J., and Hurley, L. H. (2003) *Ann. Rev. Pharm. Tox. 43*, 359.

(6) Siddiqui-Jain, A., Grand, C. L., Bearss, D. J., and Hurley, L. H. (2002) *Proc. Natl. Acad. Sci. U. S. A. 99*, 11593.

(7) Williamson, J. R., Raghuraman, M. K., and Cech, T. R. (1989) *Cell 59*, 871.

(8) Miura, T., and Thomas, G. J. Jr. (1994) *Biochemistry 33*, 7848.

(9) Hardin, C. C., Henderson, E., Watson, T., and Prosser, J. K. (1991) *Biochemistry 30*, 4460.

(10) Gilbert, D. E., and Feigon, J. (1999) *Curr. Opin. Struct. Biol. 9*, 305.

(11) Blackburn, E. H. (1991) *Nature 350*, 569.

(12) Collins, K. (2000) *Curr. Opin. Cell Biol. 12*, 378.

(13) Wright, W. E., Tesmer, V. M., Huffman, K. E., Levene, S. D., and Shay, J. W. (1997) *Genes Dev. 11*, 2801.

(14) von Zglinicki, T. (2002) *Trends Biochem. Sci. 27*, 339.

(15) Núñez, M. E., and Barton, J. K. (2000) *Curr. Opin. Chem. Biol*. *4*, 199.

(16) Schuster, G. B. (2000) *Acc. Chem. Res. 33*, 253.

(17) Giese, B. (2002) *Ann. Rev. Biochem. 71*, 51.

(18) Lewis, F. D., Letsinger, R. L., and Wasielewski, M. R. (2001) *Acc. Chem. Res*. *34*, 159.

(19) Núñez, M. E., Hall, D. B., and Barton, J. K. (1999) *Chem. Biol*. *6*, 85.

(20) Ly, D., Sanii, L., and Schuster, G. B. (1999) *J. Am. Chem. Soc*. *121*, 9400.

(21) Núñez, M. E., Noyes, K. T., Gianolio, D., McLaughlin, L. W., and Barton, J. K. (2000) *Biochemistry 39*, 6190.

(22) Núñez, M. E., Noyes, K. T., and Barton, J. K. (2002) *Chem. Biol*. *9*, 403.

(23) Núñez, M. E., Holmquist, G. P., and Barton, J. K. (2001) *Biochemistry 40*, 12465.

(24) Friedman, K. A., and Heller, A. (2001) *J. Phys. Chem. B 105*, 11859.

(25) Szalai, V. A., and Thorp, H. H. (2000) *J. Am. Chem. Soc. 122*, 4524.

(26) Beaucage, S. L., and Caruthers, M. H. (1981) *Tetrahedron Lett. 23*, 1859.

(27) Warshaw, M. M., and Tinoco, I. Jr. (1966) *J. Mol. Biol. 20*, 29.

(28) Holmlin, R. E., Dandliker, P. J., and Barton, J. K. (1999) *Bioconj. Chem. 10*, 1122.

(29) Sitlani, A., Long, E. C., Pyle, A. M., and Barton, J. K. (1992) *J. Am. Chem. Soc. 114*, 2303.

(30) Hall, D. B., Holmlin, R. E., and Barton, J. K. (1996) *Nature 382*, 731.

(31) Parkinson, G. N., Lee, M. P. H., and Neidle, S. (2002) *Nature 417*, 876.

(32) Wang, Y., and Patel, D. J. (1993) *Curr. Biol. 1*, 263.

(33) Balagurumoorthy, P., and Brahmachari, S. K. (1994) *J. Biol. Chem. 269*, 21858.

(34) Lu, M., Gao, Q., and Kallenbach, N. R. (1993) *Biochemistry 32*, 598.

(35) Risitano, A., and Fox, K. R. (2003) *Biochemistry 42*, 6507.

(36) Smith, F. W., Schultze, P., and Feigon, J. (1995) *Structure 3*, 997.

(37) Miura, T., and Thomas, G. J. (1995) *Biochemistry 34*, 9645.

(38) Wyatt, J. R., Davis, P. W., and Freier, S. M. (1996) *Biochemistry 35*, 8002.

(39) Ren, J., Qu, X., Trent, R. O., and Chaires, J. B. (2002) *Nuc. Acid Res. 30*, 2307.

(40) Hall, D. B., and Barton, J. K. (1997) *J. Am. Chem. Soc*. *119*, 5045.

(41) Bhattacharya, P. K., and Barton, J. K. (2001) *J. Am. Chem. Soc*. *123*, 8649.

(42) Rajski, S. R., and Barton, J. K. (2001) *Biochemistry 40*, 5556.

(43) Saito, I., Takayama, M., Sugiyama, H., Nakatani, K., Tsuchida, A., and Yamamoto, M. (1995) *J. Am. Chem. Soc*. *117*, 6406.

(44) Prat, F., Houk, K. N., and Foote, C. S. (1998) *J. Am. Chem. Soc*. *120*, 845.

(45) Burrows, C. J., and Muller, J. G. (1998) *Chem. Rev*. *98*, 1109.

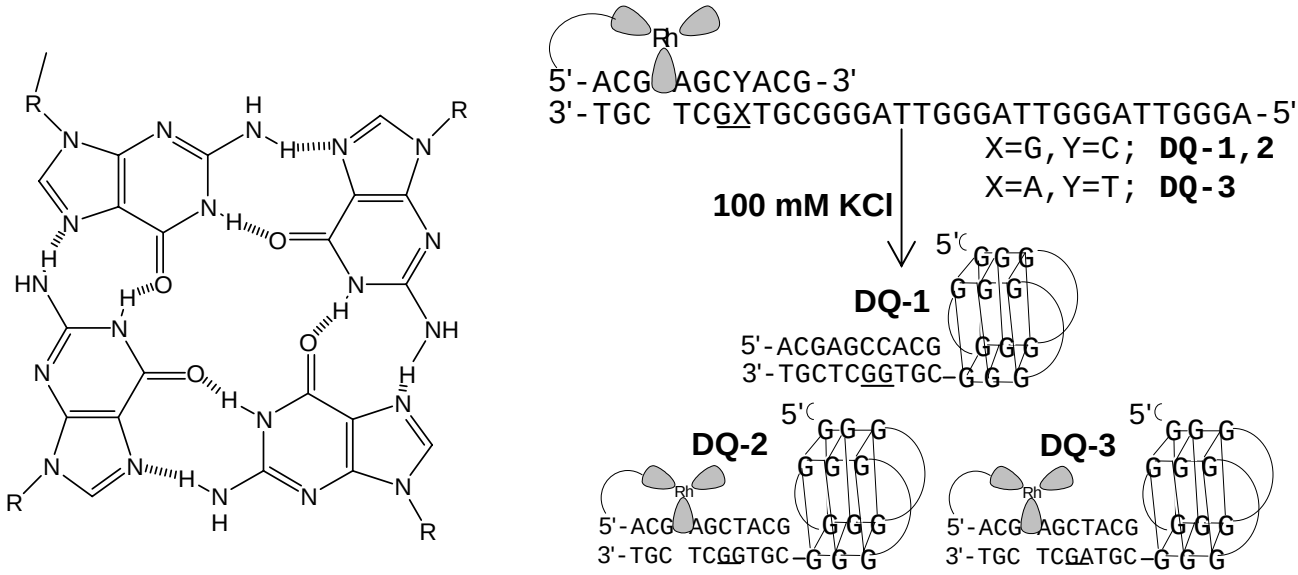

Figure 6.1. Schematic illustrations of a guanine tetrad (left) and the duplex/quadruplex conjugates **DQ-1**, **DQ-2**, and **DQ-3** (right) utilized in this work (adenines and thymines have been schematized for clarity). In the presence of 100 mM KCl, the single stranded overhang folds intramolecularly into an antiparallel quadruplex.

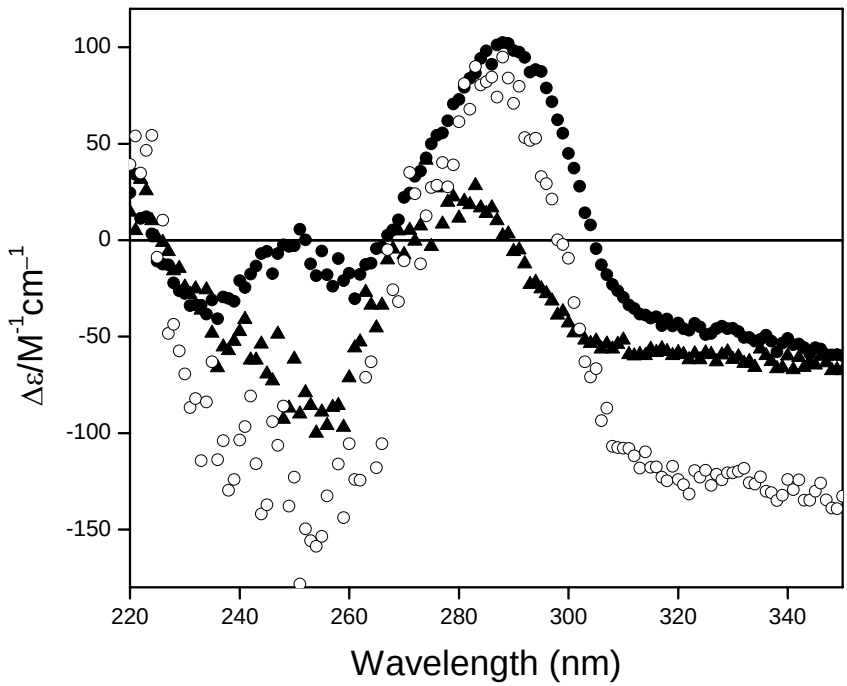

Figure 6.2. CD spectra of the quadruplex forming strand alone of **DQ-1** (closed circles), 10 base pair duplex of **DQ-1** alone (closed triangles), and **DQ-1** (open circles). The spectra were obtained at ambient temperature in 10 mM potassium phosphate, pH 7 with 100 mM KCl and at concentrations of 4 μM for the quadruplex forming strand alone and duplex and 2.5 μM for **DQ-1**.

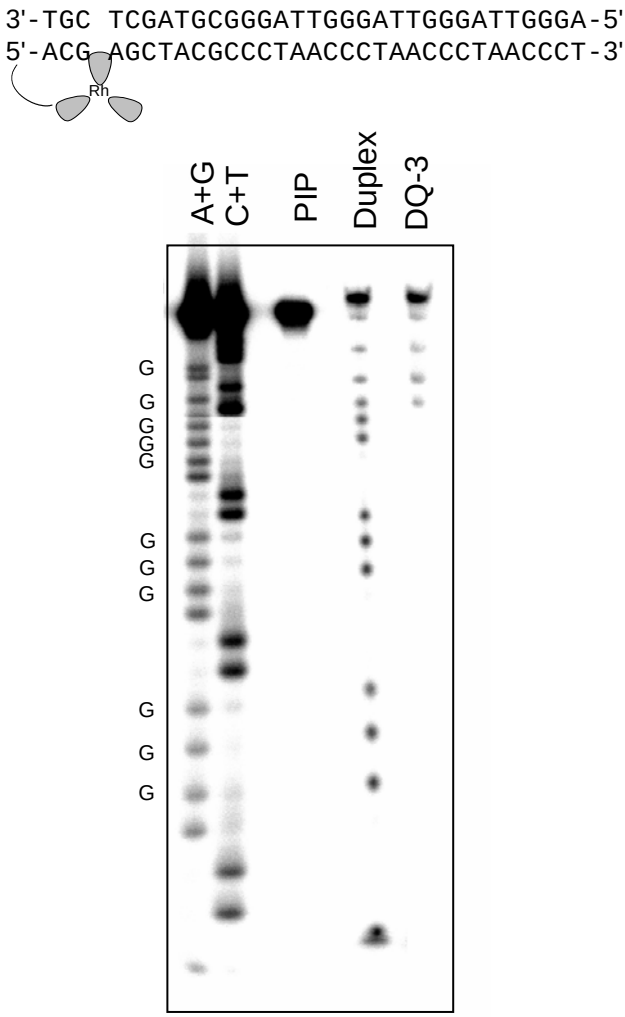

Figure 6.3. DMS methylation protection analysis of **DQ-3** and an all duplex control (sequence shown above). Maxam-Gilbert sequencing reactions A+G and C+T are shown in lanes 1 and 2, respectively. Damage of **DQ-3** treated with piperidine, but not DMS, is shown in lane 3. Lanes 4 and 5 show the methylation of the 32 base pair duplex control and **DQ-3**, respectively. The duplex and conjugate concentrations were 4 μM in 10 mM potassium phosphate, pH 7 with 100 mM KCl.

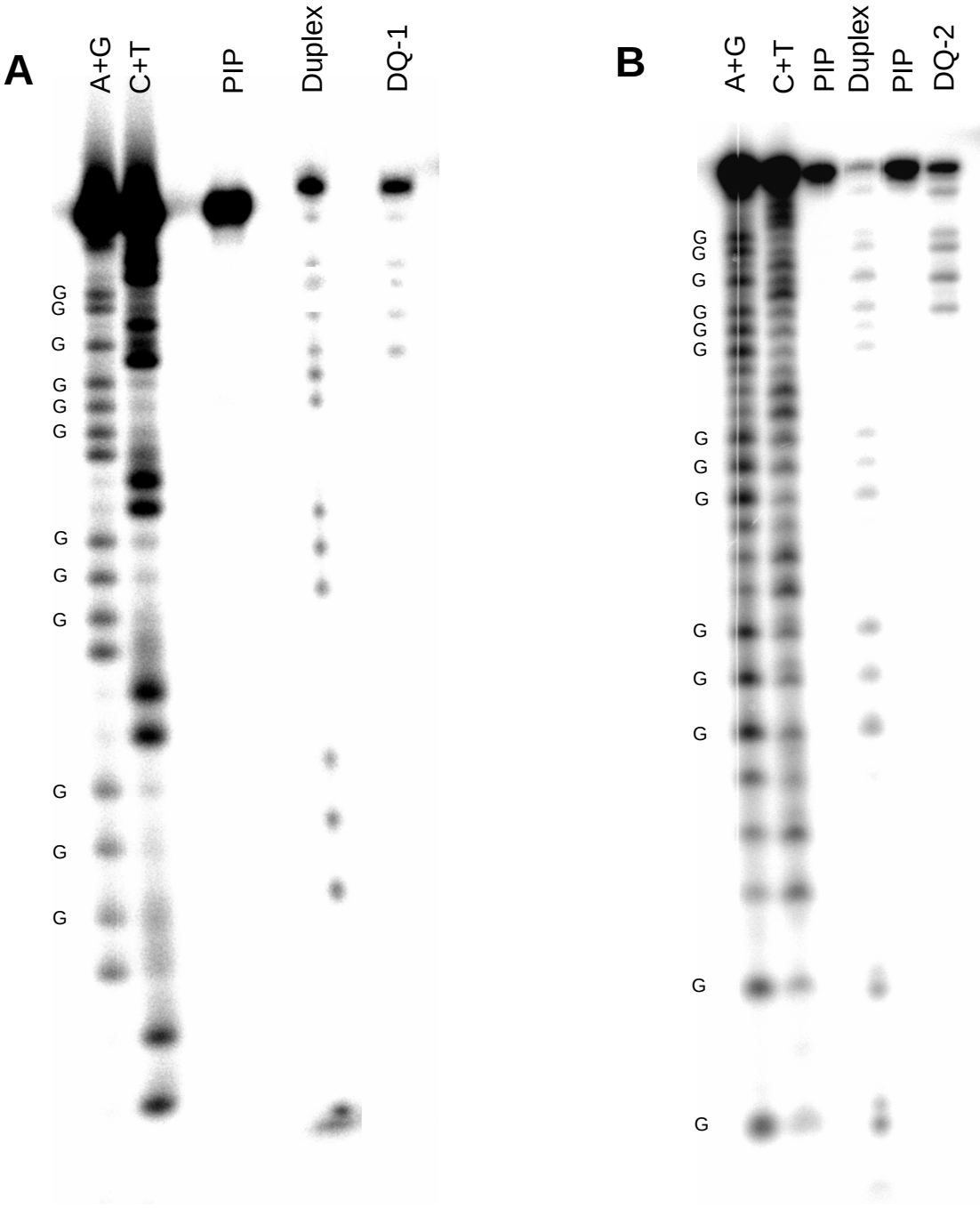

Fiugure 6.4. DMS methylation protection analysis of A) **DQ-1** and B) **DQ-2** along with duplex controls. Maxam-Gilbert sequencing reactions A+G and C+T are shown in lanes 1 and 2, respectively. Damage of duplex/quadruplex conjugates treated with piperidine, but not DMS, is shown in lanes labeled *PIP*. Methylation of the 32 base pair duplex control is shown in lanes labeled *Duplex*. Damage of duplex/quadruplex conjugates following treatment with DMS and piperdine are shown in lanes *DQ-1* and *DQ-2*. The duplex and conjugate concentrations were 4 μM in 10 mM potassium phosphate, pH 7 with 100 mM KCl.

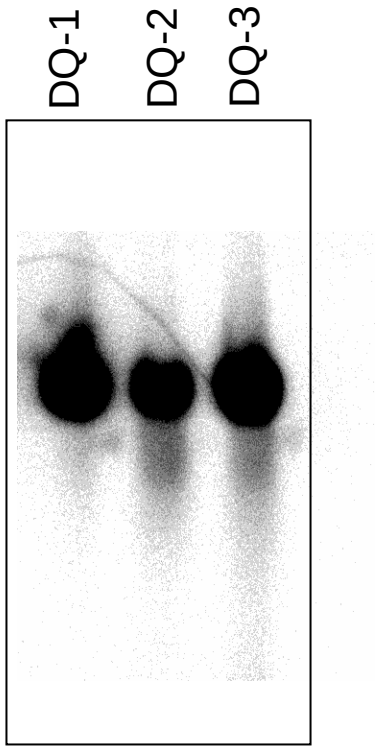

Figure 6.5. Native gel electrophoresis of **DQ-1**, **DQ-2**, and **DQ-3**. Conjugates were annealed at a concentration of 4 μM in 10 mM potassium phosphate, pH 7 with 100 mM KCl. Samples were electrophoresed at 4 °C and 10 W for ~ 12 hours through a 12% nondenaturing gel containing 100 mM KCl in the gel matrix, running buffer (0.5X TBE), and loading dye.

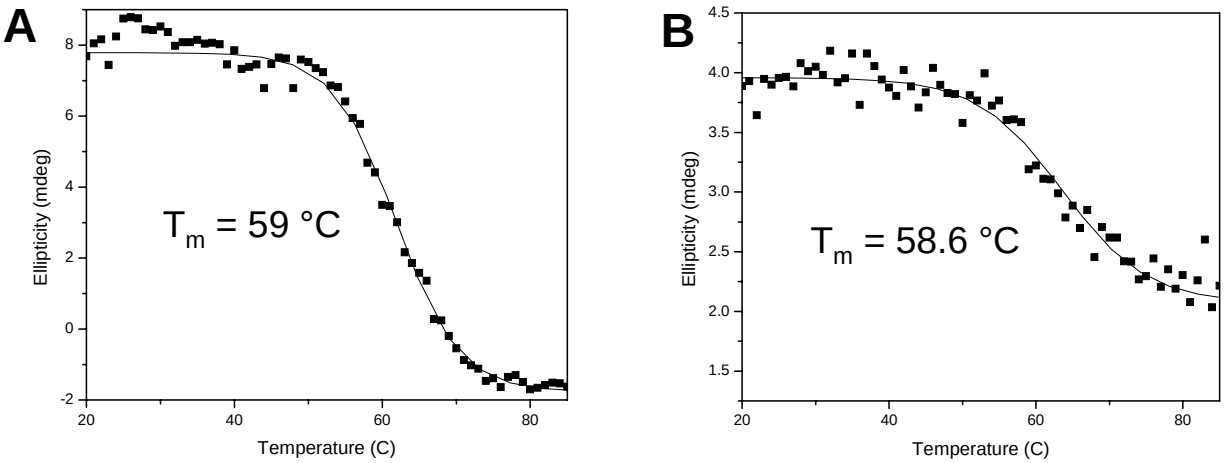

Figure 6.6. CD melting temperature profile of A) the quadruplex forming strand of **DQ-1** (4 μM) and B) duplex alone (4 μM) monitored at 285 nm, in 10 mM potassium phosphate, pH 7 with 100 mM KCl.

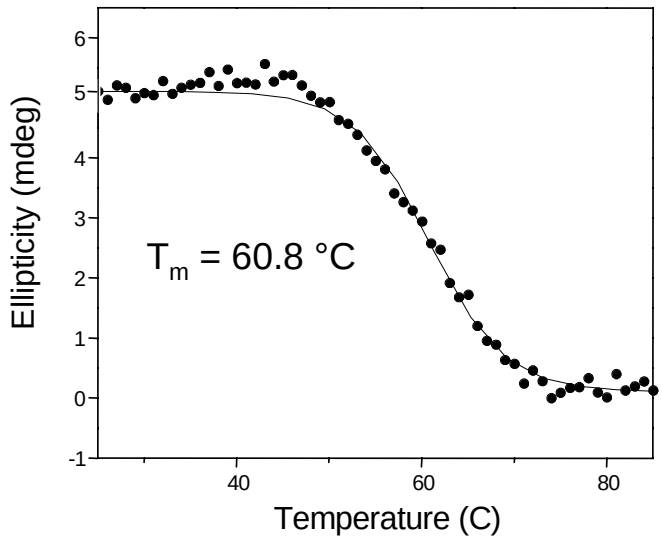

Figure 6.7. CD melting temperature profile of **DQ-1** (2.5 μM), monitored at 285 nm, in 10 mM potassium phosphate, pH 7 with 100 mM KCl. The melting temperature value of 60.8 °C represents the midpoint of the transition obtained by fitting the melting profile to a sigmoidal curve.

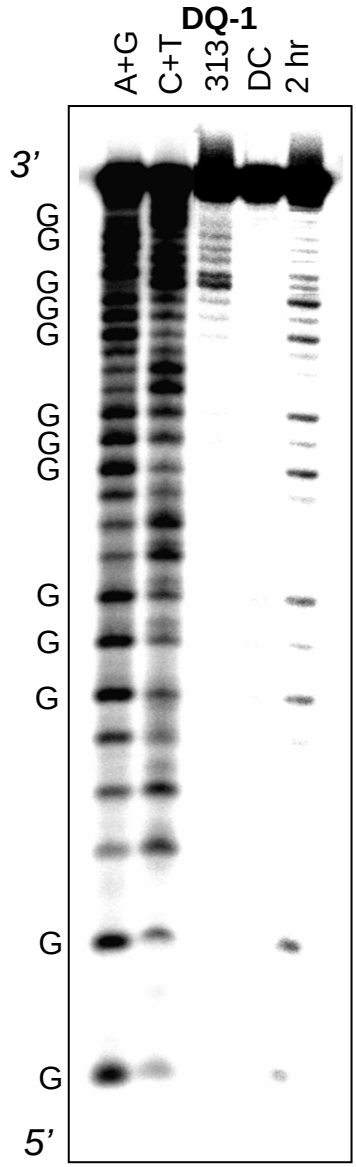

Figure 6.8. PAGE of **DQ-1** after photoactivation of noncovalently bound $[Rh(phi)_2bpy']^{3+}$. Maxam-Gilbert sequencing reactions A+G and C+T are shown in lanes 1 and 2, respectively. Lane 3 shows the direct photocleavage by the rhodium intercalator after irradiation at 313 nm for 30 min. Lanes 4 and 5 display the oxidative damage after irradiation at 365 nm for 0 and 120 min, respectively. Conjugate and noncovalent rhodium photooxidant concentrations were 4 μM in 10 mM potassium phosphate, pH 7 with 100 mM KCl.

Figure 6.9. (A) PAGE of **DQ-2** and **DQ-3** after photoactivation of covalently tethered $[Rh(phi)_2bpy']^{3+}$. On the left for **DQ-2**, Maxam-Gilbert sequencing reactions A+G and C+T are shown in lanes 1 and 2, respectively. Lane 3 shows the photocleavage of the rhodium intercalator after irradiation at 313 nm for 30 min. Lanes 4-6 display the oxidative damage after irradiation at 365 nm for 0, 60, and 120 min, respectively. On the right for **DQ-3**, Maxam-Gilbert sequencing reactions A+G and C+T are shown in lanes 1 and 2, respectively. Lane 3 shows the photocleavage of the rhodium intercalator after irradiation at 313 nm for 30 min. Lanes 4, 5 display the oxidative damage after irradiation at 365 nm for 0 and 120 min, respectively. Conjugate concentration was 4 μM in 10 mM potassium phosphate, pH 7 with 100 mM KCl. (B) Histograms of the oxidative damage observed after 120 min of 365 nm irradiation for **DQ-2** and **DQ-3**. The plots have been aligned horizontally to allow for direct comparison.

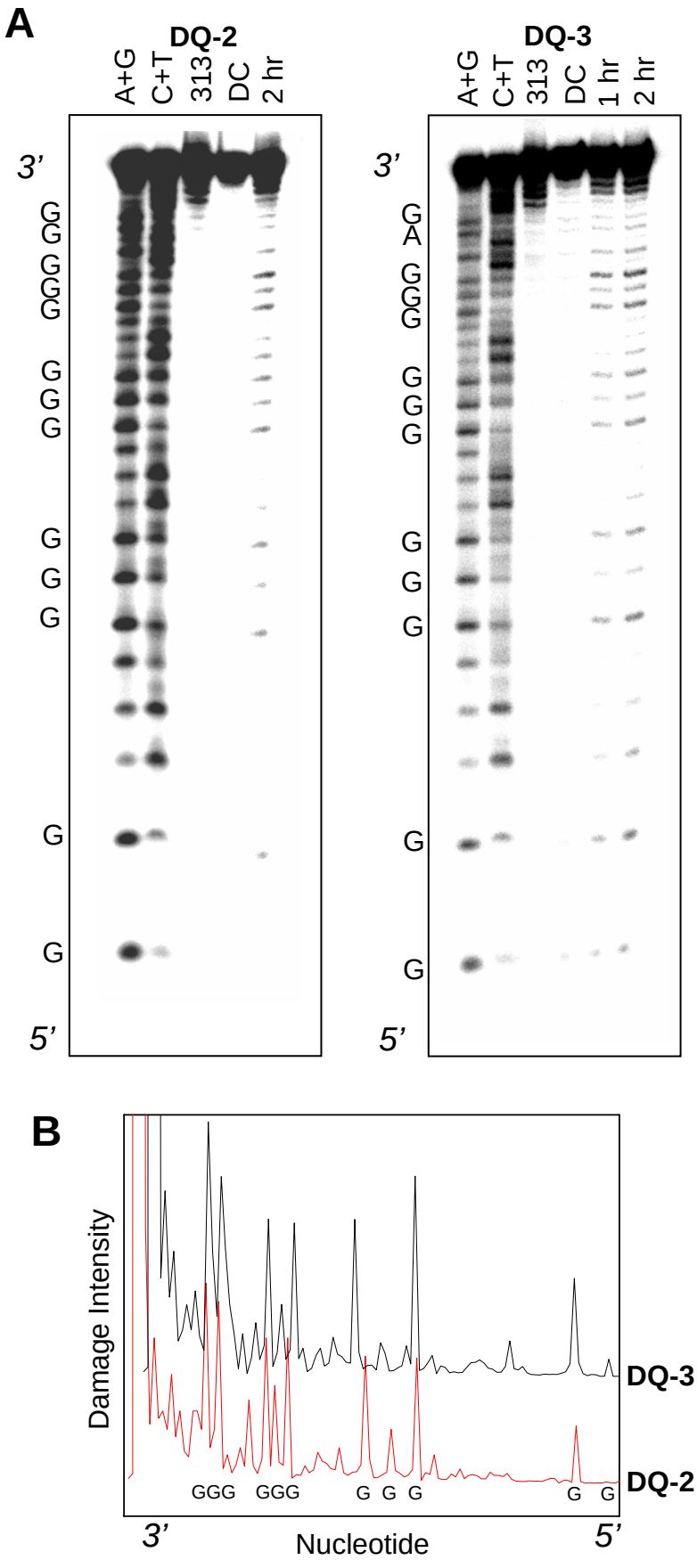
A
DQ-2
A+G
C+T
313
DC
2 hr
3'
5'
DQ-3
A+G
C+T
313
DC
1 hr
2 hr
3'
5'
B
Damage Intensity
GGG
GGG
G G G
G G
DQ-3
DQ-2
3'
Nucleotide
5'

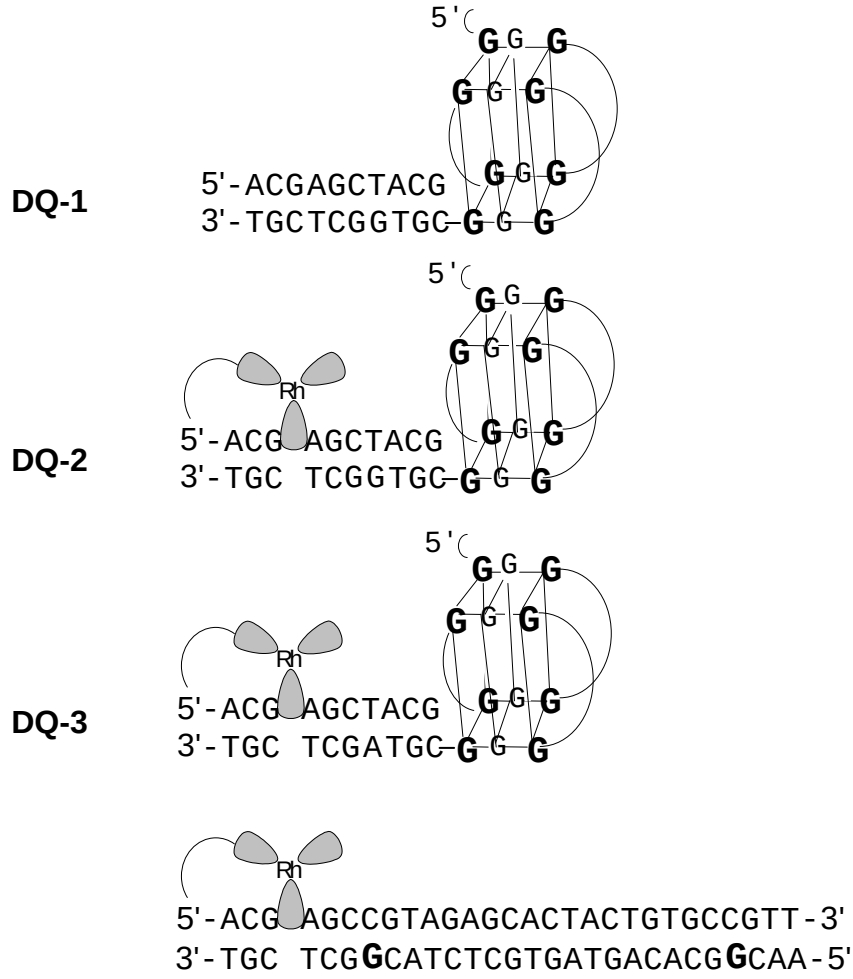

Figure 6.10. Schematic illustrations of the oxidative damage patterns in **DQ-1**, **DQ-2**, and **DQ-3** after CT from $[Rh(phi)_2bpy']^{3+}$. Damaged sites are shown in bold. A schematic of the oxidative damage in the rhodium tethered, double guanine-containing duplex, studied previously, is also shown.

G4: 5’-$G_1G_2G_3G_4T_5T_6T_7T_8G_9G_{10}G_{11}G_{12}T_{13}T_{14}T_{15}T_{16}G_{17}G_{18}G_{19}G_{20}T_{21}T_{22}T_{23}T_{24}G_{25}G_{26}G_{27}G_{28}$-3’

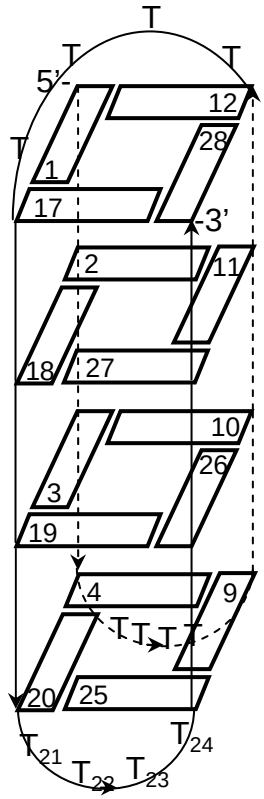

Figure 6.11. Schematic illustration of **G4** quadruplex showing the numbering of the nucleotides used in this work. The oligonucleotide sequence is shown above.

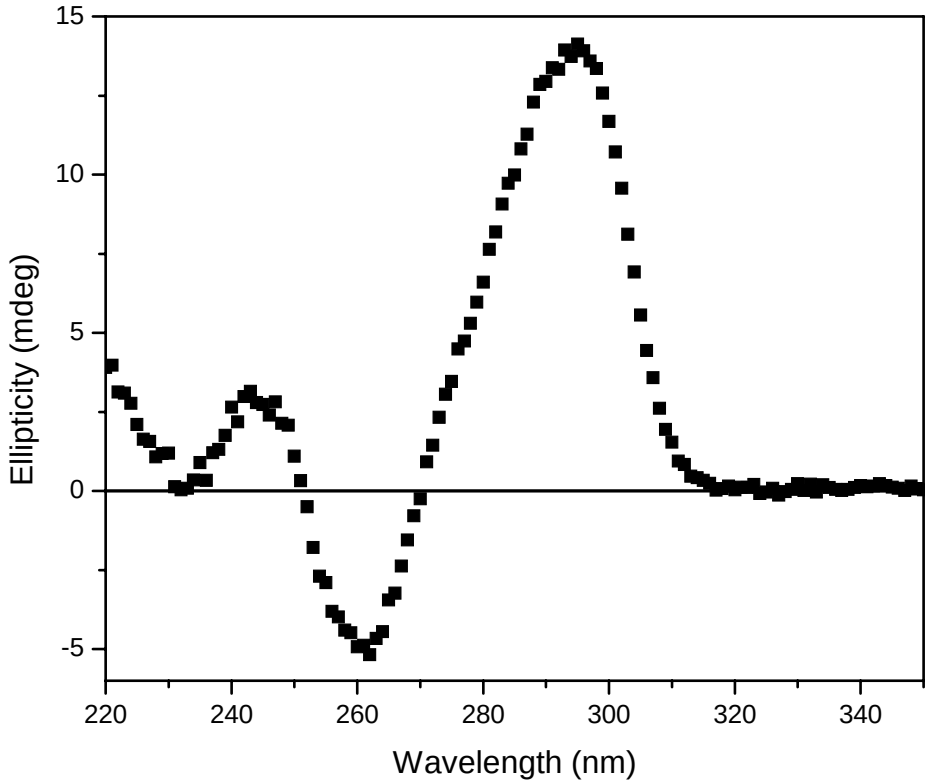

Figure 6.12. CD spectra of **G4** (4 μM). The spectra were obtained at ambient temperature in 10 mM potassium phosphate, pH 7 with 100 mM KCl.

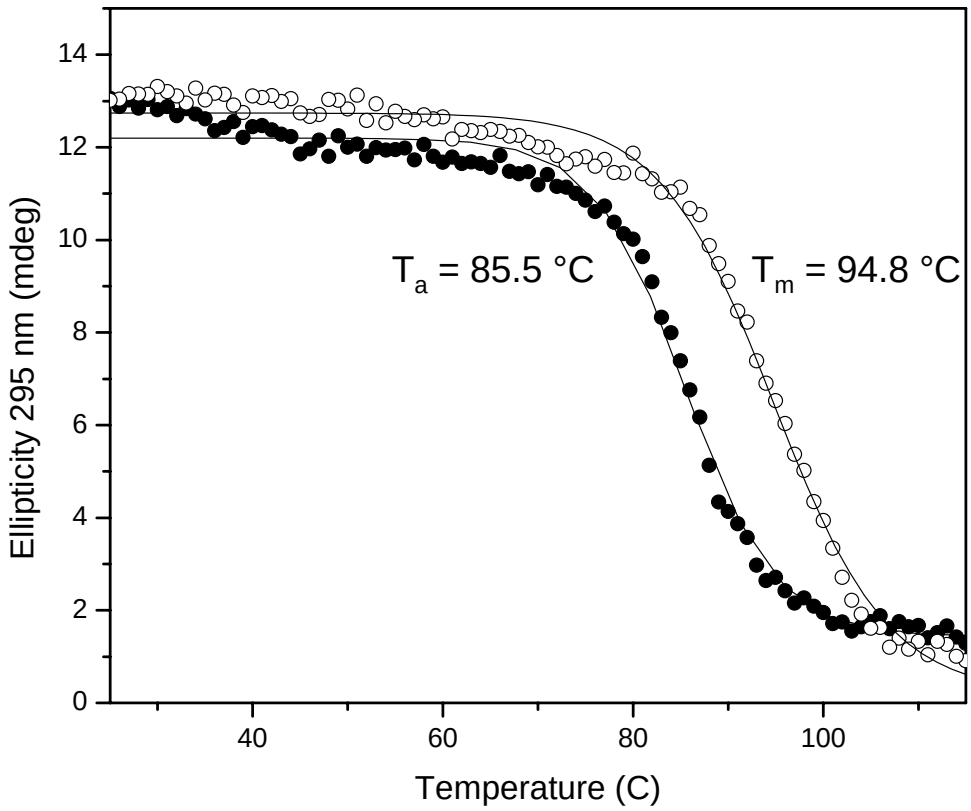

Figure 6.13. CD melting (open circles) and annealing (closed circles) temperature profile of **G4** (4 μM), monitored at 295 nm, in 10 mM potassium phosphate, pH 7 with 100 mM KCl. The melting and annealing temperatures of 94.8 °C and 85.5 °C, respectively, represent the midpoint of the transitions obtained by fitting the profile to a sigmoidal curve.

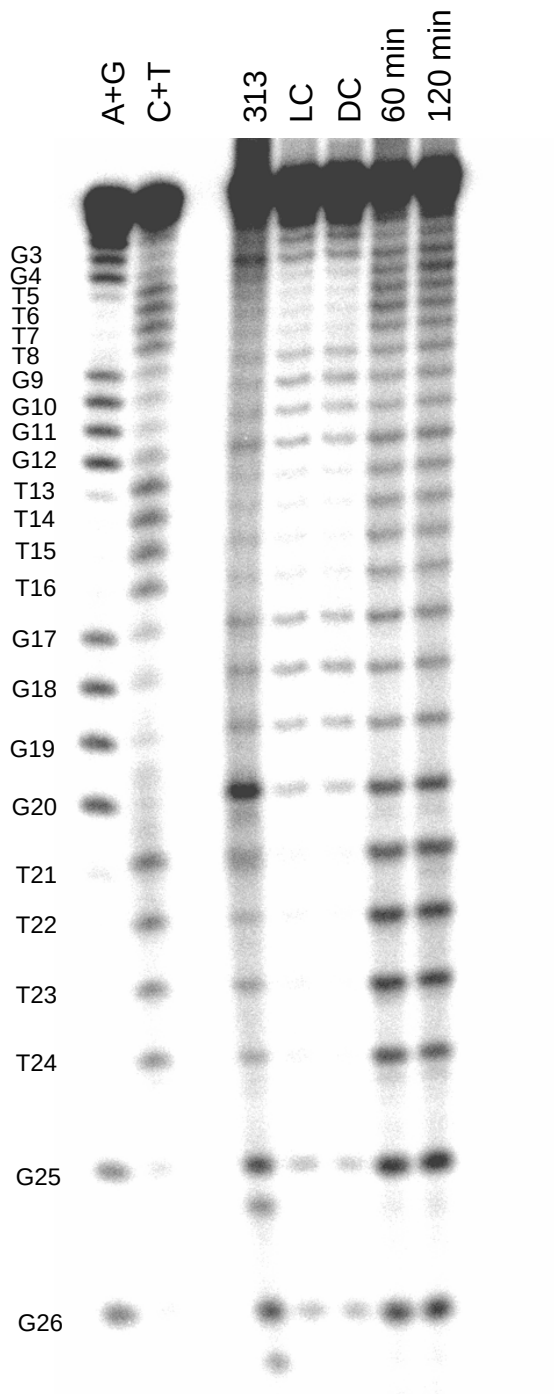

Figure 6.14. PAGE of **G4** after photoactivation of noncovalently bound $[Rh(phi)_2bpy']^{3+}$. Maxam-Gilbert sequencing reactions A+G and C+T are shown in lanes 1 and 2, respectively. Lane 3 shows the direct photocleavage by the rhodium intercalator after irradiation at 313 nm for 30 min. Lane 4 displays damage after irradiation of G4 in the absence of $[Rh(phi)_2bpy']^{3+}$. Lanes 5, 6, and 7 display the oxidative damage after irradiation at 365 nm for 0, 60, and 120 min, respectively. Quadruplex and noncovalent rhodium photooxidant concentrations were 4 μM in 10 mM potassium phosphate, pH 7 with 100 mM KCl.

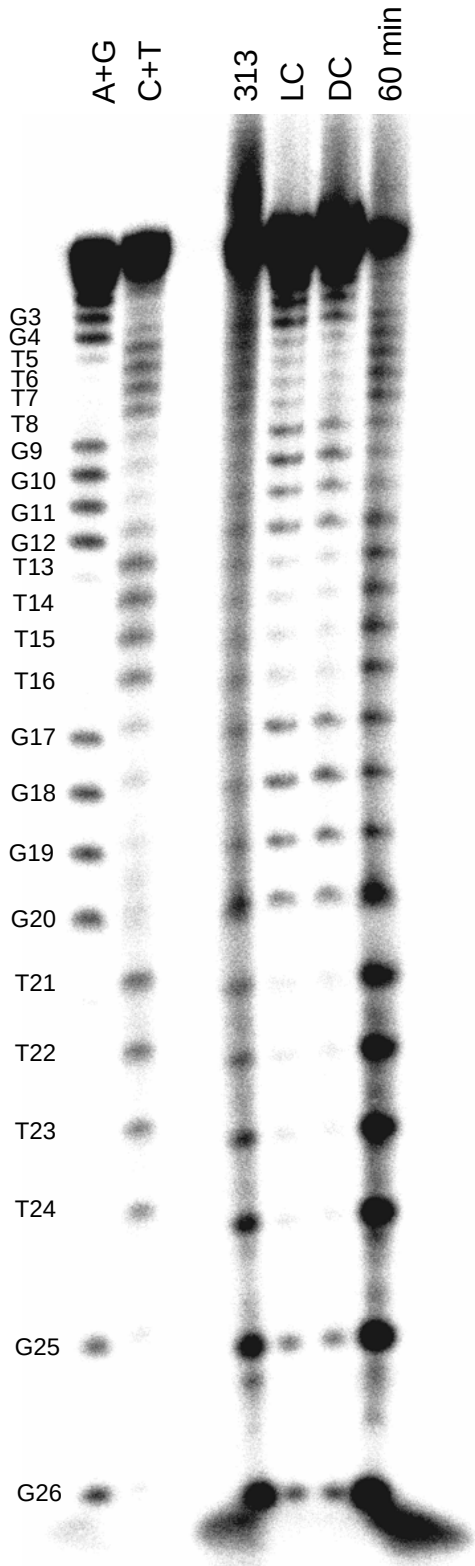

Figure 6.15. PAGE of **G4** after photoactivation of noncovalently bound $[Rh(phi)_2bpy']^{3+}$. Maxam-Gilbert sequencing reactions A+G and C+T are shown in lanes 1 and 2, respectively. Lane 3 shows the direct photocleavage by the rhodium intercalator after irradiation at 313 nm for 30 min. Lane 4 displays damage after irradiation of G4 in the absence of $[Rh(phi)_2bpy']^{3+}$. Lanes 5 and 6 display the oxidative damage after irradiation at 365 nm for 0 and 60 min, respectively. Quadruplex and noncovalent rhodium photooxidant concentrations were 4 μM and 40 μM, respectively, in 10 mM potassium phosphate, pH 7 with 100 mM KCl.

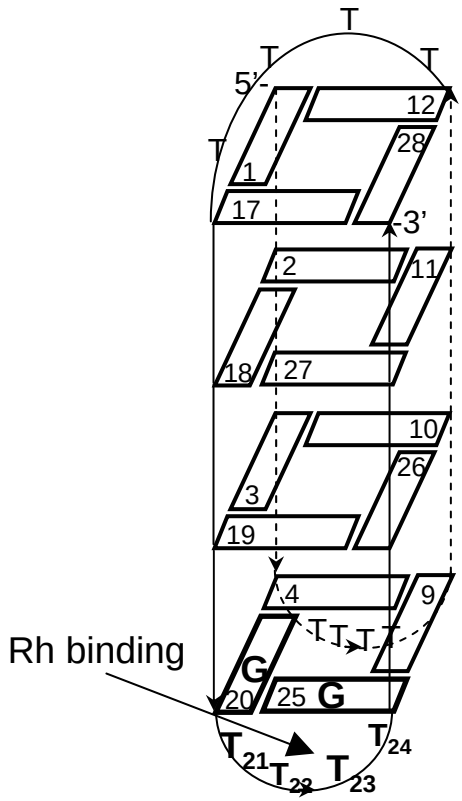

Figure 6.16. Schematic illustration of the oxidative damage patterns in **G4** after CT from $[Rh(phi)_2bpy']^{3+}$. Damaged sites are shown in bold.

CHAPTER 7

Summary and Conclusions

7.1 SUMMARY AND CONCLUSIONS

Oxidative damage to DNA from a distance has now been demonstrated using a variety of photooxidants (*1-6*) and establishes the effectiveness of DNA-mediated CT chemistry over long molecular distances. Indeed, damage has been observed 200 Å from the site of radical injection (*7, 8*). The chemical synthesis of well-defined DNA assemblies with pendant probes has been critical in the characterization of DNA-mediated CT and the parameters that affect it. Using time-resolved spectroscopy, the timescale for the rate of CT to affect long-range damage has also been probed. With our ruthenium intercalators as tethered oxidant, CT proceeds at a rate $\geq 10^7\ s^{-1}$ over 30 Å, and over this distance regime no significant variations in rate are observed (*9-11*). CT is exquisitely sensitive to sequence-dependent base stacking and may be gated by the dynamical motions within DNA. DNA CT to yield oxidative DNA damage can best be explained in the context of a hopping model, but one where holes may migrate among delocalized domains rather than from base to base, where these hopping domains are defined by sequence-dependent stacking and dynamics (*12*). Long-range oxidative damage to DNA is relevant physiologically since long-range CT damage to DNA has also been detected in cell nuclei (*13*) and nucleosome core particles (*14*).

By studying a family of ruthenium complexes containing the dppz ligand and derivatives, the ability of the complex to intercalate into the DNA π-array has been found to affect directly the extent of DNA charge transport and resultant damage (*15*). Intercalation can lead to more effective coupling into the π-stack, resulting in more efficient hole injection and charge transport. The source of charge injection into DNA is therefore a critical parameter in determining the extent of oxidative DNA damage from a

distance. These results require consideration in comparing reactions on DNA with different photooxidants.

Back electron transport has emerged as a critical parameter in examining long-range oxidative DNA damage. Using dipyridophenazine complexes of ruthenium, the sequence at the charge injection site was found to directly modulate the extent of long-range damage (*10*). Biochemical analyses suggest these differences depend upon the extent of radical delocalization at the injection site by allowing (with G) or inhibiting (with I) a non-productive back reaction with reduced quencher. A fast rate of BET may also explain the lack of damage products observed in the reductive flash/quench scheme; BET may be faster than radical trapping.

Through a series of spectroscopic and biochemical analyses on duplexes containing two oxidatively sensitive sites, we have observed charge equilibration over the DNA duplex (*11*). Charge migration leads to a sampling of the entire duplex on a time scale that is fast compared to localization and trapping. Charge transport through DNA can not be considered statically with conclusions based upon measurements of yield. Instead, the reaction must be viewed dynamically with rates of CT across the duplex in both forward and reverse directions being considered.

A potential biological opportunity for DNA CT has been explored by examining oxidative damage in guanine quadruplexes (*16*). Interestingly, the results obtained in this work may aid in elucidating the DNA sequences that form guanine quadruplexes *in vivo*. The 5'-GGG-3' guanine triplets composing the guanine quadruplexes show an oxidative damage pattern of 5'-G ~ 3'-G >> center-G after CT from a rhodium photooxidant. In contrast, the oxidative damage pattern observed at 5'-GGG-3' guanine triplets in duplex

DNA packaged within nuclei after incubation and photoactivation of a rhodium intercalator is 5'-G > center-G > 3'-G; this is the damage pattern typically observed after long-range CT in duplex DNA. Therefore, by observing CT damage patterns in different regions of the genome, one may be able to distinguish purine rich sequences that *in vivo* form quadruplex structures. Hence studies of long-range oxidative DNA damage *in vivo* by CT may provide a tool to assess quadruplex formation.

The characteristics of DNA CT chemistry that have been delineated prompt many more questions. Given that DNA CT can occur over long molecular distances, does this reaction play a role in oxidative damage within the genome? Can radicals generated at one site in the base stack migrate or be funneled through the helix to other regions? Perhaps even more intriguing, DNA-binding proteins can modulate CT both positively and negatively; is the base pair stack used for signaling between proteins, to scan for DNA damage and mismatches or possibly for transcriptional activation from a distance? Can we describe the DNA CT chemistry we have developed using DNA assemblies with pendant redox probes truly as biomimetic chemistry, modeling what can occur within the cell? Designing experiments to probe these questions, both in the test tube and within the cell, provides us with still more tantalizing challenges.

7.2 REFERENCES

(1) Hall, D. B., Holmlin, R. E., and Barton, J. K. (1996) *Nature 382*, 731.

(2) Núñez, M. E., Noyes, K. T., Gianolio, D., McLaughlin, L. W., and Barton, J. K. (2000) *Biochemistry 39*, 6190.

(3) Hall, D. B., Kelley, S. O., and Barton, J. K. (1998) *Biochemistry 37*, 15933.

(4) Gasper, S. M., and Schuster, G. B. (1997) *J. Am. Chem. Soc*. *119*, 12762.

(5) Nakatani, K., Dohno, C., and Saito, I. (1999) *J. Am. Chem. Soc*. *121*, 10854.

(6) Meggers, E., Kusch, D., Spichty, M., Wille, U., and Giese, B. (1998) *Angew. Chem., Int. Ed*. *37*, 460.

(7) Núñez, M. E., Hall, D. B., and Barton, J. K. (1999) *Chem. Biol*. *6*, 85.

(8) Ly, D., Sanii, L., and Schuster, G. B. (1999) *J. Am. Chem. Soc*. *121*, 9400.

(9) Pascaly, M., Yoo, J., and Barton, J. K. (2002) *J. Am. Chem. Soc*. *124*, 9083.

(10) Yoo, J., Delaney, S., Stemp, E. D. A., and Barton, J. K. (2003) *J. Am. Chem. Soc*. *125*, 664.

(11) Delaney, S., Yoo, J., Stemp, E. D. A., and Barton, J. K. (2004) Manuscript submitted.

(12) O'Neill, M. A., and Barton, J. K. (2004) Manuscript submitted.

(13) Núñez, M. E., Holmquist, G. P., and Barton, J. K. (2001) *Biochemistry 40*, 12465.

(14) Núñez, M. E., Noyes, K. T., and Barton, J. K. (2002) *Chem. Biol*. *9*, 403.

(15) Delaney, S., Pascaly, M., Bhattacharya, P., Koun, H., and Barton, J. K. (2002) *Inorg. Chem*. *41*, 1966.

(16) Delaney, S., and Barton, J. K. (2003) *Biochemistry 42*, 14159.